Spring 5-1-2015

Material Coefficient of Thermal Expansion Investigation for Use in Additive Manufacturing Fused Deposition Modeling for Composite Tooling

Daniel Joseph Miller
University of Southern Mississippi

The University of Southern Mississippi

MATERIAL COEFFICIENT OF THERMAL EXPANSION INVESTIGATION FOR USE IN ADDITIVE MANUFACTURING FUSED DEPOSITION MODELING FOR COMPOSITE TOOLING

by

Daniel Joseph Miller

A Thesis
Submitted to the Graduate School
of The University of Southern Mississippi
in Partial Fulfillment of the Requirements
for the Degree of Master of Science

Approved:

Dr. Jeffery S. Wiggins
Committee Chair

Dr. Sarah E. Morgan

Dr. Sergei I. Nazarenko

Dr. Karen S. Coats
Dean of the Graduate School

May 2015

ABSTRACT

MATERIAL COEFFICIENT OF THERMAL EXPANSION INVESTIGATION FOR USE IN ADDITIVE MANUFACTURING FUSED DEPOSITION MODELING FOR COMPOSITE TOOLING

by Daniel Joseph Miller

May 2015

Polymer matrix composites are being used to manufacture light weight, high stiffness aircraft structures. These structures are often manufactured from carbon fiber reinforced epoxy. When these structures are damaged, they must be repaired to restore strength to the component to avoid the cost and logistics of having replacement parts. Occasionally, these repairs require tooling in order to make a quality repair, however, tooling generally has a long lead time. Additive manufacturing could be used to manufacture rapid tooling to create tooling for composite repairs. The issue is that polymer printed tooling has a much higher coefficient of thermal expansion (CTE) than the composites that are being cured on them. This research investigates the addition of negative CTE fillers in polymers to reduce CTE to more closely match composites to reduce CTE mismatch and part distortion during elevated temperature cure.

ACKNOWLEDGMENTS

I would like to extend a special thank you to the following individuals who contributed to this effort. These individuals contributed by either specimen manufacturing, aiding in experiments, or by advising me on my efforts.

I would like to thank my thesis advisor, Jeffrey Wiggins, for helping guide me through the thesis process, reading my multiple drafts, and helping me to form good conclusions based off the testing results I found.

The following individuals aided by helping synthesize experimental specimen in the Polymer Science Laboratory in Hattiesburg MS: John Misasi, Kyler Knowles, and Andrew Frazee.

I would like to thank Justin Massey for supporting me through his parallel efforts as well as helping to provide information and expertise on FDM.

I would like to thank folks at NAVAIR; Anton Geiz and Mallory Knott for aiding me with running the thermal laboratory equipment, Ryan Davis, Tracy Larson, Chris Rethmel, Tara Kovacs, Andre Turner, Anthony Mara, and Brent Stickle for all helping with specimen prep and synthesis, Chad Gerdish for his laboratory management, John Brennan as my supervisor for helping me with my proposal writing, Jerry Rubinsky for aiding me with funding and development support, and finally Chris Coughlin for helping with thermal testing, advising, and interpretation of results.

TABLE OF CONTENTS

LIST OF TABLES

Table

LIST OF ILLUSTRATIONS

Figure

LIST OF EQUATIONS

Equation

CHAPTER I

INTRODUCTION

Problem Statement

Due to its high stiffness to weight ratio, many military aircraft utilize carbon fiber reinforced epoxy matrix composite material systems to create heavily loaded air craft structures. In a report produced by AeroStrategy for NIAR at Wichita State University, the increase in the percentages by weight of modern aircraft was captured. The graph that was generated can be found in Figure 1, showing the steep increase in composite materials in the aerospace industry. Military aircraft can be seen in blue and show that the current fleet of aircraft fielded is around the 25-40% by weight composites. When taking into account the many metal and ceramic engine components, this means that most of the structural components of fielded military aircraft are composite structures.

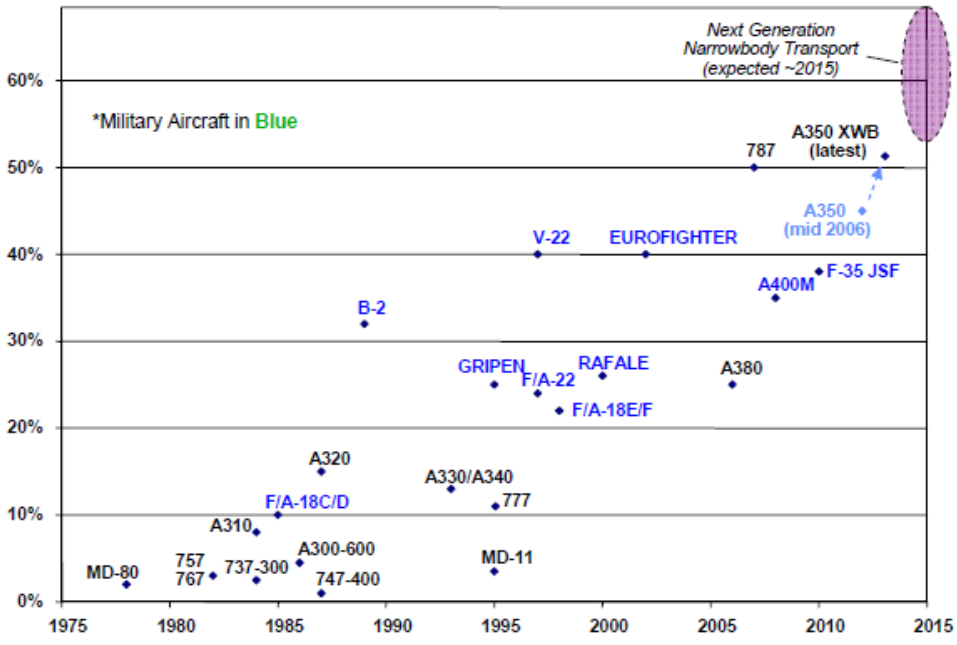

Figure 1. Percentage by weight of composite in modern aircraft (Tomblin 2014).

In the extreme environment that these military aircraft see, composite structures will often become damaged during use. Aircraft carbon fiber epoxy matrix composite structures can become damaged in many ways. The damage can be induced by overloading, impacts as well as many other types of environmental exposure damage such as high temperature exposures, or even bullet holes due to the harsh environment in which they are used. Because a larger percentage of military aircraft are using composites, more structures are becoming larger monocoque, or bonded structures. Once damaged, these structures must be repaired to reduce the "remove and replace" costs of scrapping and buying new aircraft components. Because composite components are becoming larger and more complex, removing fasteners and replacing parts is not financially or logistically sustainable, so repairs must be used to return structural integrity to composite aircraft structures.

Repairs can be performed with metal doublers fastened onto the aircraft to restore strength. These types are repairs are not preferred from an aircraft performance standpoint because they add significant weight and affect the center of gravity of the aircraft as well as potentially affecting airfoil performance. Due to these problems, fair, composite repairs are preferred from a weight and performance standpoint. The problem is that performing certain kinds of composite structural repairs requires special tooling to create the structural geometry of the carbon fiber epoxy matrix composites. Due to the fact that many repairs are unique, a unique tool is needed for each repair. These tools traditionally have long lead times due to forming or machining processes because they are made by machining metals or creating composite molds. This long time to create tooling increases aircraft downtime, which in turn reduces fleet readiness. The other issue

with using traditional tooling, such as machined metals, is that the tooling will have a coefficient of thermal expansion (CTE) that is different than that of a typical carbon fiber epoxy matrix composite system. The 304 stainless steel CTE is 17.3µm/m/ºC and 6061 Al is 23.6µm/m/ºC (Matweb 2014). Typical carbon fiber reinforced epoxy composites of quasi isotropic layup are around 2.1µm/m/ºC and 11.6µm/m/ºC for fiber glass reinforced epoxy composites (Goodfellow 2014). This CTE mismatch causes the composite and the tooling to expand at different rates during the elevated temperature cure cycle needed to crosslink the thermoset matrix material. This creates fit up issues from warpage and spring in as well as creates internal stresses cured into the component that may reduce the effectiveness of the repair. A representation of spring in from Wucher can be seen in Figure 2. The gradient in Figure 2 shows the displacement of the composite cured part from the tooling after the elevated cure cycle due to spring in.

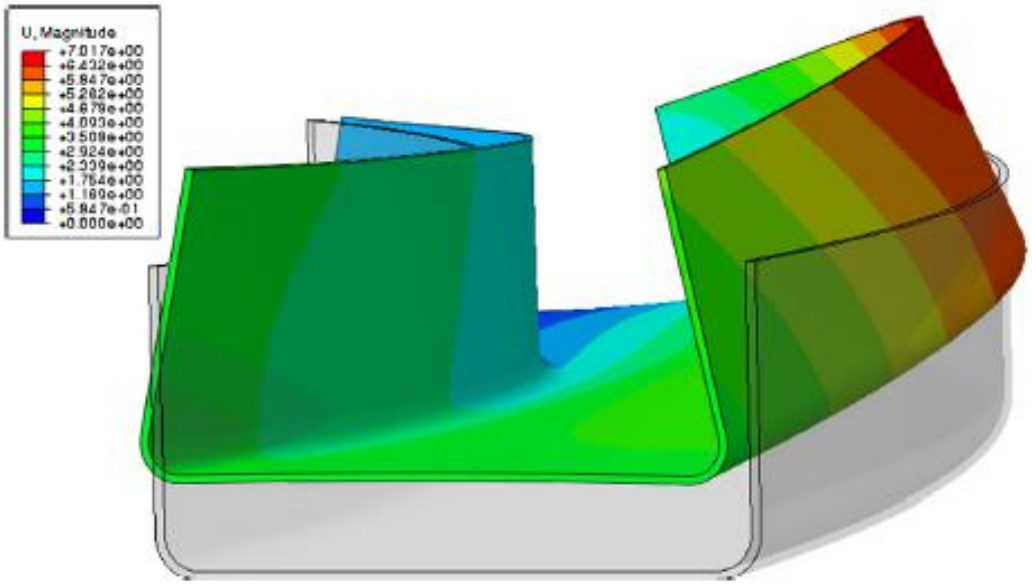

Figure 2. CTE Mismatch Part Distortion.

Tooling CTE Mismatch Correction Approaches

There are three general approaches to mitigate the issue of having a CTE mismatch between the composite component that is being cured, and the tooling that the part is being cured and formed onto. The three general approaches are to make changes to the process, material, or mold.

The first general approach is to change the process, or the way that the composite is processed and cured, also known as crosslinking. One common way that the process is changed in order to reduce the CTE mismatch impacts is to use multistage curing. This is when the part is ramped up to a lower cure temperature then held to start the crosslinking process. This is done to reduce the temperature change from where the part is crosslinked to the usage temperature. The part would then be ramped up higher after the component starts to crosslink, which reduces the rate it moves as it is ramped up further. The problem is that changing the ramp rate may impact the rheology during cure, potentially impacting the flow, increasing void content and altering the compaction of plies. Also crosslinking at a lower temperature at a lower reaction rate has been shown to significantly change the way the polymer crosslinks. It has been shown that at slow ramp rates one sees linear growth in crosslinking, but at higher ramp rates, one sees a more microgel type of growth. When making composites, the process is very important and changing it could significantly change the material properties of the final structure (Wucher et al. 2013).

The second general approach is to change the material itself. This is done during material selection for the application, and the CTE of the component is often manipulated by adding fillers to beneficially alter the CTE mismatch, or to change the cure

temperature to reduce the impact of CTE mismatch. The main problem is these approaches is that the material properties of the composite part you are trying to make are changed. This makes this very design limiting when designing and creating composite aircraft structures (Wucher et al. 2013).

The final generic approach is to make changes to the tooling. Wucher et al have developed a model to design the spring back into the mold. The researchers then designed the mold so that it was not the correct final dimensions of the desired part. However, during the cure cycle the tooling would "distort" because of thermal expansion, to the desired geometry and the component would then be cross-linked at the desired geometry. This is opposed to currently used methods of tooling design in which the tool is designed to the final part dimensions and distorting during the cure cycle and causing a problem. This method was used so the desired designed material properties and process could be kept without having the CTE issues that would cause part distortion, spring-back and internal stresses.

Proposed Solution

The proposed solution is to use a derivative of the third approach of manipulating the mold, but instead of using modeling to design the geometry of the mold, manipulate the CTE material properties of the tooling in order to reduce the CTE mismatch. In order to address the issue of fleet readiness and aircraft down time, additive manufacturing could be used to 3D print tooling to quickly turn around tooling for repairs.

To reduce the lead time of these tools, Fleet Readiness Center South West (FRCSW) located in North Island, California Naval Base, has used Fused Deposition

Modeling (FDM) to 3D print polymer molds and tooling on which to lay up carbon fiber reinforced epoxy matrix composites.

A schematic of the FDM process can be seen in Figure 3. The figure shows how a thread of thermoplastic material is fed through the extruder into the heated nozzle of the machine. The gantry moves back and forth across the stage in both X and Y directions to deposits the material one layer at a time. As layers are deposited by the extruder and nozzle, the stage moves down in the Z to allow the next layer to be printed onto the previous layer. As the molten polymer exits the nozzle and is deposited onto the previous layer, it cools and solidifies to create the three dimensional shape. Figure 4 shows the steps in the process as the polymer is deposited one layer at a time (Massey, Haris, et al. 2011).

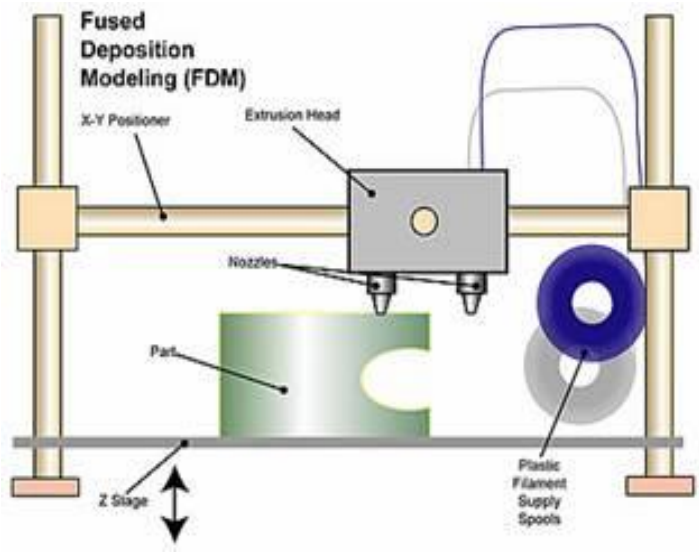

Figure 3. Fused Deposition Modeling.

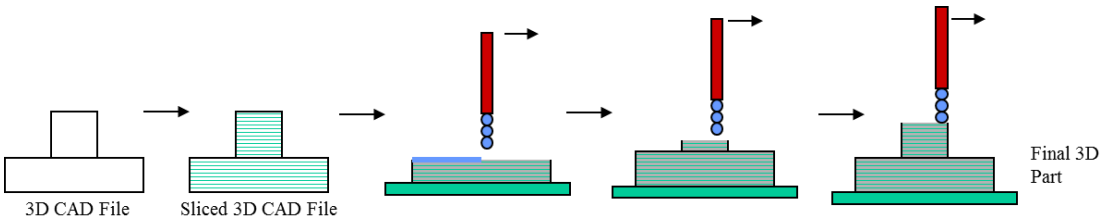

Figure 4. FDM Process.

The materials that FRCSW selected were, Polyphenylsulfone (PPSF) and Polyetherimide (PEI), which could be processed through the FDM process. These polymers were selected due to their high thermal stability and glass transition temperatures, targeting use in an autoclave for high temperatures and high pressures. A Stratasys Fortus 400mc FDM machine was used due to its ability to process the polymers at the high melt temperature needed to melt and deposit them layer by layer. Using an additive manufacturing approach can create a tool within a matter of hours, rather than months that the traditional metal machined subtracting manufacturing methods take. This approach alleviates the down time issue from needing "one off" tooling to perform composite repairs. However, due to the CTE mismatch, the composites distort. The CTE of most thermoplastic polymers is approximately 55µm/m/ºC, while the CTE of a 50% carbon fiber epoxy composite is closer to 2.1µm/m/ºC and 11.6µm/m/ºC for fiber glass epoxy composites (Unknown 2009) (www.goodfellow.com 2014). FRCSW chose to use the FDM 3D printing process to create a splash of the tooling then from that create a sand mold that has a lower CTE, similar to that of the composite part they were curing. The following research is an effort to lower the CTE of the FDM material in an attempt to eliminate a step in processing as well as avoid having to use a more fragile compressed sand mold (Massey, Haris et al. 2011; Massey, Heacock, and Harris 2014).

In this effort to lower the CTE of an FDM material, a particle filler was selected with negative CTE properties to reduce the bulk CTE properties of the material. In order to investigate this hypothesis, the following research describes how samples of PEI with various levels of fillers were prepared and the CTE was measured and compare to theoretical predictions. The following document will describe why the materials that were used were selected. Additionally, due to manufacturing issues with the PEI specimen, samples of an unfilled epoxy with multiple levels of the same filler were prepared and those CTEs were measured and compared with theoretical prediction.

It was also predicted that adding a filler would increase the viscosity of the polymer. This increase of viscosity would affect the processing of the PEI as it flowed out of the FDM nozzle during the melting and deposition process. In this thesis research effort, the temperature increase needed to achieve the same viscosity in polymer samples with filler versus neat resin samples based on a particular shear rate was characterized. If this can be understood, then the nozzle temperature can be increased to run the lower CTE filled polymer through the FDM nozzle.

Polyetherimide

Polymerization

Polyetherimides are polyimides that contain ethers and other structural units that increase the ability for it to be processed in the melt. This makes Polyetherimides good for injection molding and extrusion processing. Polyetherimides are synthesized by nucleophilic aromatic substitution between 1,3-bis(4-nitrophthalimido) benzene and disodiumsalt of bisphenol A. Polymerization is performed at 80-130°C in a polar solvent solution usually NMP or DMAC. This polymerization reaction can be seen in Figure 5.

Polyetherimides can also be polymerized using a reaction of diamine-dianhydride (Odian 2004).

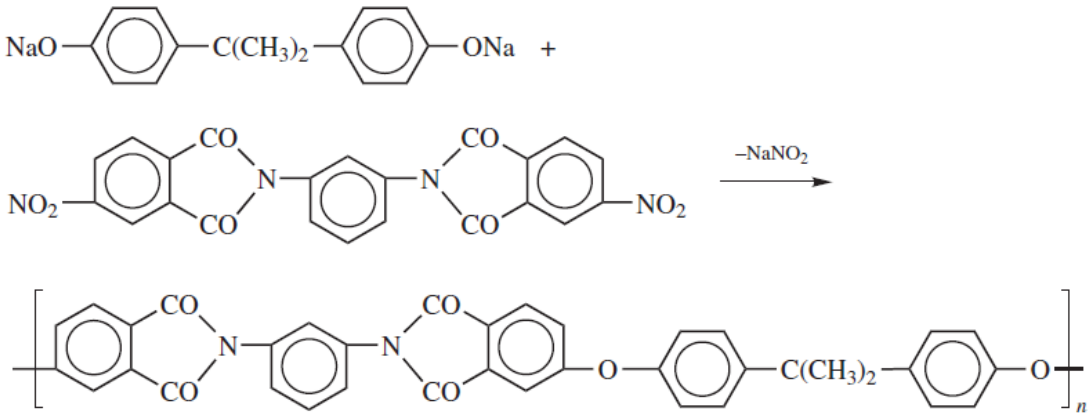

Figure 5. Polymerization of Polyetherimide (Odian 2004).

Characteristics

Polyetherimide is an amorphous polymer that has a glass transition temperature of approximately 215°C and can be used structurally up to 170-180°C. Polyetherimides also have good solvent resistance, with the exception that it is soluble in partially halogenated organic solvents. Another benefit of this polymer is that is does not produce volatile byproducts during processing. This reduces the voids that would be produced during processing if there was such off gassing during processing (Odian 2004).

For these reasons, Polyetherimide is a good polymer selection for the proposed solution. Polyetherimide has a use temperature in the 170-180°C which would be good for a typical high temperature carbon fiber/aerospace epoxy matrix composite cure cycle, which peaks around 177°C. If desired, this material could be used in an autoclave to cure these components because it has structural stability at those cure temperatures. Polyetherimide also does not produce volatile byproducts during reprocessing. This is beneficial for creating tooling using FDM because as the polymer is heated and deposited

on previous layers voids will not be created in the layers of between the layers. Voids within the tooling would cause issues during the composite cure cycle.

Nextrema

Nextrema is a silicate based ceramic provided by SCHOTT. The processing parameters were kept proprietary by SCHOTT. A technical data sheet was provided that detailed mechanical, electrical, spectral emission, as well as thermal properties. Nextrema is thermally stable up to 710°C. Nextrema was selected due to its relative inexpensive cost as a filler, and the technical data sheet documented a CTE of -0.28 µm/m/°C useful for reducing the overall bulk CTE when blended into the neat PEI polymer. Nextrema was also selected due to its high stiffness which allows it to have a larger effect on the bulk CTE due to the interactions between it and the softer polymer that it is mixed into. This is explained further in the calculations and predictions section.

Literature Search

Equations from Hashin can predict the bulk material properties of a heterogeneous material that has round spheres included in it. As discussed previously, Hashin found that edge effects from the particles caused interactions that could not be explained by the rule of mixtures so he model the interactions and created his own equations to model the interaction (Hashin 1962). Equations were used based on work that Hashin performed to predict the bulk modulus changes that were experienced in polymers with fillers in it that did not follow the traditional rule of mixtures. This interaction is based on the fact that the two materials have different stiffnesses so when they are expanding and contracting, they will put mechanical strain on one another in addition to the thermal strain from the changing temperatures. (Hashin and Rosen, The

Elastic Moduli of Fiber-reinforced Materials 1964). This is explained further in the calculations and predictions section. Due to the concern of timing to procure and synthesize PEI specimen work performed by Togana showed that epoxy's would follow similar predictions that Hashin found, deviating from the traditional rule of mixtures. (Tognana et al. 2009).

CHAPTER II

EQUATIONS AND CALCULATIONS

Equations

In order to calculate the CTE of a heterogeneous material using the individual material properties, Zvi Hashin proposed the following list of equations (Hashin, The Elastic Moduli of Heterogeneous Materials 1962). He found that the traditional rule of mixtures, Equation 1, was not sufficient for modeling the thermal expansion of the bulk material.

$$CTE = CTE_M(1 - \emptyset) + CTE_F\emptyset$$

Equation 1. Rule of Mixtures.

Where the CTE_M and CTE_F are the coefficient of thermal expansion for the matrix and the filler respectively and $\emptyset$ is the volumetric fraction of the filler particle.

This insufficiency was due to the modulus interactions of the material on the CTE. With rule of mixtures, the stiffnesses of the materials are not taken into account and their interactions on each other are not factored in. Hashin's assumption is that the material boundaries are bonded together and the stiffness of the two material when they are expanding or contracting during temperature changes, also push and pull on one another having an effect in addition to the thermal stresses. Equation 2 shows the calculation to determine the CTE of a heterogeneous material system with a matrix and a filler material.

$$\boldsymbol{CTE = CTE_M + \frac{CTE_F - CTE_M}{1/K_F - 1/K_M}\left(\frac{1}{K_C} - \frac{1}{K_M}\right)}$$

Equation 2. The Hashin-Shtrikman Equation.

Where the CTE_M and CTE_F are the coefficient of thermal expansion for the matrix and the filler respectively and K_c is the bulk modulus and K_M and K_F are the bulk modulus of the Matrix and Filler. The upper and lower bounds can be found using Equation 3 and Equation 4,

$$K_C(Up) = K_F + \frac{1 - \emptyset}{1/(K_M - K_F) + 3\emptyset/(3K_F + 4G_F)}$$

Equation 3. Upper Composite Bulk Modulus.

$$K_C(Low) = K_M + \frac{\emptyset}{1/(K_F - K_M) + 3(1 - \emptyset)/(3K_M + 4G_M)}$$

Equation 4. Lower Composite Bulk Modulus.

where the K_M and K_F are the bulk modulus of the Matrix and Filler and the G_M and G_F are the shear modulus of the matrix and filler. $\emptyset$ is the volumetric fraction of the filler particle. Bulk and shear modulus are related to the elastic modulus and Poisson's ratio as seen in Equation 5 and Equation 6.

$$K = \frac{E}{3(1 - 2v)}$$

Equation 5. Bulk Modulus.

$$\boldsymbol{G = \frac{E}{2(1 + v)}}$$

Equation 6. Shear Modulus.

v is the poisons rato of the material.

Predictions and Calculations

As reported below, the average CTE of the Nextrema was measured across the useful temperature, from room temperature, 30°C, up to 177°C. The average CTE was found to be -4.64µm/m/°C. Neat Polyetherimide was measured the same way and was found to be 53.38µm/m/°C. Details on the measurement and set up and graphical

representation of dimensional changes during temperature sweeps can be found in the Experimental section of this thesis. The elastic modulus and Poisson's ratio were documented to be 3.58GPa and 0.30 for Ultem 1000 from Sabic (www.matweb.com 2014) and 89.0GPa and 0.25 for Schott Nextrema (www.schott.com/nextrema 2014). These values were based on documented supplier datasheets and were not measured for use in the theoretical calculations. Due to the higher stiffness of the Nextrema, it is predicted that the bulk CTE of the will be closer to the Hashin lower bound due to the Nextrema stiffness overpowering the polyetherimide and having a larger effect on the overall CTE of the mixed material.

In an attempt to make the graphical representations compatible with the specimen that were manufactured, the density ratio was calculated into the volume fraction so that the axis could be graphed as the weight percent of additive into the polymer material. In order to do this, the weight percent was multiplied by the ratio of density of the polymer of the material and the Nextrema particles. The density of Nextrema is 2.6g/cm^3, PEI is 1.27 g/cm^3, and Epoxy used is 1.38 g/cm^3. Equation 7 shows the conversion from weight percent to volumetric fraction.

$$\emptyset = \frac{p_M}{p_F} W_P$$

Equation 7. Volumetric fraction conversion equation.

Where p_M is the density of the matrix material, p_F is the density of the filler, and W_P is the weight percent of filler that is added to the material.

Hashin's equations are designed out for bulk modulus calculations. The measurements that were going to be made were going to be linear thermal expansion with a TMA, discussed in the experimental section of this thesis. Hashins calculations can be

used for this approximation because linear thermal expansion was and linear modulus were used in the calculations below. Table 1 shows the calculations using the equations from the previous section to calculate the upper and lower limits of the coefficient of thermal expansion (CTE) using Hashin's method. The following figure, Figure 6, visually shows the bounds of the predicted calculations and also compares it to the traditional rule of mixtures calculations.

Table **2** and Figure 7 show the calculations and the bounds for Epoxy calculations.

Table 1

PEI Calculations

	CTE (µm/m/°C)	CTEM (µm/m/°C)	CTEF (µm/m/°C)	KC (GPa)	KM (GPa)	KF (GPa)	GM (GPa)	GF (GPa)	EM (GPa)	EF (GPa)	vM	vF	p Fraction	Weight %
Lower	53.38	53.38	-4.64	2.98	2.98	59.33	1.38	35.60	3.58	89.00	0.30	0.25	0.4792	0.00
Upper	53.38			2.98										
Lower	50.87	53.38	-4.64	3.11	2.98	59.33	1.38	35.60	3.58	89.00	0.30	0.25	0.4792	0.01
Upper	52.95			3.00										
Lower	48.54	53.38	-4.64	3.24	2.98	59.33	1.38	35.60	3.58	89.00	0.30	0.25	0.4792	0.02
Upper	52.51			3.03										
Lower	46.39	53.38	-4.64	3.37	2.98	59.33	1.38	35.60	3.58	89.00	0.30	0.25	0.4792	0.03
Upper	52.08			3.05										
Lower	44.38	53.38	-4.64	3.50	2.98	59.33	1.38	35.60	3.58	89.00	0.30	0.25	0.4792	0.04
Upper	51.66			3.07										
Lower	42.51	53.38	-4.64	3.63	2.98	59.33	1.38	35.60	3.58	89.00	0.30	0.25	0.4792	0.05
Upper	51.23			3.09										
Lower	40.75	53.38	-4.64	3.76	2.98	59.33	1.38	35.60	3.58	89.00	0.30	0.25	0.4792	0.06
Upper	50.81			3.11										
Lower	39.11	53.38	-4.64	3.89	2.98	59.33	1.38	35.60	3.58	89.00	0.30	0.25	0.4792	0.07
Upper	50.39			3.14										
Lower	37.57	53.38	-4.64	4.02	2.98	59.33	1.38	35.60	3.58	89.00	0.30	0.25	0.4792	0.08
Upper	49.97			3.16										
Lower	36.12	53.38	-4.64	4.16	2.98	59.33	1.38	35.60	3.58	89.00	0.30	0.25	0.4792	0.09
Upper	49.55			3.18										
Lower	34.75	53.38	-4.64	4.29	2.98	59.33	1.38	35.60	3.58	89.00	0.30	0.25	0.4792	0.10
Upper	49.14			3.21										
Lower	33.46	53.38	-4.64	4.43	2.98	59.33	1.38	35.60	3.58	89.00	0.30	0.25	0.4792	0.11
Upper	48.73			3.23										
Lower	32.24	53.38	-4.64	4.56	2.98	59.33	1.38	35.60	3.58	89.00	0.30	0.25	0.4792	0.12
Upper	48.32			3.25										
Lower	31.08	53.38	-4.64	4.70	2.98	59.33	1.38	35.60	3.58	89.00	0.30	0.25	0.4792	0.13
Upper	47.91			3.28										
Lower	29.98	53.38	-4.64	4.83	2.98	59.33	1.38	35.60	3.58	89.00	0.30	0.25	0.4792	0.14
Upper	47.50			3.30										
Lower	28.94	53.38	-4.64	4.97	2.98	59.33	1.38	35.60	3.58	89.00	0.30	0.25	0.4792	0.15
Upper	47.10			3.33										
Lower	27.95	53.38	-4.64	5.11	2.98	59.33	1.38	35.60	3.58	89.00	0.30	0.25	0.4792	0.16
Upper	46.70			3.35										
Lower	27.01	53.38	-4.64	5.25	2.98	59.33	1.38	35.60	3.58	89.00	0.30	0.25	0.4792	0.17
Upper	46.30			3.37										
Lower	26.11	53.38	-4.64	5.39	2.98	59.33	1.38	35.60	3.58	89.00	0.30	0.25	0.4792	0.18
Upper	45.90			3.40										
Lower	25.25	53.38	-4.64	5.53	2.98	59.33	1.38	35.60	3.58	89.00	0.30	0.25	0.4792	0.19
Upper	45.51			3.42										
Lower	24.43	53.38	-4.64	5.67	2.98	59.33	1.38	35.60	3.58	89.00	0.30	0.25	0.4792	0.20
Upper	45.12			3.45										

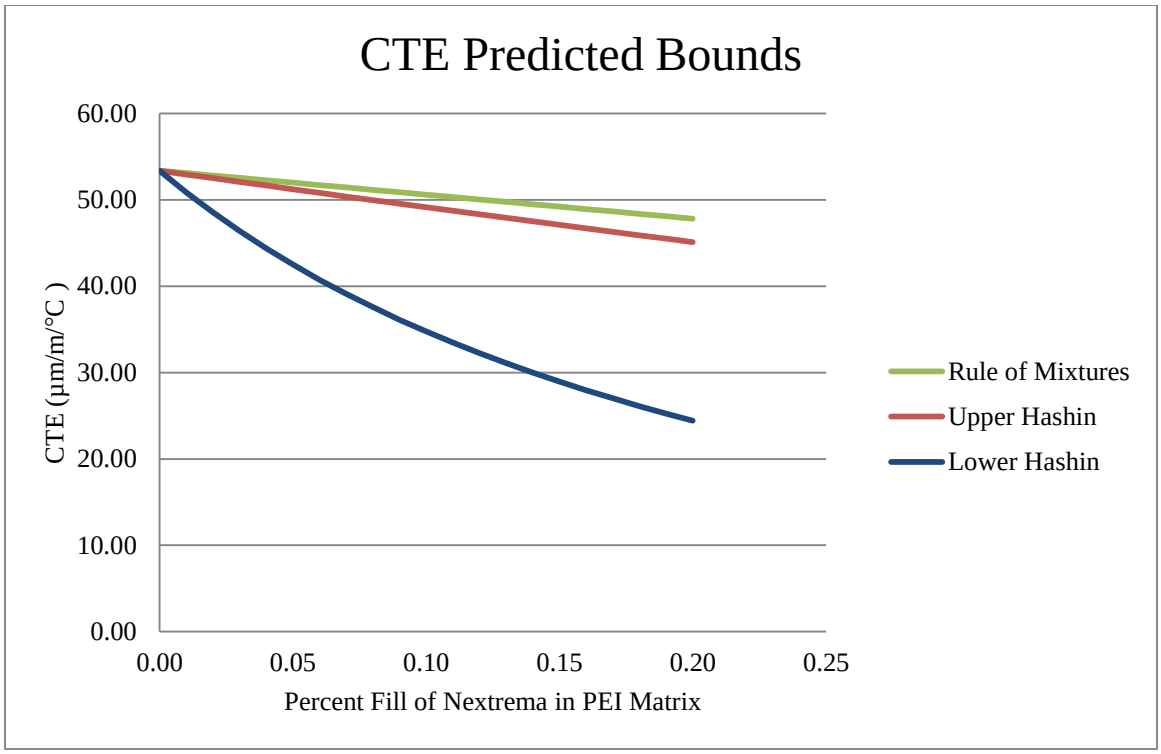

Figure 6. PEI Hashin and Rule of Mixtures Bounds.

Table 2

Calculations Epoxy

	CTE (µm/m/°C)	CTEM (µm/m/°C)	CTEF (µm/m/°C)	KC (GPa)	KM (GPa)	KF (GPa)	GM (GPa)	GF (GPa)	EM (GPa)	EF (GPa)	vM	vF	p Fraction	Weight %
Lower	74.00	74.00	-4.64	2.98	2.98	59.33	1.38	35.60	3.58	89.00	0.30	0.25	0.5208	0.00
Upper	74.00			2.98									0.5208	
Lower	70.31	74.00	-4.64	3.12	2.98	59.33	1.38	35.60	3.58	89.00	0.30	0.25	0.5208	0.01
Upper	73.36			3.01									0.5208	
Lower	66.92	74.00	-4.64	3.26	2.98	59.33	1.38	35.60	3.58	89.00	0.30	0.25	0.5208	0.02
Upper	72.72			3.03									0.5208	
Lower	63.80	74.00	-4.64	3.40	2.98	59.33	1.38	35.60	3.58	89.00	0.30	0.25	0.5208	0.03
Upper	72.09			3.05									0.5208	
Lower	60.90	74.00	-4.64	3.54	2.98	59.33	1.38	35.60	3.58	89.00	0.30	0.25	0.5208	0.04
Upper	71.46			3.08									0.5208	
Lower	58.21	74.00	-4.64	3.69	2.98	59.33	1.38	35.60	3.58	89.00	0.30	0.25	0.5208	0.05
Upper	70.84			3.10									0.5208	
Lower	55.71	74.00	-4.64	3.83	2.98	59.33	1.38	35.60	3.58	89.00	0.30	0.25	0.5208	0.06
Upper	70.22			3.13									0.5208	
Lower	53.38	74.00	-4.64	3.97	2.98	59.33	1.38	35.60	3.58	89.00	0.30	0.25	0.5208	0.07
Upper	69.60			3.15									0.5208	
Lower	51.20	74.00	-4.64	4.12	2.98	59.33	1.38	35.60	3.58	89.00	0.30	0.25	0.5208	0.08
Upper	68.99			3.18									0.5208	
Lower	49.15	74.00	-4.64	4.26	2.98	59.33	1.38	35.60	3.58	89.00	0.30	0.25	0.5208	0.09
Upper	68.37			3.20									0.5208	
Lower	47.23	74.00	-4.64	4.41	2.98	59.33	1.38	35.60	3.58	89.00	0.30	0.25	0.5208	0.10
Upper	67.77			3.23									0.5208	
Lower	45.42	74.00	-4.64	4.56	2.98	59.33	1.38	35.60	3.58	89.00	0.30	0.25	0.5208	0.11
Upper	67.16			3.25									0.5208	
Lower	43.72	74.00	-4.64	4.70	2.98	59.33	1.38	35.60	3.58	89.00	0.30	0.25	0.5208	0.12
Upper	66.56			3.28									0.5208	
Lower	42.11	74.00	-4.64	4.85	2.98	59.33	1.38	35.60	3.58	89.00	0.30	0.25	0.5208	0.13
Upper	65.97			3.30									0.5208	
Lower	40.59	74.00	-4.64	5.00	2.98	59.33	1.38	35.60	3.58	89.00	0.30	0.25	0.5208	0.14
Upper	65.37			3.33									0.5208	
Lower	39.15	74.00	-4.64	5.15	2.98	59.33	1.38	35.60	3.58	89.00	0.30	0.25	0.5208	0.15
Upper	64.78			3.36									0.5208	
Lower	37.78	74.00	-4.64	5.30	2.98	59.33	1.38	35.60	3.58	89.00	0.30	0.25	0.5208	0.16
Upper	64.20			3.38									0.5208	
Lower	36.48	74.00	-4.64	5.46	2.98	59.33	1.38	35.60	3.58	89.00	0.30	0.25	0.5208	0.17
Upper	63.61			3.41									0.5208	
Lower	35.24	74.00	-4.64	5.61	2.98	59.33	1.38	35.60	3.58	89.00	0.30	0.25	0.5208	0.18
Upper	63.03			3.44									0.5208	
Lower	34.07	74.00	-4.64	5.76	2.98	59.33	1.38	35.60	3.58	89.00	0.30	0.25	0.5208	0.19
Upper	62.46			3.47									0.5208	
Lower	32.95	74.00	-4.64	5.92	2.98	59.33	1.38	35.60	3.58	89.00	0.30	0.25	0.5208	0.20
Upper	61.88			3.49										

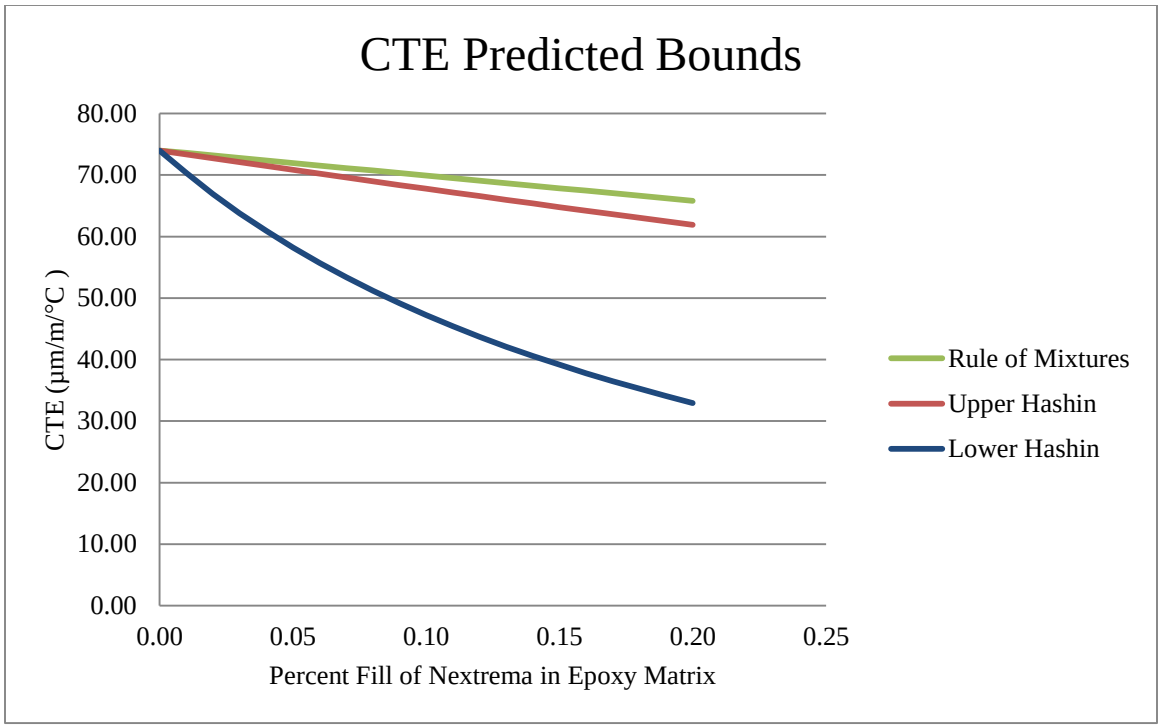

Figure 7. Epoxy Hashin and Rule of Mixtures Bounds.

CHAPTER III

EXPERIMENTATION

Specimen Manufacturing

Samples were made from a mixture of polymer matrix material and a filler material that was selected based on its negative CTE properties. Polyetherimide (PEI), trade name Ultem manufactured by SABIC, grade 1000, was selected as the polymer matrix material due to its thermal properties as described previously. The high melt temperature approximately 400°C, and glass transition temperature, 216°C make it useful for tooling with a desired use temperature of 177°C. Nextrema, a silicate particulate was selected from supplier SCHOTT, due to its relatively low cost and negative CTE to be used as the filler. Figure 8 is an image of the bulk Nextrema before the glass is crushed to create small particles.

Figure 8. Bulk Nextrema 2.63 cm in the longest direction.

Nextrema was pulverized using a hydraulic press to crush it between two parallel plates at a pressure of 25,000 psi. The filler particles were then run through a series of sieves to create a particle size distribution. Two different sieves were used, 40 mesh and 80 mesh. Three different particle distributions were created. Particles were collected after passing through the 40 mesh sized sieve to create the first distribution. The second two distributions were made of particles that could pass through the 40 but not the 80 mesh, then the particles that could pass through the 80 mesh, respectively. The openings in the 40 mesh and 80 mesh are 0.0145 inches and 0.0071 inches respectively. This means that the particles for the 3 different distributions would be 0.00 inches to 0.0145 inches now on referred to as 40 mesh, 0.00 inches to 0.007 inches now on referred to as 80 mesh, and finally 0.007 inches to 0.0145 inches, from now on referred to as 40-80 mesh.

Extrusion

Samples were created by extruding the two materials using a double screw extruder to mix together the Polyetherimide matrix and the Nextrema filler. The laboratory in the Wiggins Research group uses a Prism co rotating twin screw extruder. The machine has an upper temperature limit of 300 °C, and a torque limit of aproximately 25 N*m. Table 3 shows the processing conditions for neat Ultem 1000, as well as with Nextrama particles at 1 and 5 percent by weight (i.e. for 300g PEI, 3g Nextrama was added). Both PEI pellets and Nextrema particles were weighed on an analytical balance, then combined in a polypropylene mixing container and thoroughly mixed manually. The material was then placed on a vibrating feeder trough as seen in Figure 9, whose vibrational speed was chosen such that the material was “starve fed” into the extruder feed zone (temperature zone 1). Upon exiting the extruder, the solid string of material was then pelletized for reprocessing.

Figure 9. PEI/Nextrema particles fed into the extruder by the vibrating feeder trough.

Table 3

Prism Extruder settings for PEI with 0,1,and 5 phr Nextrema particle additives

Nextrema Content	**Temperature (°C)**					**Screw Speed**	**Machine Torque**	**Torque Capacity**
(phr)	**Zone 1**	**Zone 2**	**Zone 3**	**Zone 4**	**Zone 5**	**(RPM)**	**(N*m)**	**% (approx)**
0	200	280	300	300	300	60	14.1	50
1	200	290	300	300	300	49	18.3	70
5	200	290	300	300	300	40	18.8	80

The screws for the twin screw extruder that was used to compound the Polyetherimide and the Nextrema together are seen in Figure 10 and Figure 11. The two screws used simotaniosly are a compounding screw and a reaction extrusion screw. The first sample set of specimen were manufactured in one pass through the extruder. This sample set were the specimens that had no filler in them and the 40 mesh specimen that contained the larger dispersion of filler particle sizes. During the second sampling of specimen that were manufactured, incolving the 80 mesh and 40-80 mesh specimen, it was visually observed that upon pelletization after extrusion that the Nextrema filler was

not uniformly dispersed, so the blended pellets were run through the extruder two more times, for a total of 3 passes through the extruder to fully mix and blend the Nextrema filler into the Polyetherimide.

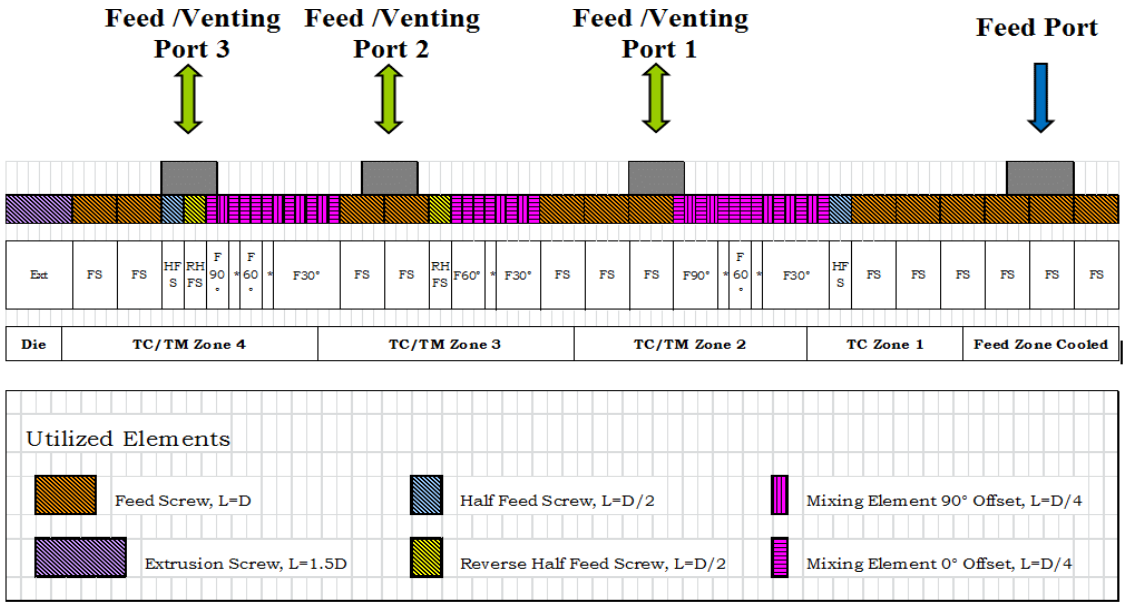

Figure 10. Reaction Extrusion Screw.

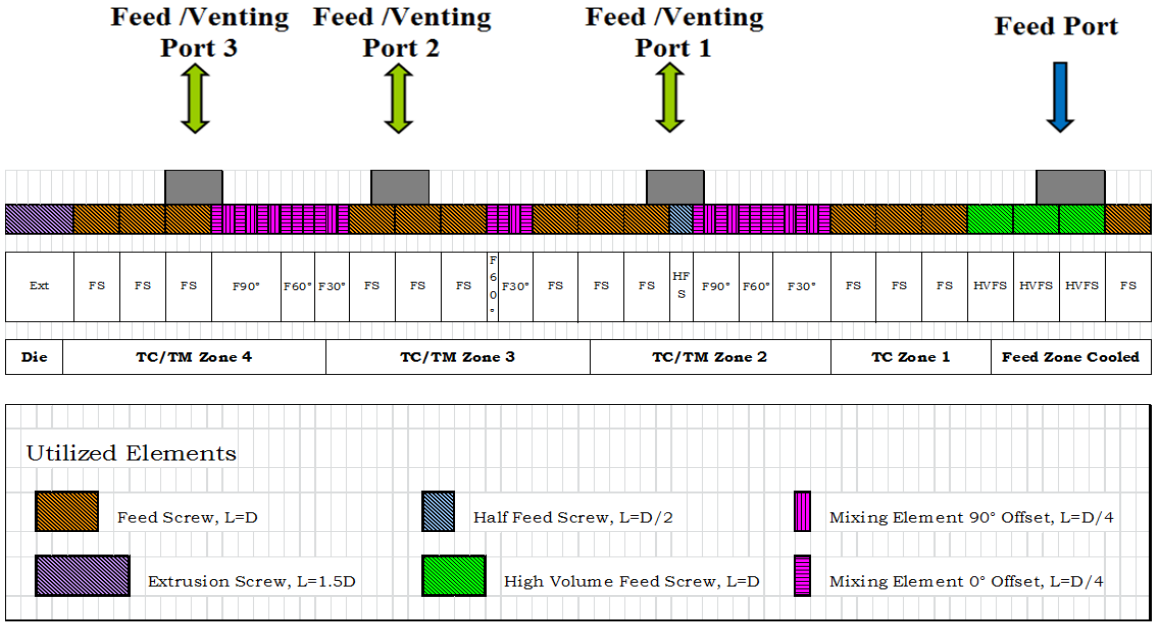

Figure 11. Compounding Screw.

Melt-Pressing

Both the neat Polyetherimide and the compounded pellets made of the Polyetherimide and Nextrema were melt-pressed at 300 °C (572 °F) with 27.6 MPa (4000 psi). Teflon coated release paper was used to keep the specimen from sticking to the mold. The size of the specimens was 26.0mm in diameter and 1.6mm thick. The 40 mesh discs showed homogenous surface texture and appeared void free. This size of specimen was ideal for use as rheological specimen for the parallel plate rheology measured in the RDA. The 80 mesh and the 40-80 mesh disks had intermittent voids as well as surface pitting and appeared blotchy. An example photograph is seen in Figure 12, the remainder of the specimen photographs are contained in the results section. Specimens were trimmed down to be able to fit into the TMA for CTE measurements.

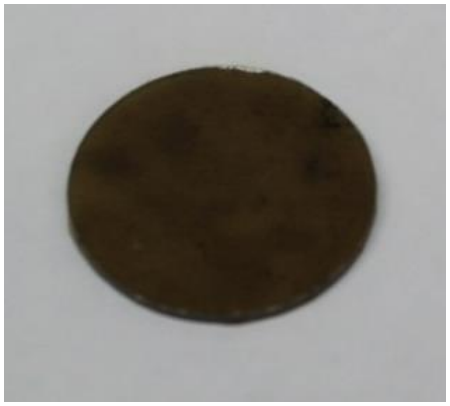

Figure 12. Photograph of press melted PEI Specimen.

Making Epoxy Specimens

Due to suspicion of thermal degradation of the polyetherimide resulting from multiple passes through the extruder, it was decided to also create epoxy specimens for the purpose of collecting TMA data and correlate that back to the theoretical model.

The epoxy specimens were manufactured by first selecting an epoxy that did not have any other thickening agent or fillers in it. Magnolia Plastics engineered and

manufactured Magnolia 136-553 as an epoxy system that does not contain any fumed silica filler for thickening. Figure 13 is a photograph of a package of Magnolia 136-553 after it was thawed for used.

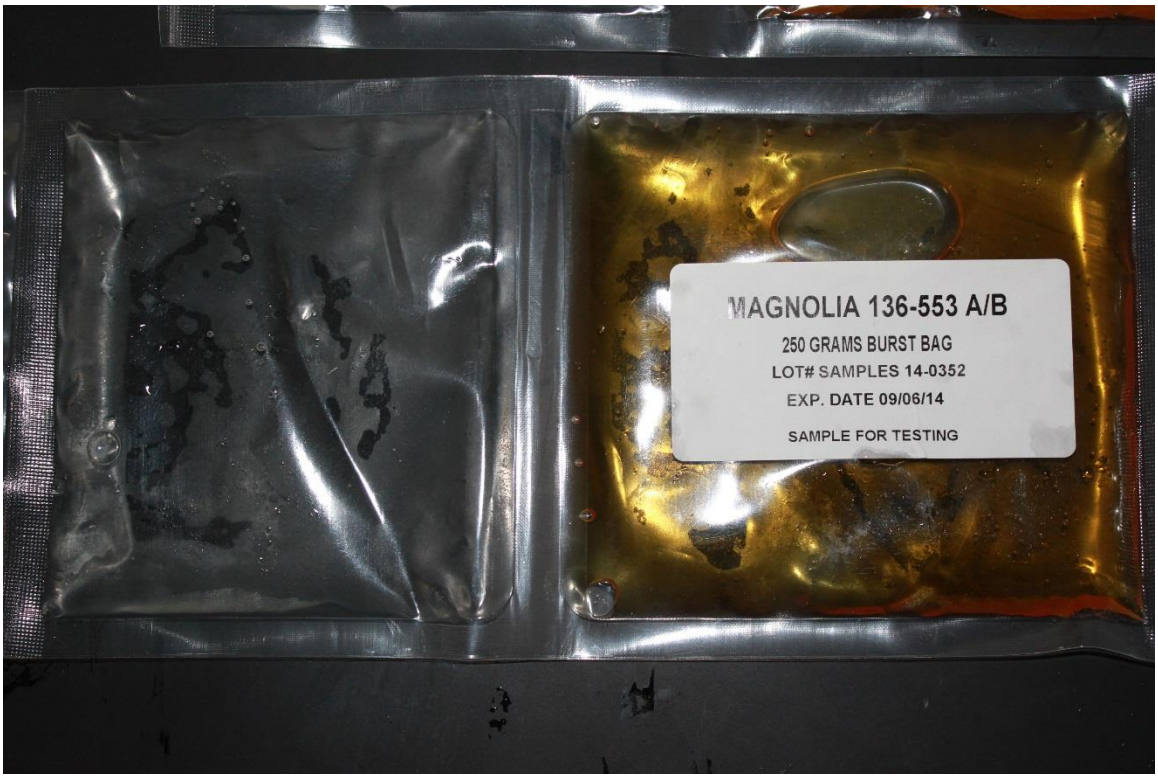

Figure 13. Thawed Magnolia 136-553 bi-pack.

After the epoxy was thawed, the packaging was cut open with a pair of shears and the contents of the package was emptied into a nylon graduated beaker, seen in Figure 14. The beaker was placed on a scale accurate to 0.01grams to measure out the correct mixture ratio of the epoxy and amine components by weight.

Figure 14. Filling Graduated Beaker with Epoxy.

Figure 15. Weighing Magnolia 136-553 Epoxy.

After the Magnolia 136-553 epoxy was weighed, it was thoroughly mixed with a stir rod. It was then placed in a water bath, mixed mechanically at 190 of RPMs while the water bath was within an ultrasonic mixer, agitating the water at 60 MHz frequency using a Branson B-220H Ultrasonic Cleaner. This mixing was performed for 10 minutes. The overhead stirrer was cleaned thoroughly with 100 percent acetone and a small cleaning brush between samples to avoid cross contaminating samples. This mixing method was used to increase dispersion of the micro particles, and reduce clumping. The mixing apparatus set up is seen in Figure 16.

Figure 16. Mixing Apparatus.

After the samples of epoxy with Nextrema were mixed, they were degassed in a vacuum chamber for one hour at around -30inches of mercury. Then the epoxy specimen were moved to a silicone mold with a disposable pipette. The mold can be seen in Figure 17. Specimen were cured at room temperature for 48 hours, then post cured for 2 hours at 177˚C. Specimen were cut and polished to fit into the Thermo Mechanical Analysis (TMA) for CTE measurements.

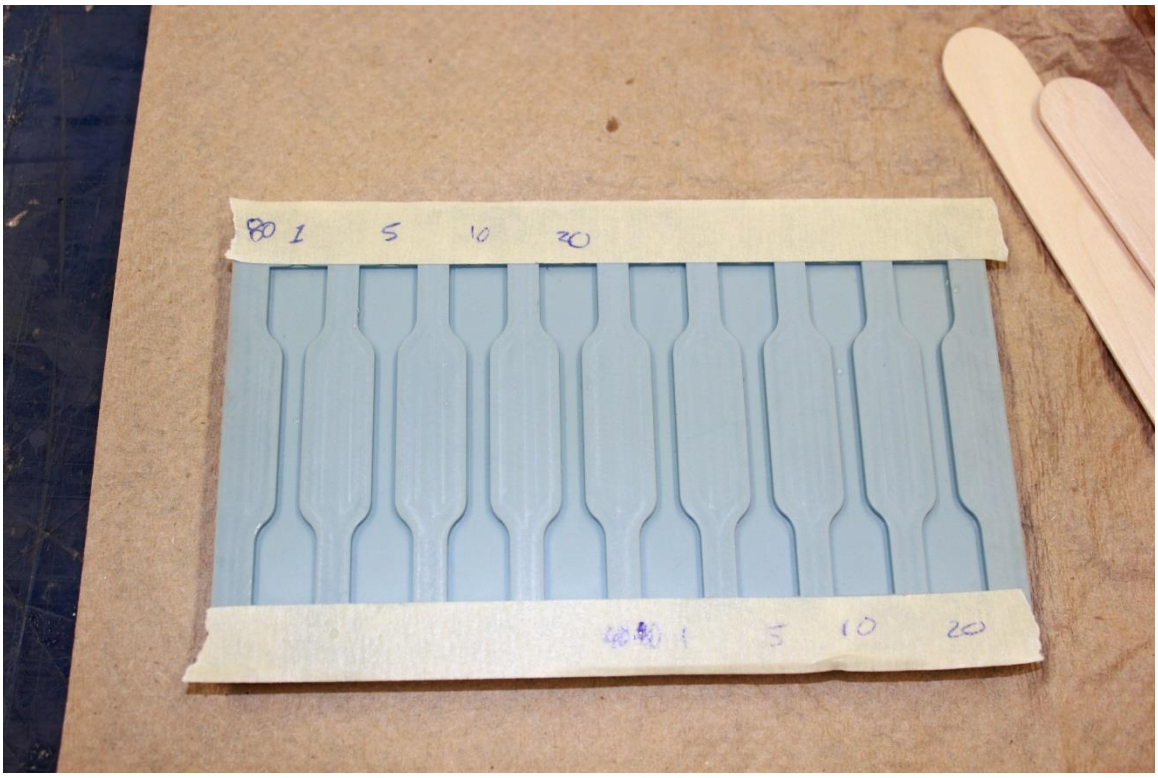

Figure 17. Epoxy Specimen Silicone Mold.

Testing

The overall intent of the testing performed was to evaluate the calculations from Hashin on the CTE of heterogeneous polymer mixtures, as well as to understand how the processing of the Ultem would change with the different percentages of Nextrema filler in the specimen.

Thermo Mechanical Analysis (TMA) was used to measure the changes in the coefficient of thermal expansion (CTE) in the polyetherimide based on the percentage of Nextrema filler. The CTE of the neat polymer and the filler were measured for performing the modeling calculations, then the polymer was measured with the different percent fills of the Nextrema.

A TA instruments ARES-RDA was used to characterize the rheology of the specimen. The intent was to identify the temperature increase needed at the head of the

fused deposition modeling (FDM) machine, when processing a filled PEI to match the viscosity of the unfilled PEI.

Cross-sectional micrographs were used to observe the dispersion and confirm the percent fill of the Polyetherimide specimen. Optical microscopy was used to visually confirm the fill percentage on selected specimens.

TMA

TMA is a polymer characterization technique that is used to measure thermal expansion of a sample. A polymer specimen is placed on a stage inside the TMA and a probe is used to measure the expansion of the specimen during a temperature sweep. TMA is often used to understand the glass transition but for this research it was used to characterize the coefficient of thermal expansion of the specimen over the temperature range of interest. The probe is made from quartz due to its low thermal expansion coefficient when compared to most polymers in the usage temperature range of most polymers. (Campbell, Pethrick, and White 2000). Diagrams of the TMA can be seen in Figure 18 and Figure 19.

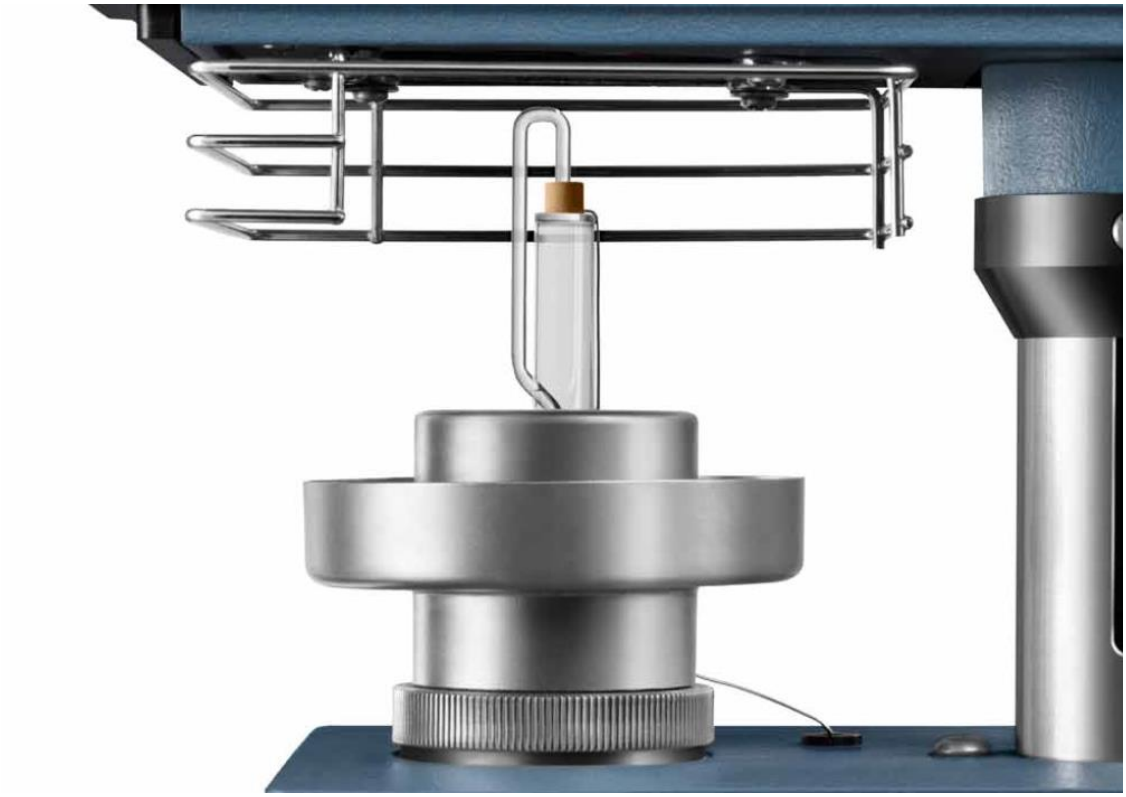

Figure 18. Sample stage (TMA 2014).

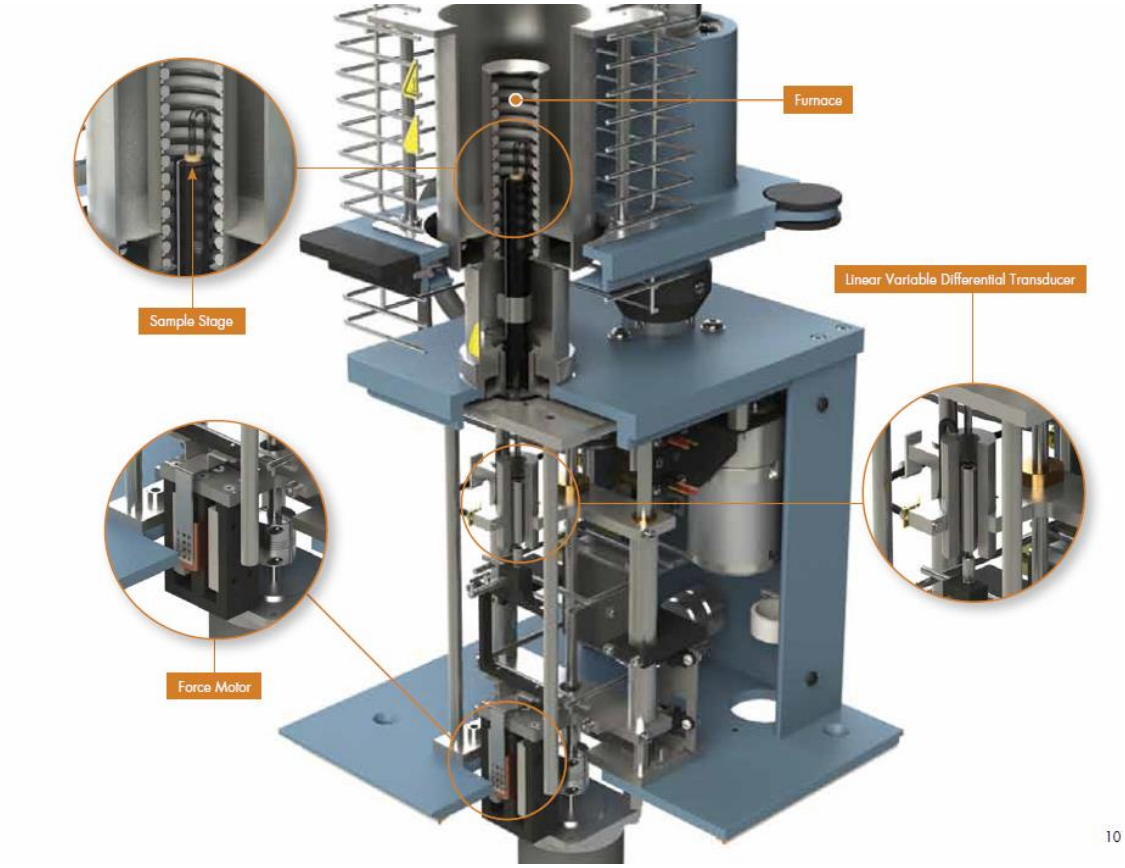

Figure 19. TMA cross section (TMA 2014).

TA Instruments TMA Q400 was used to make thickness measurements during a temperature sweep to calculate the coefficient of thermal expansion. The TA Instruments TMA Q400 measured the thickness of the specimen with a quartz probe. The force applied to the specimen during the experiment was 0.25 Newtons. This force was chosen because during preliminary runs it was found that a lower force created a noisy measurement of the thickness dimensional change, while a higher force started to press into the softening polymer and gave false results at higher temperatures. The specimen was brought to thermal equilibrium at 30°C and ramped to 225°C at 5°C per min. CTE was calculated from 35°C to 150°C and from 35°C to 177°C. These temperatures were

chosen to simulate the ramp up of a piece of tooling from room temperature to typical composite cure temperatures of 300°F and 350°F.

RDA

Rheology of the different fill percentages and particle sizes of the Nextrema in Polyetherimide was investigated with TA Instruments ARES-RDA. The general idea what temperature increase is needed to achieve the same viscosity in polymer samples with filler in them versus neat resin samples based on a particular shear rate. If this can be understood, then the nozzle temperature can be increased to run the lower CTE filled polymer through the FDM nozzle.

Approximately eight specimens of neat resin samples, and filled samples with 1% by weight and 5% by weight, with three different particle sizes of each were investigated. There were six different filled configurations with 8 specimen each, and 1 configuration of neat, eight specimen each.

The parameters of the RDA were a shear rate of 1Htz, a ramp rate of 5˚C/min, 2% strain, and a 1.4mm Gap between the plates with a 25 gram sensitivity. Measurements were taken every 10 seconds over the temperature range of 325-425˚C. These settings were selected to create a squeeze out when the 1.6mm specimen were place in between the parallel plates. The excess was removed so as not to impact the test results from the edge resistant of the plates. The shear and strain rates were selected to represent a large enough strain rate that good data could be collected from the runs.

Cross-sectional Micrographs

Due to the varying results that were seen in the RDA and TMA measurements, Cross sectional micrographs were taken of the various samples to look for void content or other anomalies in the specimen. Samples were mounted in a room temperature polymer

cure matrix as to not introduce thermal damage to the polyetherimide samples. Once mounted the samples were then polished on a series of polishing wheels down to a 1000 grit and photographs were captured using a microscope.

Particle Size Distribution

The size of the Nextrema particles was attempted to be investigated at PAX River as a part of the effort of understanding the distribution of particle sizes within the ranges that were made with the sieves. The investigation was going to be done with an oil suspension particle size counter. The issue was that the Nextrema particles were so large and dense that they did not stay suspended in the standard oil that is used to count particles and measure their sizes.

As a result, the polymer institute was able to use optical microscopy function to measure and characterize the particle size distribution. The particle size distributions were investigated using an Olympus GX51 Optical Microscope then using the particle size function included with the Olympus software, Olympus Stream Essentials. Due to the different size particle ranges, different settings were used on the Olympus to get data on the distribution of the particle sizes that were included in the PEI and Epoxy matrices. For the 40-80 mesh, as well as 80 mesh images, 10 times magnification was used on the optical microscope, while for the 40 mesh images, 20 times magnification was used. Samples were spooned onto a glass slide which was then physically tapped against the glass particle containers to remove most of the particles, allowing for a transparent glass slide with residual glass particles stuck to the surface.

For each mesh size, three images were taken in separate areas of the slide. These images were separated into "Particle" and "Background" through Red/Green/Blue

intensities which was determined by the Olympus software. The user manually selects points determined to be the particle, and all pixels sharing that RGB intensity are also selected. The user can then define maximum and minimum limits for particle diameters to remove any errors such as dust spots, shadows, or blemishes on the lenses. A minimum of 1 micrometer (0.00003937 inches) was used for each image. For 40 mesh, a maximum of 20 micrometers (0.0007878 inches) was used. For 40-80 as well as 80 mesh, a maximum of 100 micrometers (0.00397 inches) was used. The particles for the three different distributions based on the sieves used should be 0.00 inches to 0.0145 inches for 40 mesh, 0.00 inches to 0.007 inches for 80 mesh, and finally 0.007 inches to 0.0145 inches for 40-80 mesh.

The particle diameters were then exported to Excel, sorted smallest to largest, and rounded to either the nearest tenth or whole micrometer. The diameters were sorted into bins for the creation of a particle count versus frequency histogram.

Results

TMA

Table **4** records the CTE measurements that were recorded by the TMA TMA Q400 V7.3 Build 91 that was used at PAX River Maryland in the Robert Becker thermal laboratory for PEI specimen. The weight percent fill and particle sizes are recorded as well as the average CTE across multiple specimen.

Table 4

PEI TMA Data

Percent Fill by Weight	Particle Size	CTE (µm/m/°C)	Average CTE (µm/m/°C)
0	0	53.28	58.19
0	0	57.35	
0	0	60.70	
0	0	61.16	
0	0	62.31	
0	0	54.34	
1	40	58.11	45.90
1	40	37.54	
1	40	42.04	
1	40-80	56.31	47.55
1	40-80	38.78	
1	80	44.17	37.62
1	80	31.06	
5	40	44.65	44.87
5	40	45.31	
5	40	44.65	
5	40-80	60.03	56.08
5	40-80	52.13	
5	80	19.15	29.92
5	80	40.68	

Figure 20 shows a graph of the CTE average measurements for the larger particle distribution, 40 mesh, that were recorded overlaid on the CTE predicted bounds from Hashin's equations.

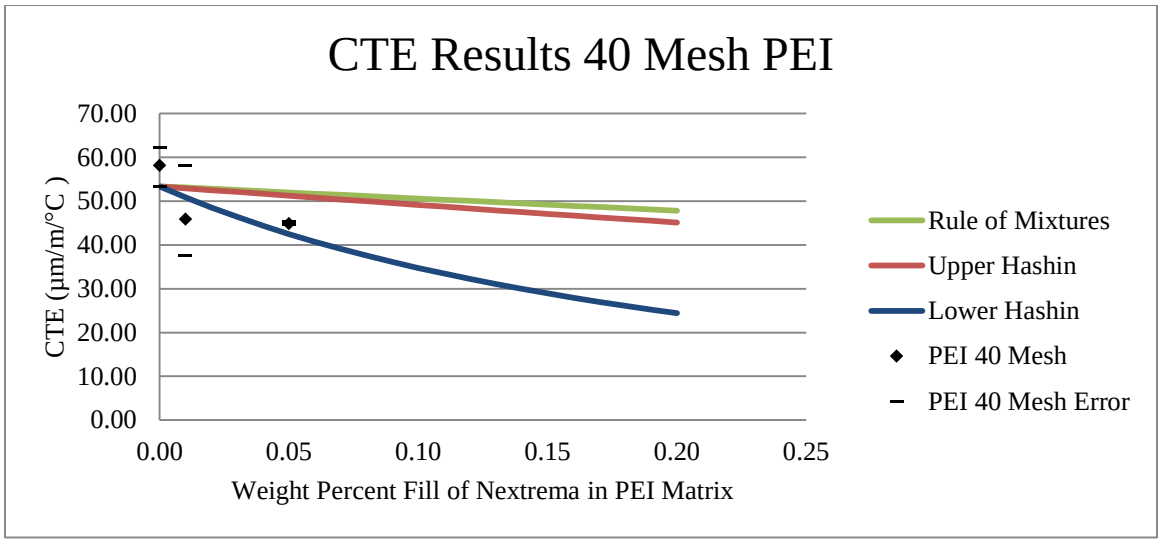

Figure 20. CTE Measurements PEI 40 Mesh.

Figure 21 shows a graph of the CTE average measurements for the smaller particle distribution with larger particles, 40-80 mesh, that were recorded, overlaid on the CTE predicted bounds from Hashin's equations.

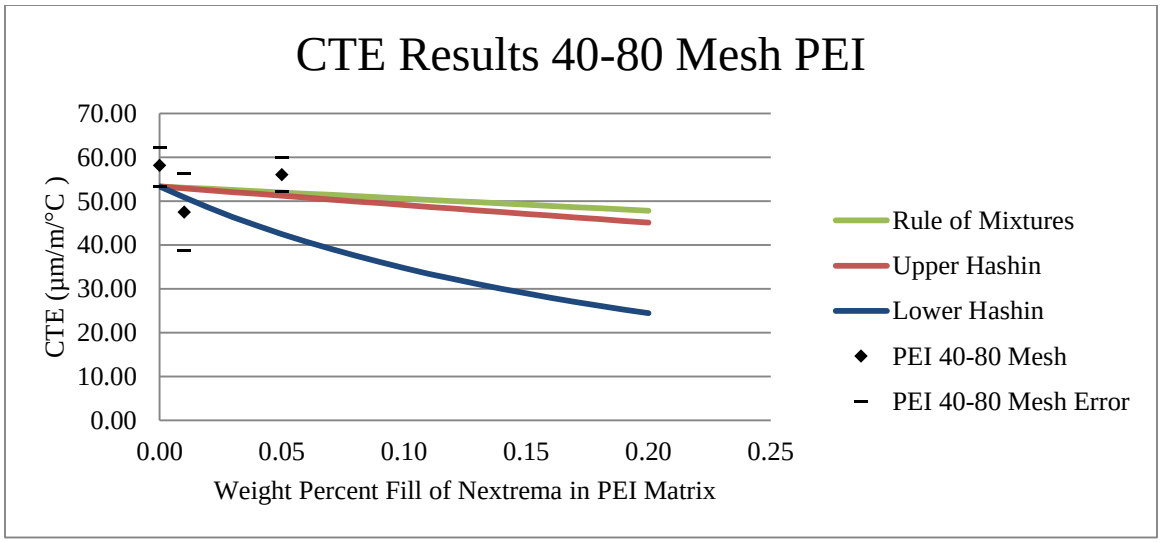

Figure 21. CTE Measurements PEI 40-80 Mesh.

Figure 22 shows a graph of the CTE average measurements for the smaller particle distribution with smaller particles, 80 mesh, that were recorded, overlaid on the CTE predicted bounds from Hashin's equations.

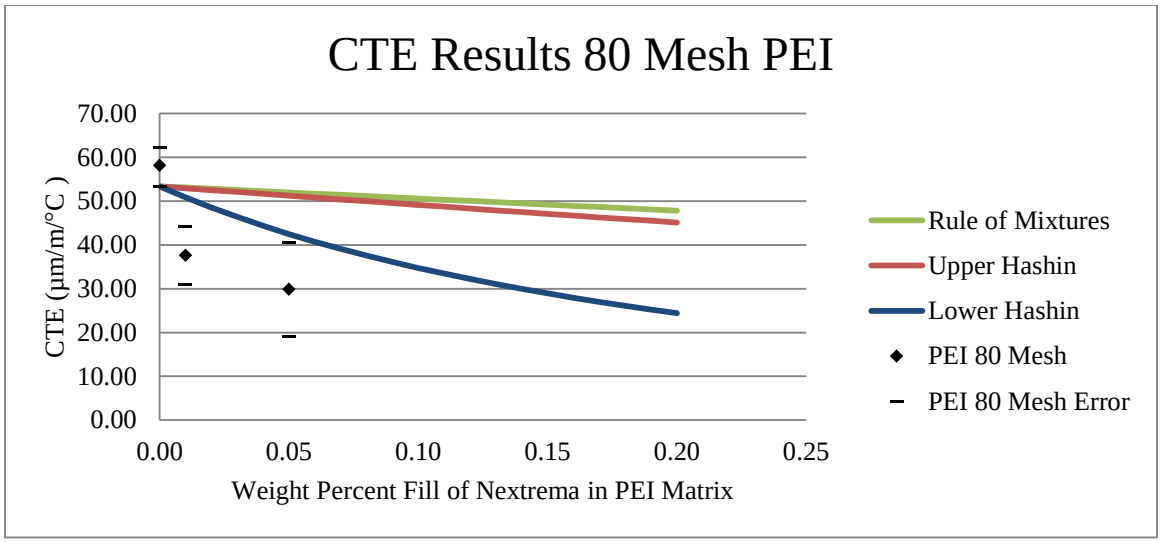

Figure 22. CTE Measurements PEI 80 Mesh.

Table 5 records the CTE measurements that were recorded by the TMA Q400 V7.3 Build 91 that was used at PAX River Maryland in the Robert Becker thermal laboratory for epoxy specimen. The weight percent fill and particle sizes are recorded as well as the average CTE across multiple specimen.

Table 5

Epoxy TMA Data

Percent Fill by Weight	Particle Size	CTE (µm/m/°C)	Average CTE (µm/m/°C)
0	0	72.06	72.06
1	40-80	75.56	74.86
1	40-80	74.15	
1	80	72.81	72.78
1	80	72.75	
5	40-80	76.81	75.25
5	40-80	73.68	
5	80	69.21	69.13
5	80	69.04	
10	40-80	81.93	72.47
10	40-80	63.01	
10	80	41.85	56.30
10	80	70.75	
20	40-80	75.65	75.38
20	40-80	75.10	
20	80	79.04	71.50
20	80	63.95	

Figure 23 shows a graph of the epoxy CTE average measurements for the smaller particle distribution with larger particles, 40-80 mesh, that were recorded, overlaid on the CTE predicted bounds from Hashin's equations.

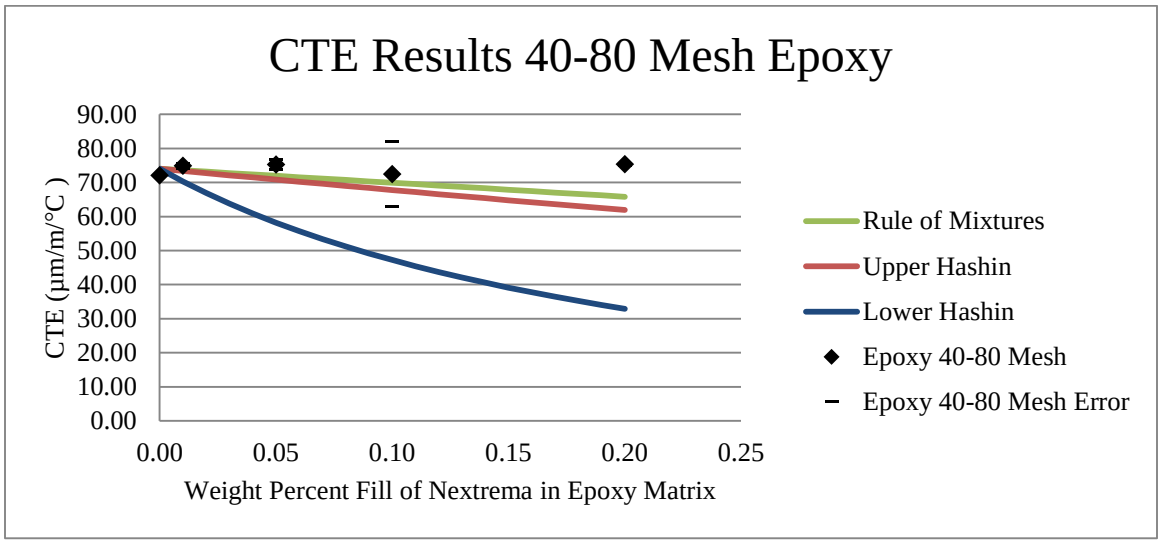

Figure 23. CTE Measurements Epoxy 40-80 Mesh.

Figure 24 shows a graph of the epoxy CTE average measurements for the smaller particle distribution with larger particles, 80 mesh, that were recorded, overlaid on the CTE predicted bounds from Hashin's equations.

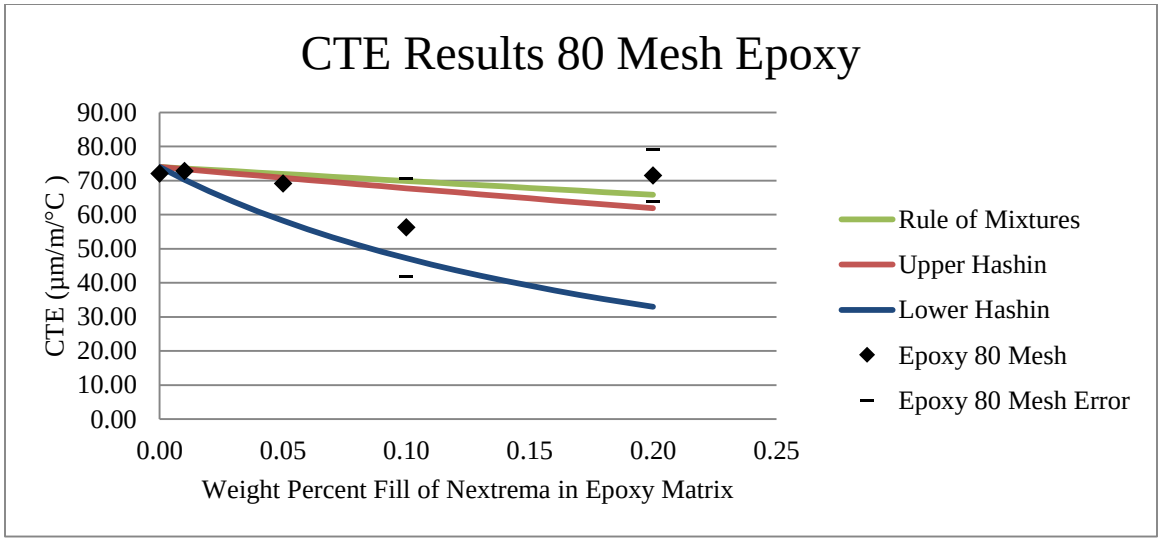

Figure 24. CTE Measurements Epoxy 80 Mesh.

RDA

Table 6 records temperature points and average viscosity that was captured and recorded by the ARES TA Instruments RDA.

Table 6

Pascale measurements of samples as temperature ramps up.

Temperature Degrees C, Poise											
		330	340	350	360	370	380	390	400	410	420
5% 80 Mesh	Run 1	39571	31499	23132	17026	12940	10280	8898	8699	9133	11187
	Run 2	32138	22441	16507	12421	9239	6890	5138	4039	3076	2936
	AVG	35855	26970	19820	14724	11090	8585	7018	6369	6105	7062
1% 80 Mesh	Run 1	70819	32456	16956	9928	6167	4179	3080	2427	2587	4515
	Run 2	31060	22441	16738	12421	9024	6890	5074	3933	3076	2936
	AVG	50940	27449	16847	11175	7596	5535	4077	3180	2832	3726
5% 40-80 Mesh	Run 1	49205	35721	24936	17679	11738	8312	5979	4902	4354	4675
	Run 2	38234	25956	18188	12857	9268	6918	5053	3904	3232	3011
	AVG	43720	30839	21562	15268	10503	7615	5516	4403	3793	3843
1% 40-80 Mesh	Run 1	40656	32283	23742	17481	13204	10350	7943	6637	6091	6126
	Run 2	40538	27584	19387	13420	9315	6367	4340	3052	2468	2675
	AVG	40597	29934	21565	15451	11260	8359	6142	4845	4280	4401
5% 40 Mesh	Run 1	88226	56965	40086	28582	20812	15904	12762	10651	9044	9152
	Run 2	56720	40603	27614	19059	12908	9451	7051	5581	5294	6708
	AVG	72473	48784	33850	23821	16860	12678	9907	8116	7169	7930
1% 40 Mesh	Run 1	72272	50512	34309	24760	16951	12282	9277	7293	6932	7588
	Run 2	72256	45264	29332	19850	13909	10084	7464	5198	4248	6258
	AVG	72264	47888	31821	22305	15430	11183	8371	6246	5590	6923
Neat	Run 1	52137	40452	28763	20383	14762	10611	8148	6953	6280	6035
	Run 2	35126	30142	22522	16866	12596	9844	7920	6815	6699	7664
	AVG	43632	35297	25643	18625	13679	10228	8034	6884	6490	6850

Figure 25 records the viscosity curves of all the different specimen that were run with their average viscosity recorded.

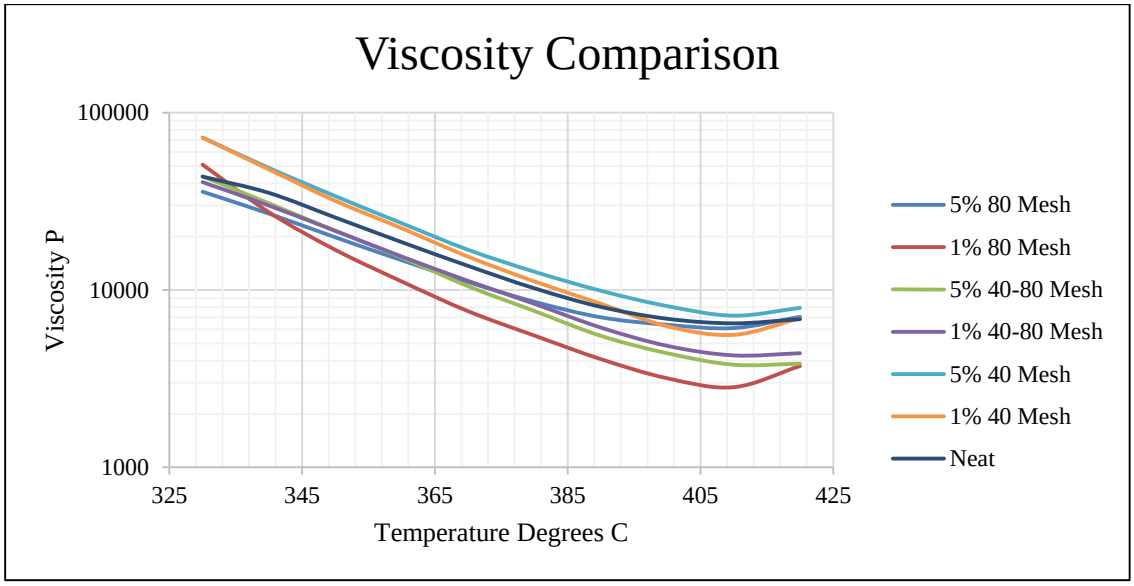

Figure 25. Viscosity Curves of average viscosities across data samples.

Figure 26 shows the comparison of the 5% by weight Nextrema 80 mesh filled PEI versus the neat PEI across the temperature range of 325-425˚C

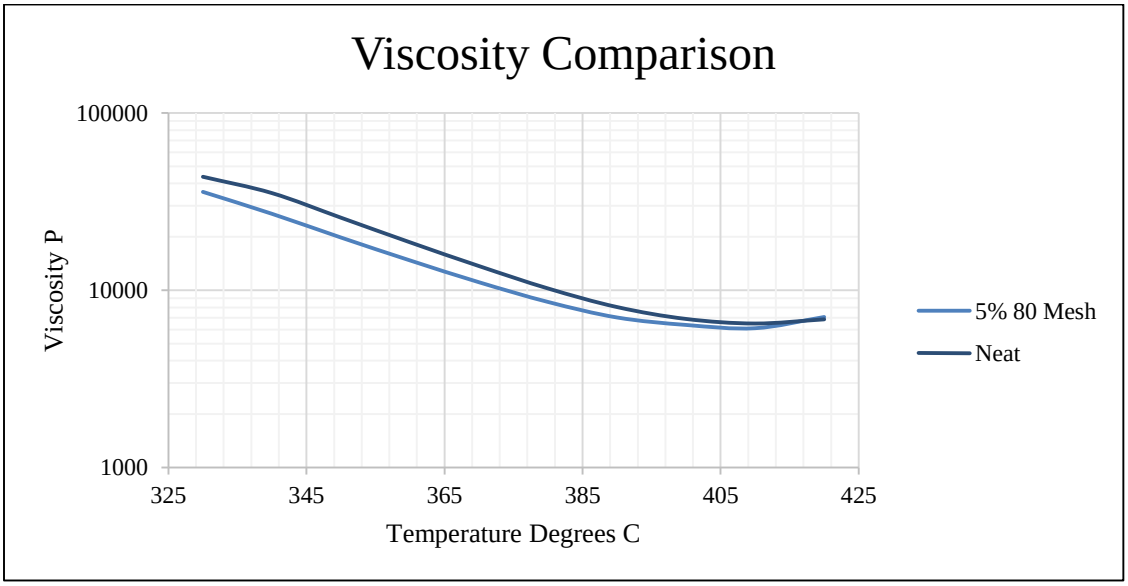

Figure 26. Neat vs 5% 80 Mesh.

Figure 27 Shows the comparison of the 1% by weight Nextrema 80 mesh filled PEI versus the neat PEI across the temperature range of 325-425˚C

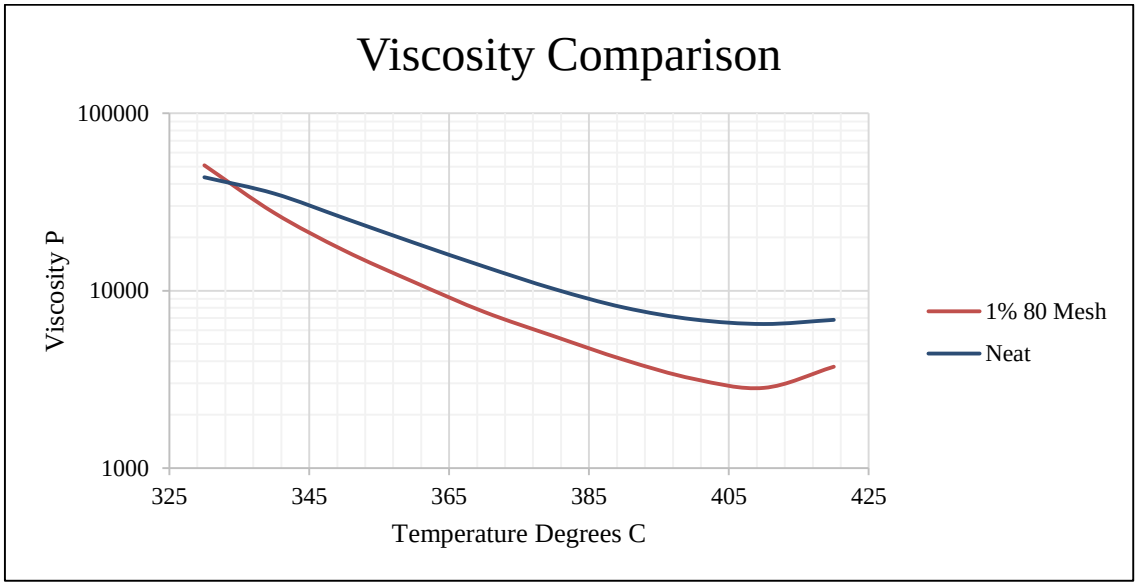

Figure 27. Neat vs 1% 80 Mesh.

Figure 28 shows the comparison of the 5% by weight Nextrema 40-80 mesh filled PEI versus the neat PEI across the temperature range of 325-425˚C

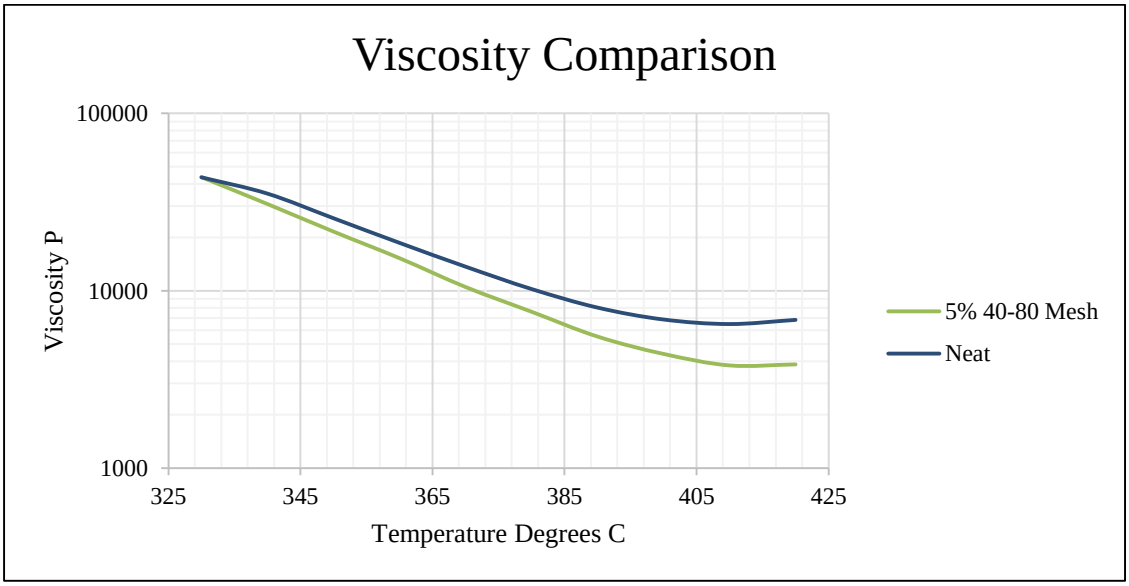

Figure 28. Neat vs 5% 40-80 Mesh.

Figure 29 shows the comparison of the 1% by weight Nextrema 40-80 mesh filled PEI versus the neat PEI across the temperature range of 325-425˚C

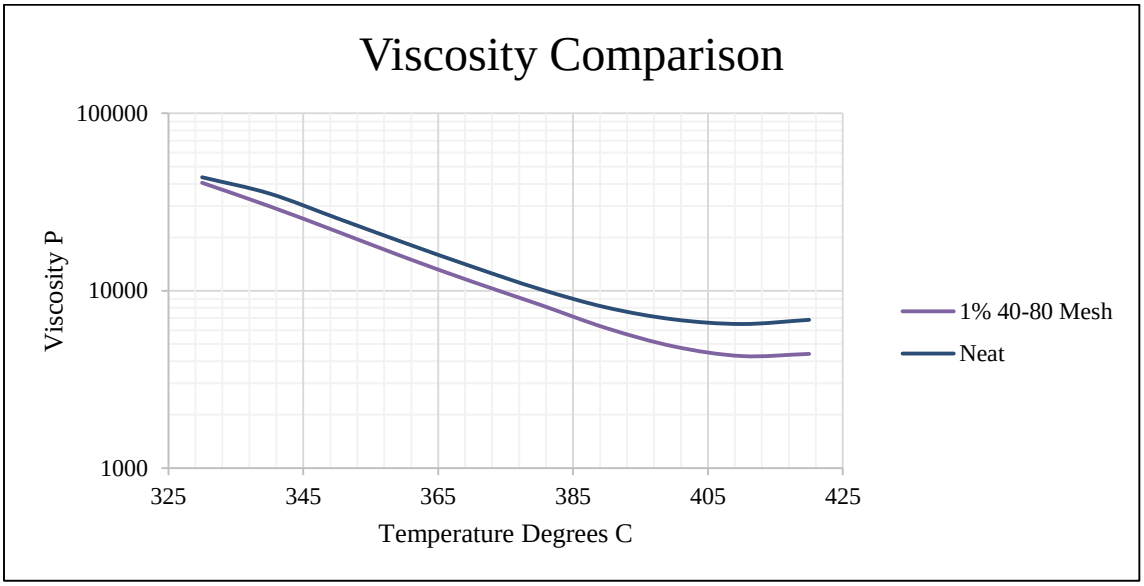

Figure 29. Neat vs 1% 40-80 Mesh.

Figure 30 shows the comparison of the 5% by weight Nextrema 40mesh filled PEI versus the neat PEI across the temperature range of 325-425˚C

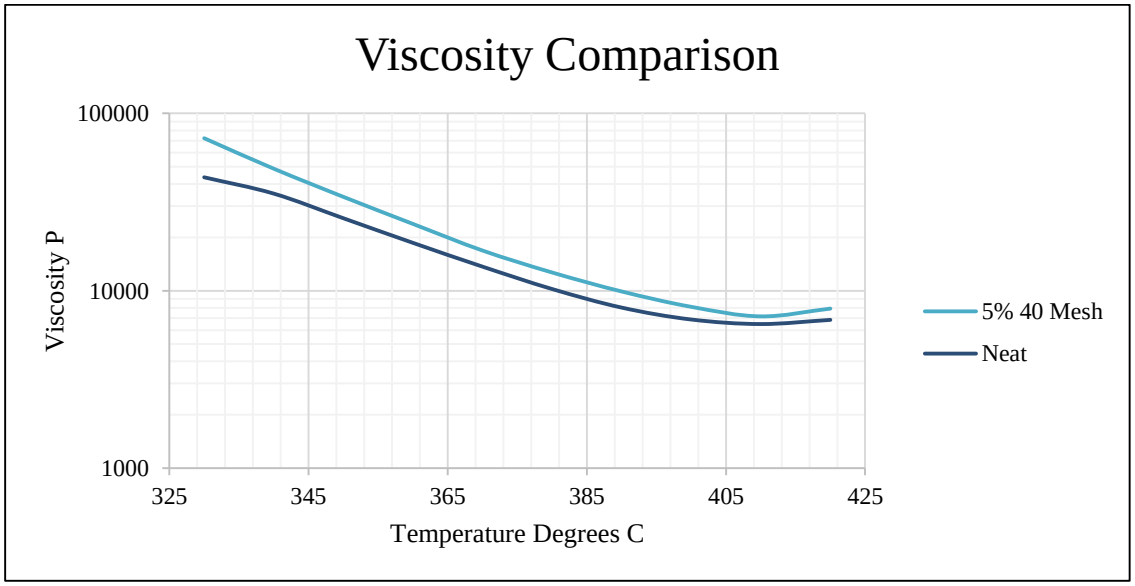

Figure 30. Neat vs 5% 40 Mesh.

Figure 31 Shows the comparison of the 1% by weight Nextrema 40 mesh filled PEI versus the neat PEI across the temperature range of 325-425˚C

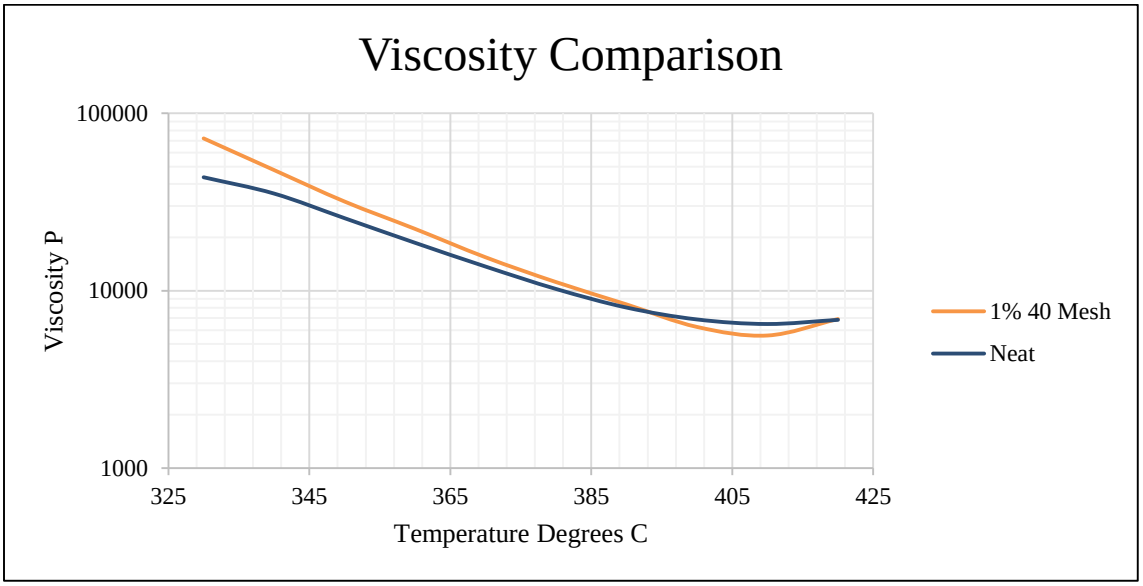

Figure 31. Neat vs 1% 40 Mesh.

Cross-sectional Micrographs

Figure 32 is a photograph of one of the PEI 1% fill by weight with 40 mesh Nextrema disks that were melt-pressed at 300 °C (572 °F) with 27.6 MPa (4000 psi). Teflon coated release paper was used to keep the specimen from sticking to the mold. The size of the specimens was 26.0mm in diameter and 1.6mm thick. Generally uniform color was observed on these specimen and no voids were visually observed to the naked eye.

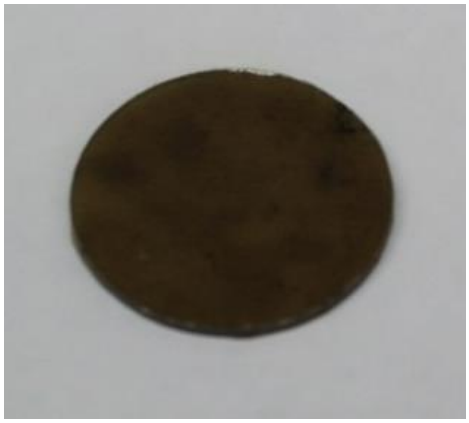

Figure 32. Macroscopic Photo PEI 1% fill by weight 40 mesh.

Figure 33 is a photograph of one of the PEI 5% fill by weight with 40 mesh Nextrema disks that were melt-pressed at 300 °C (572 °F) with 27.6 MPa (4000 psi). Teflon coated release paper was used to keep the specimen from sticking to the mold. The size of the specimens was 26.0mm in diameter and 1.6mm thick. Generally uniform color was observed and no voids were visible to the naked eye. It was observed that the color of these particular set of specimen were darker in color than the other sets of specimen.

Figure 33. Macroscopic Photo PEI 5% fill by weight 40 mesh.

Figure 34 is a photograph of one of the PEI 1% fill by weight with 40-80 mesh Nextrema disks that were melt-pressed at 300 °C (572 °F) with 27.6 MPa (4000 psi). Teflon coated release paper was used to keep the specimen from sticking to the mold. The size of the specimens was 26.0mm in diameter and 1.6mm thick. Non-uniform color

across all the specimen in this class was observed, with patches of lighter and darker material. Voids and short fills were able to be observed with the naked eye.

Figure 34. Macroscopic Photo PEI 1% fill by weight 40-80 mesh.

Figure 35 is a photograph of one of the PEI 5% fill by weight with 40-80 mesh Nextrema disks that were melt-pressed at 300 °C (572 °F) with 27.6 MPa (4000 psi). Teflon coated release paper was used to keep the specimen from sticking to the mold. The size of the specimens was 26.0mm in diameter and 1.6mm thick. Again non-uniform color was observed as well as some voids with the naked eye.

Figure 35. Macroscopic Photo PEI 5% fill by weight 40-80 mesh.

Figure 36 is a photograph of one of the PEI 1% fill by weight with 80 mesh Nextrema disks that were melt-pressed at 300 °C (572 °F) with 27.6 MPa (4000 psi). Teflon coated release paper was used to keep the specimen from sticking to the mold.

The size of the specimens was 26.0mm in diameter and 1.6mm thick. Non-uniform color across the specimen were observed as well as some voids being visible to the naked eye.

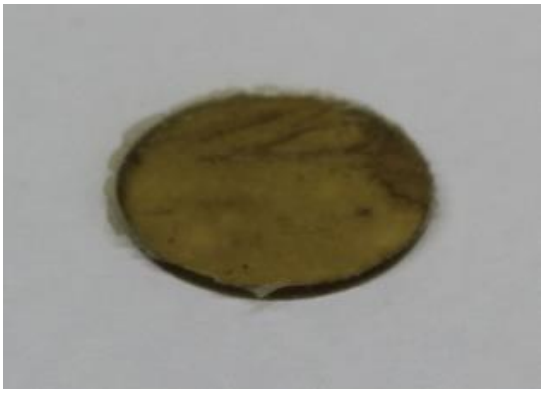

Figure 36. Macroscopic Photo PEI 1% fill by weight 80 mesh.

Figure 37 is a photograph of one of the PEI 5% fill by weight with 80 mesh Nextrema disks that were melt-pressed at 300 °C (572 °F) with 27.6 MPa (4000 psi). Teflon coated release paper was used to keep the specimen from sticking to the mold. The size of the specimens was 26.0mm in diameter and 1.6mm thick. Non-uniform color can be observed as well as voids throughout all the specimen.

Figure 37. Macroscopic Photo PEI 5% fill by weight 80 mesh.

Figure 38 is a cross sectional micrograph of polyetherimide disk that was heat pressed by the University of Southern Mississippi. The scratchers that are observed are remnants of polishing the piece. A limited number of voids and imperfects can be seen in this sample.

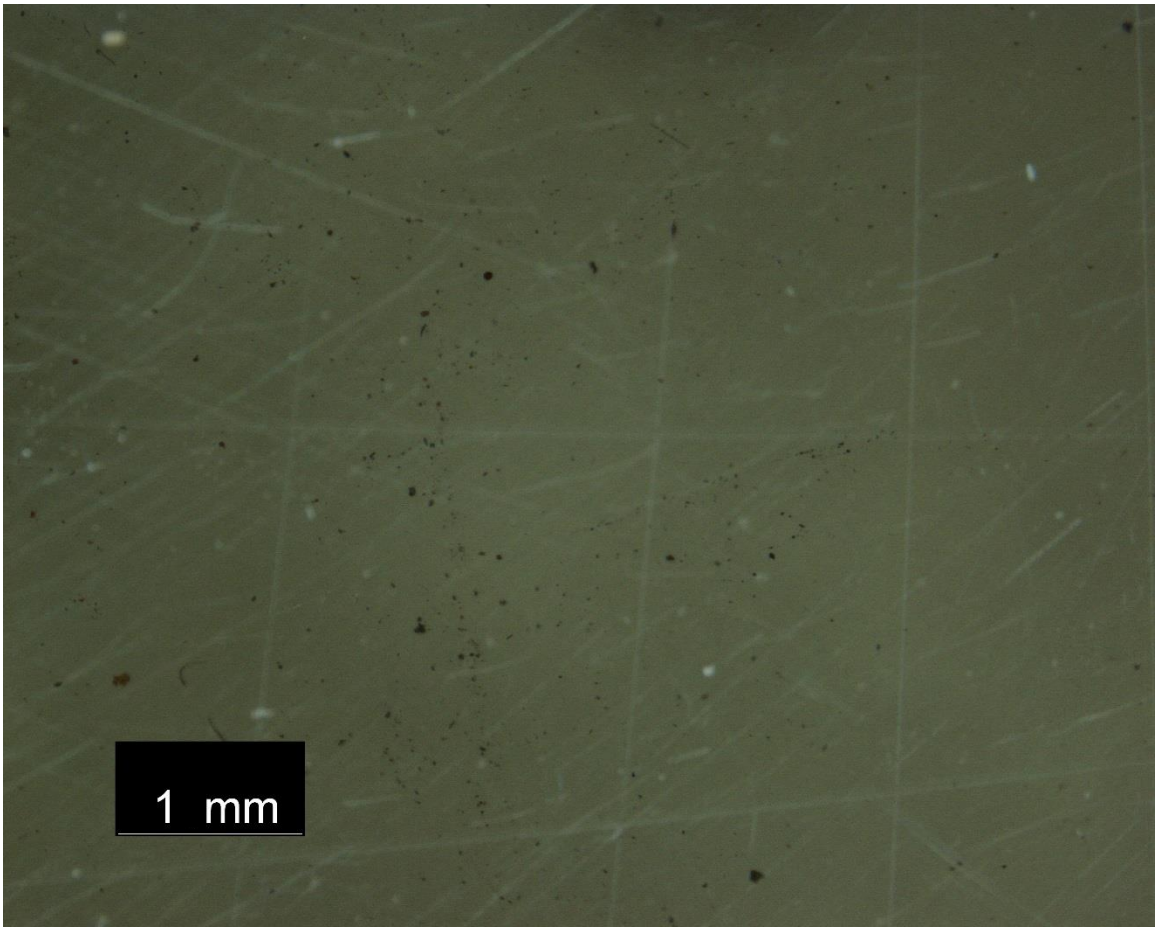

Figure 38. PEI Neat cross sectional micrograph.

Figure 39 is a cross sectional micrograph picture of polyetherimide with one percent by weight of the 40 mesh Nextrema particles. Scratches that are observed in the cross section are remnants of aggressive polishing.

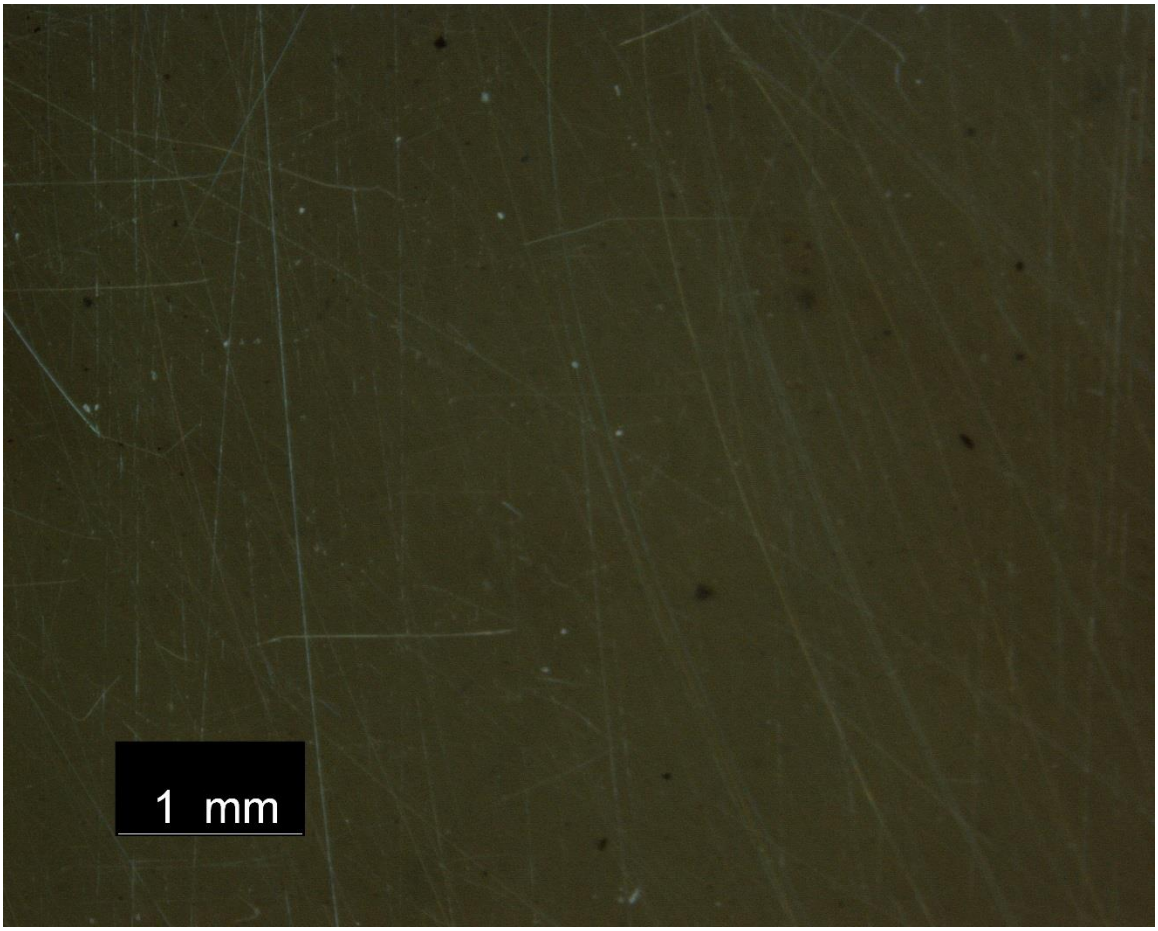

Figure 39. PEI with 1% of 40 mesh Nextrema cross sectional micrograph.

Figure 40 is a cross sectional micrograph picture of polyetherimide with five percent by weight of the 40 mesh Nextrema particles. Scratches that are observed in the cross section are remnants of aggressive polishing

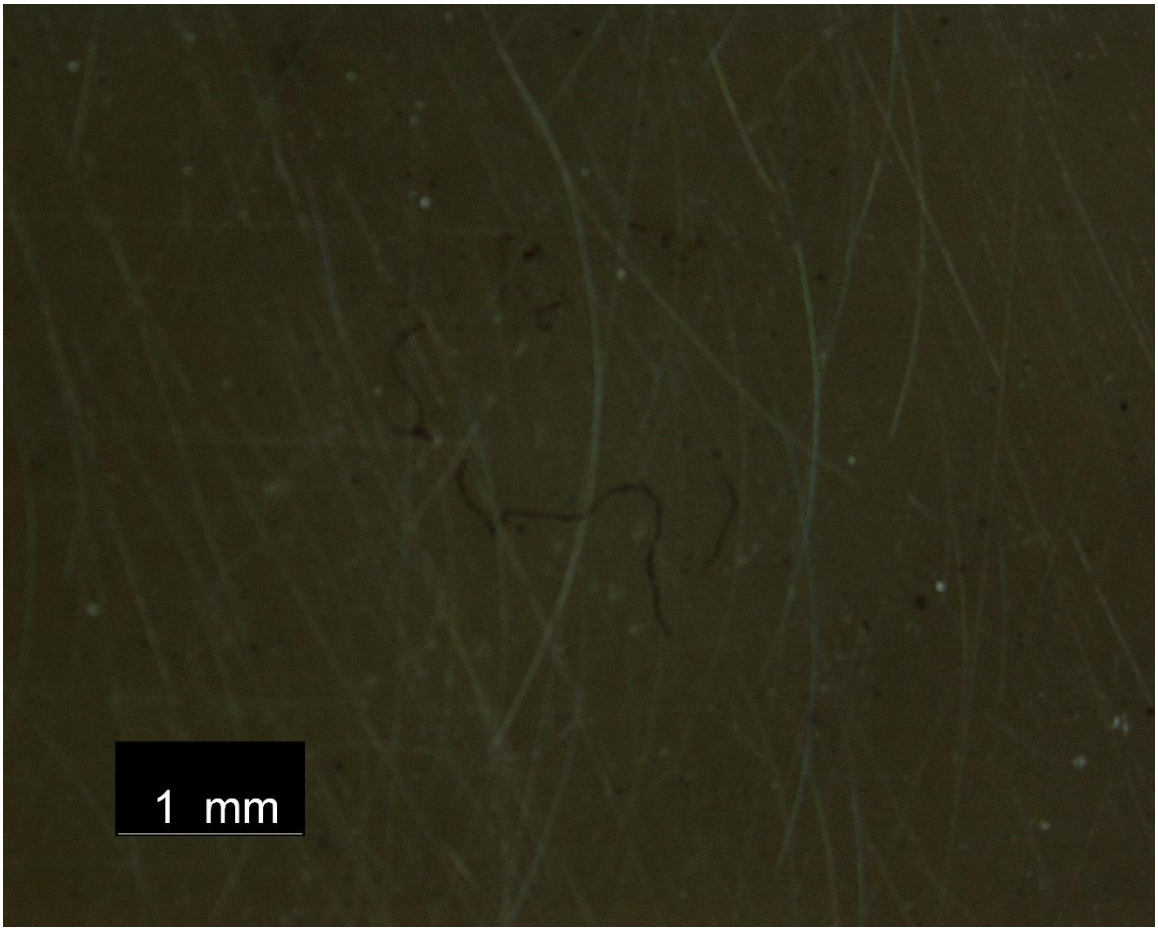

Figure 40. PEI with 5% of 40 mesh Nextrema cross sectional micrograph.

Figure 41 is a cross sectional micrograph picture of polyetherimide with one percent by weight of the 40-80 mesh Nextrema particles. Scratches that are observed in the cross section are remnants of aggressive polishing. Some voids are also observed in the cross section.

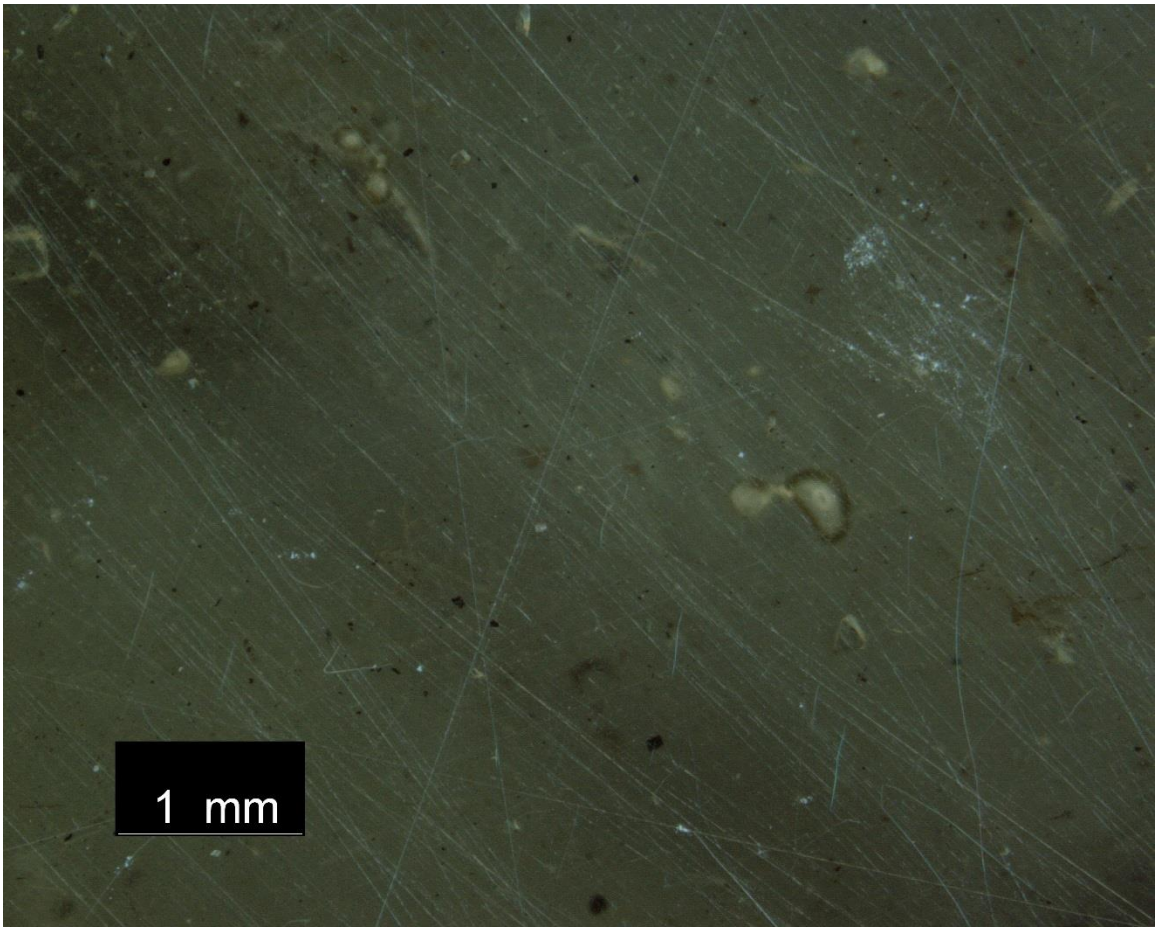

Figure 41. PEI with 1% of 40-80 mesh Nextrema cross sectional micrograph.

Figure 42 is a cross sectional micrograph picture of polyetherimide with five percent by weight of the 40-80 mesh Nextrema particles. Scratches that are observed in the cross section are remnants of aggressive polishing. Voids can be observed in the cross section.

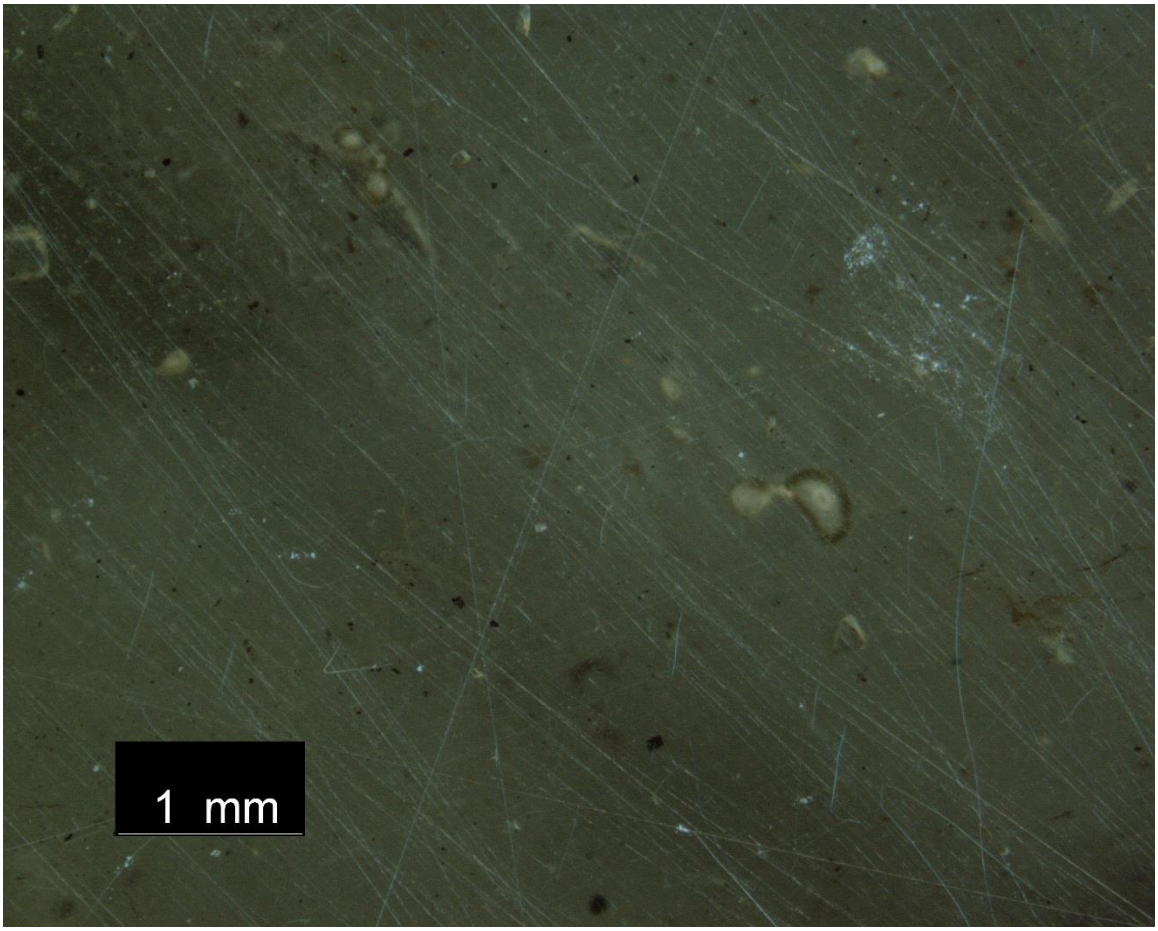

Figure 42. PEI with 5% of 40-80 mesh Nextrema cross sectional micrograph.

Figure 43 is a cross sectional micrograph picture of polyetherimide with one percent by weight of the 80 mesh Nextrema particles. Scratches that are observed in the cross section are remnants of aggressive polishing. A significant number of voids are observed in this sample.

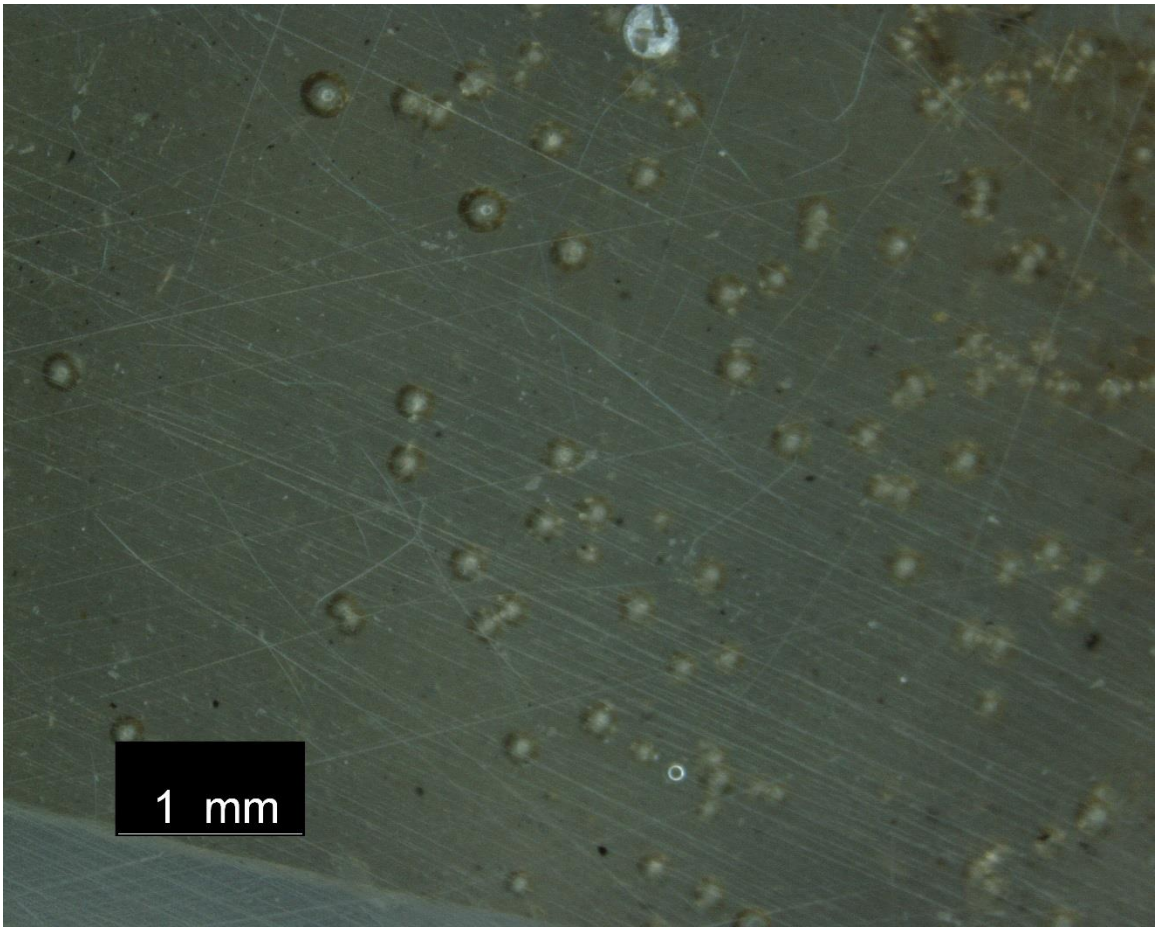

Figure 43. PEI with 1% of 80 mesh Nextrema cross sectional micrograph.

Figure 44 is a cross sectional micrograph picture of polyetherimide with five percent by weight of the 80 mesh Nextrema particles. Scratches that are observed in the cross section are remnants of aggressive polishing. Excessive voids are observed in this sample.

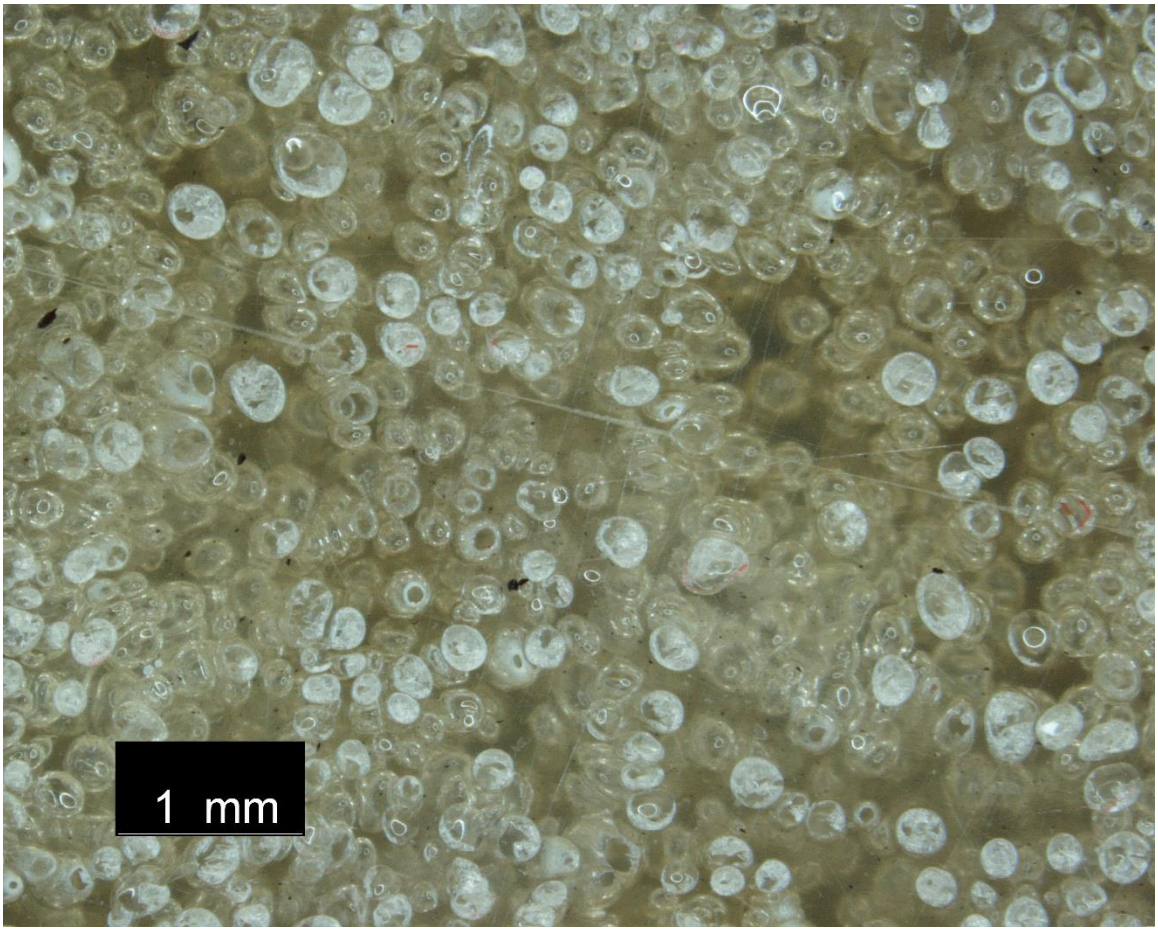

Figure 44. PEI with 5% of 80 mesh Nextrema cross sectional micrograph.

Particle Size Distribution

The particle diameters were then exported to Excel, sorted smallest to largest, and rounded to either the nearest tenth or whole micrometer. The diameters were sorted into bins for the creation of a particle count versus frequency histogram.

Figure 45 is one of the three images of the 40 mesh that were taken with the Olympus optical microscope and further analyzed with the pre-loaded features to count the particles and record their sizes.

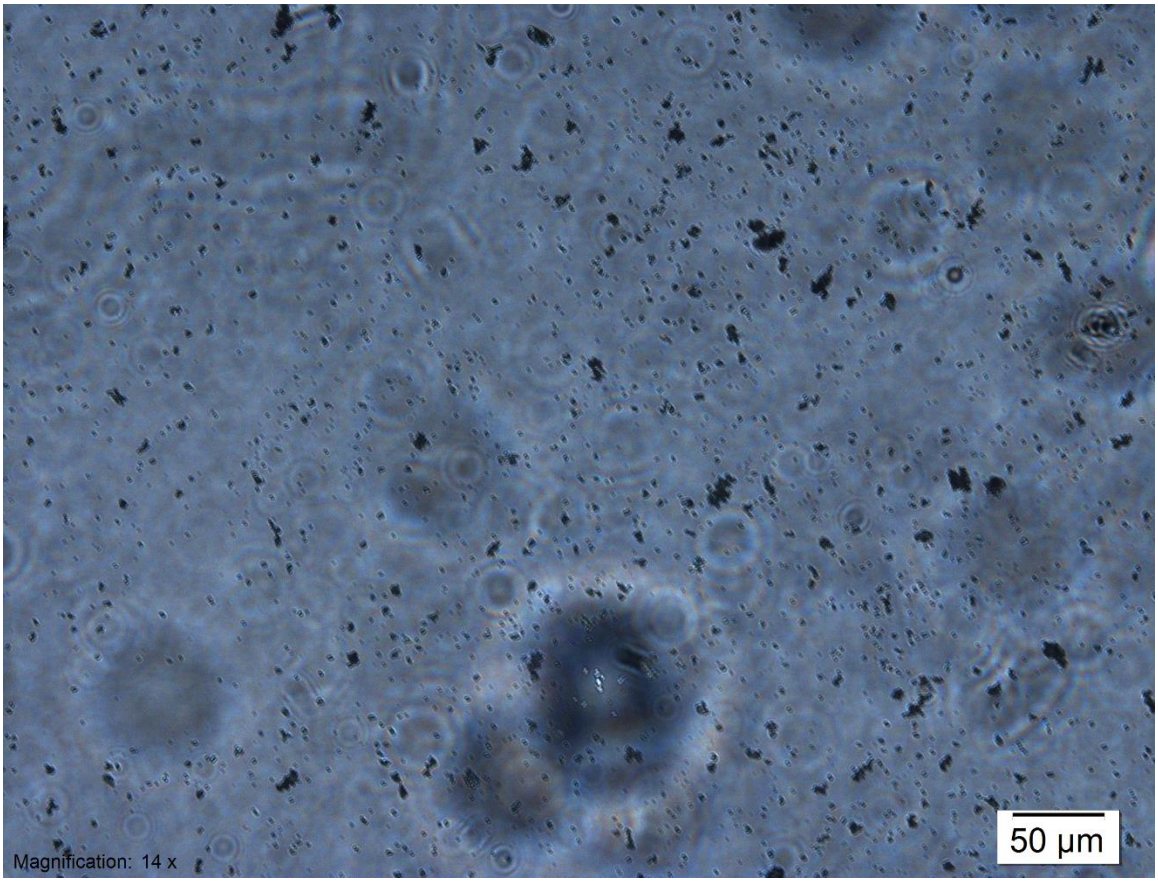

Figure 45. Optical microscope image of the 40 mesh particles.

Figure 46 is one of the three images of the 40-80 mesh that were taken with the Olympus optical microscope and further analyzed with the pre-loaded features to count the particles and record their sizes.

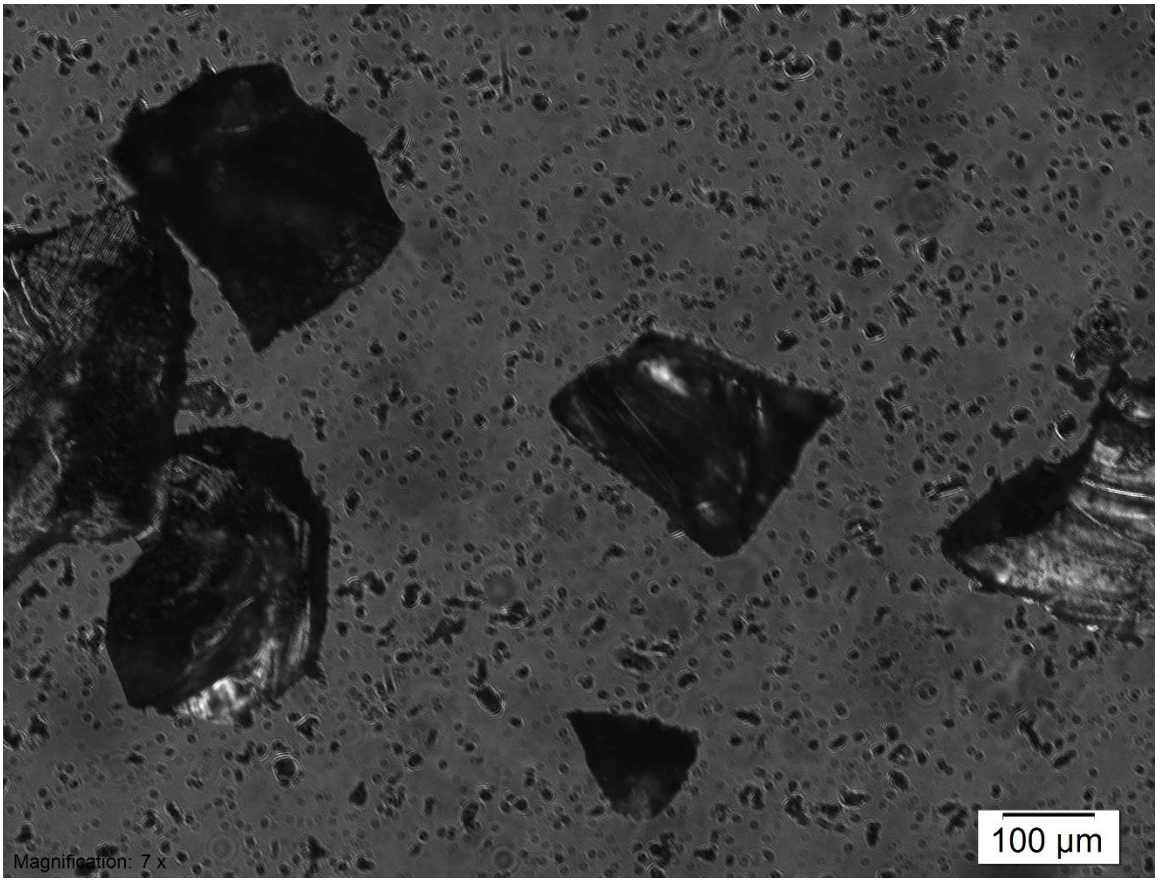

Figure 46. Optical microscope image of the 40-80 mesh particles.

Figure 47 is one of the three images of the 40 mesh that were taken with the Olympus optical microscope and further analyzed with the pre-loaded features to count the particles and record their sizes.

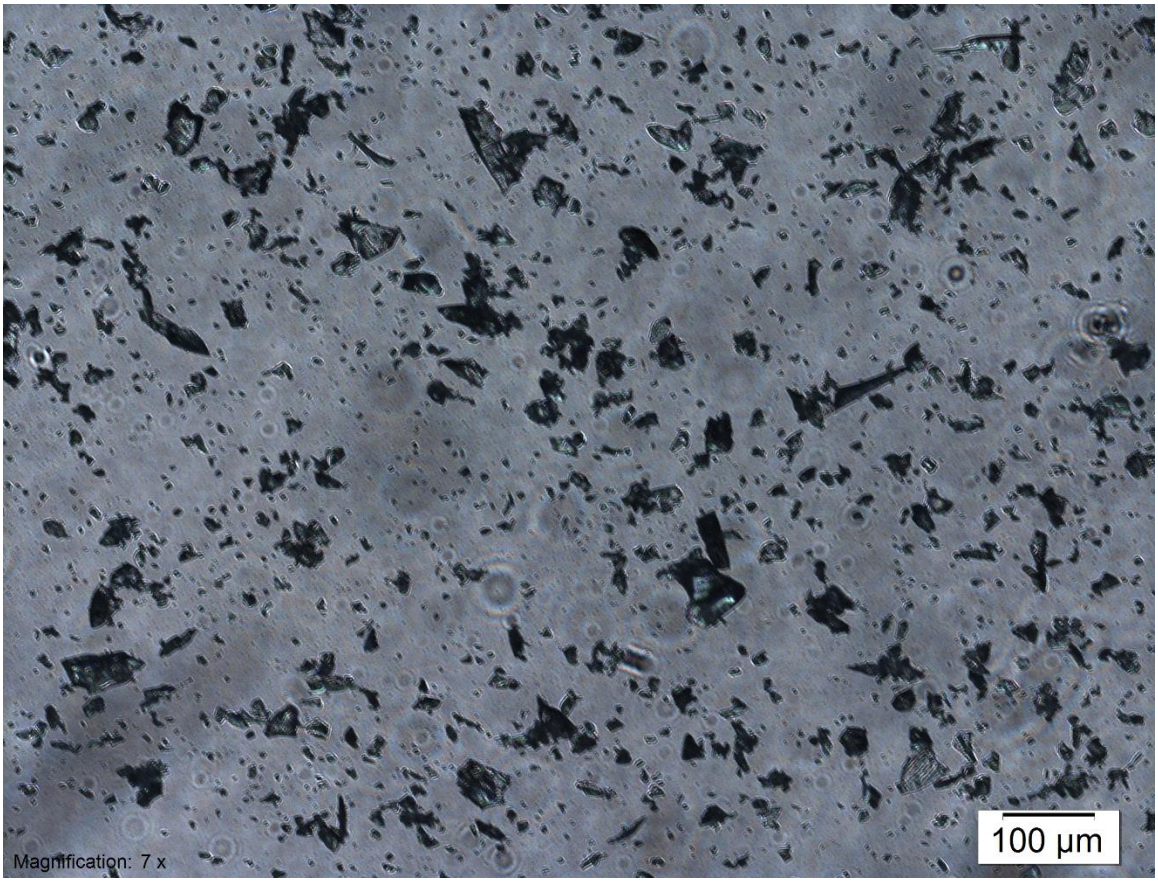

Figure 47. Optical microscope image of the 80 mesh particles.

The frequency of different particles sizes was determined and recorded then tabulated in separate sizes by rounding to the nearest tenth of a micrometer. Below, different distributions of the particles can be seen through a histogram visual. Though it is important to understand the distribution of the different particle sizes and the number of those sizes, it is perhaps more important to understand the volumetric composition of the distribution, how much of the volume of the glass is a particular size.

The equation for the volume of a sphere is below.

$$V = \frac{4}{3}\pi r^3$$

Equation 8. Volume of a sphere.

Where *V* is the volume, and *r* is the radius of the sphere. A volumetric bias can be generated by multiplying the size of the particle by the frequency that size particle appears. In this case particles were approximated to be spheres.

Figure 48 Histogram of 40 mesh. The X axis is the particle diameter. The Y axis is the frequency that that particular particle size was recorded by the optical microscope.

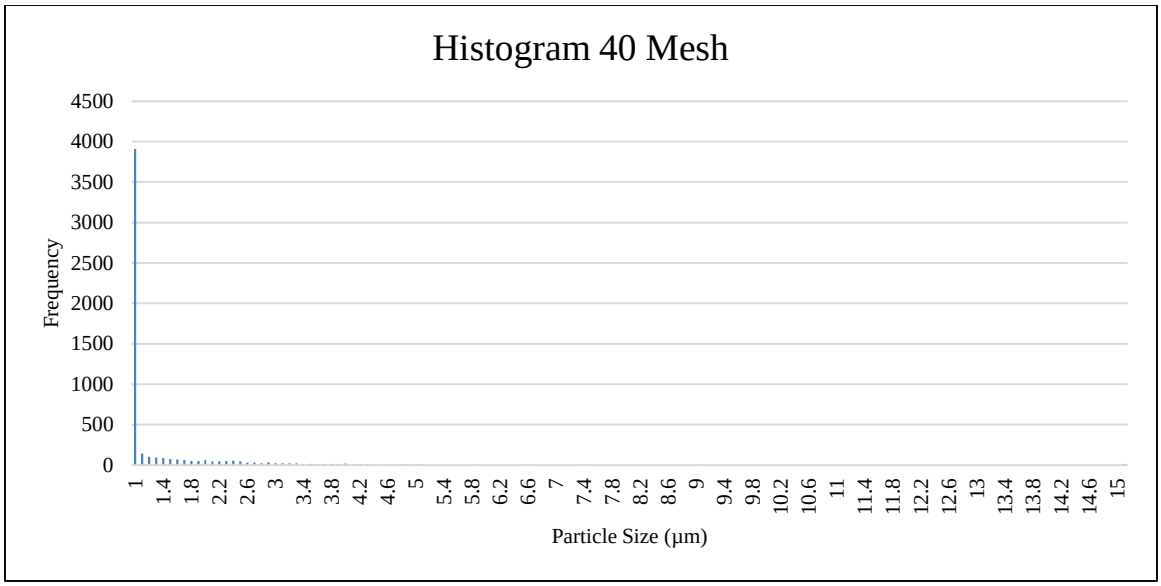

Figure 48. Histogram of 40 mesh.

Figure 49 Volumetric bias with the 40 mesh. The X axis is the particle diameter. The Y axis is the volume of the particles are that size particle recorded by the optical microscope.

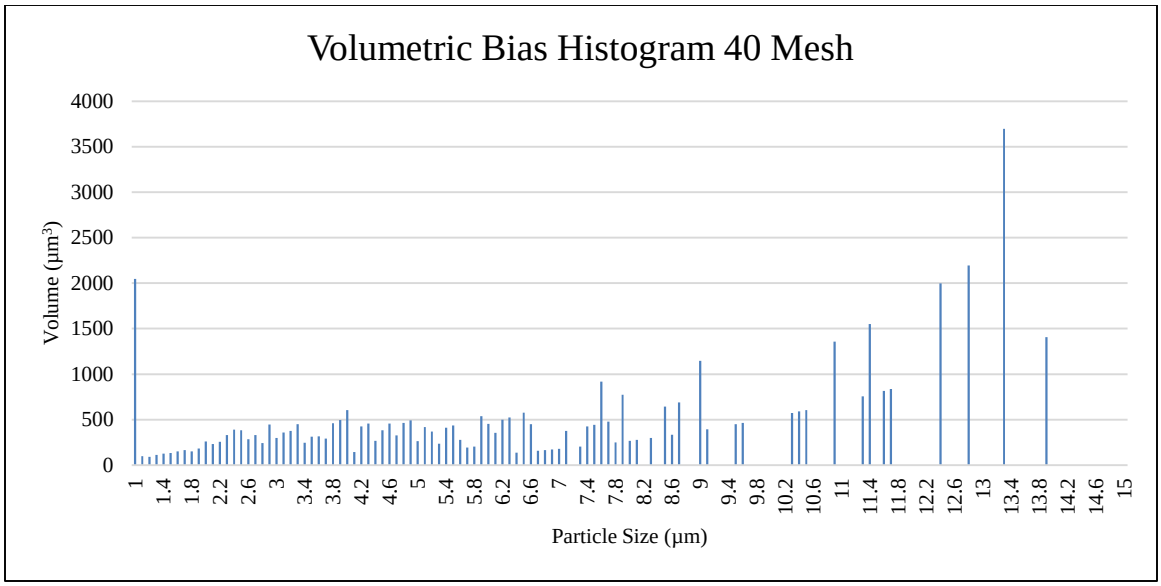

Figure 49. Volumetric bias histogram of 40 mesh.

Figure 50 Histogram of 40-80 mesh. The X axis is the particle diameter. The Y axis is the frequency that that particular particle size was recorded by the optical microscope.

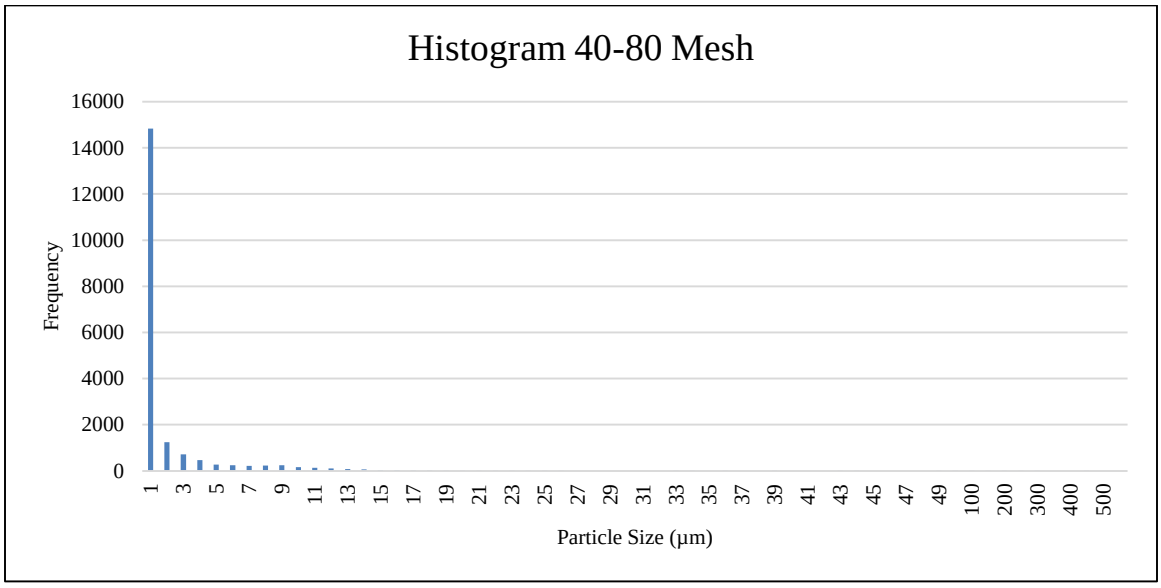

Figure 50. Histogram of 40-80 mesh.

Figure 51 Volumetric bias of 40-80 mesh. The X axis is the particle diameter. The Y axis is the volume of the particles are that size particle recorded by the optical microscope.

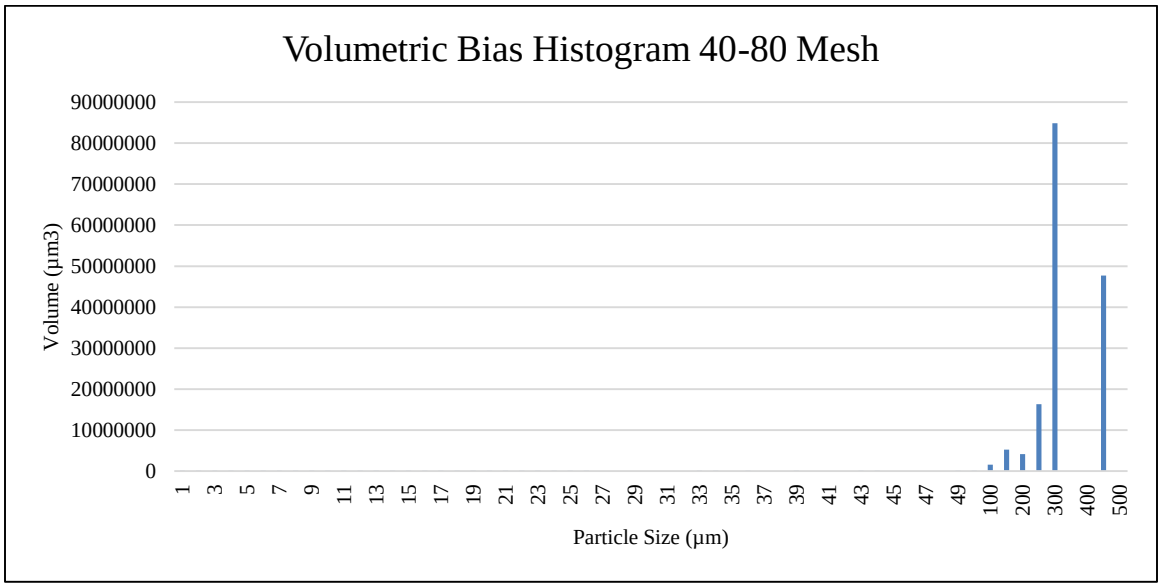

Figure 51. Volumetric bias histogram of 40-80 mesh.

Figure 52 Histogram of the 80 mesh. The X axis is the particle diameter. The Y axis is the frequency that that particular particle size was recorded by the optical microscope.

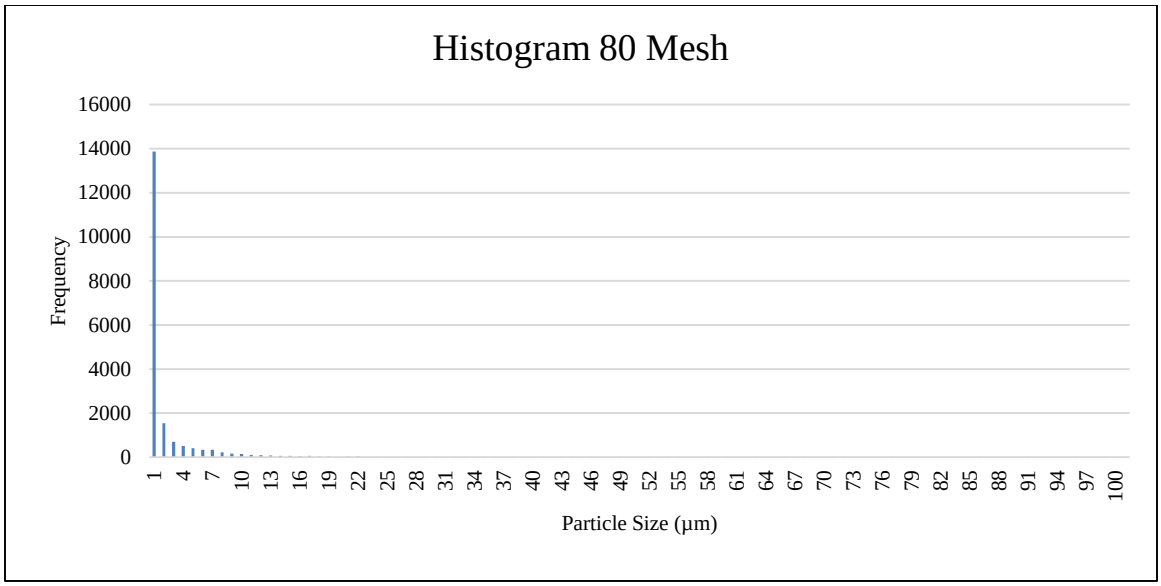

Figure 52. Histogram of 80 mesh.

Figure 53 is a volumetric bias histogram of the 80 mesh. The X axis is the particle diameter. The Y axis is the volume of the particles are that size particle recorded by the optical microscope.

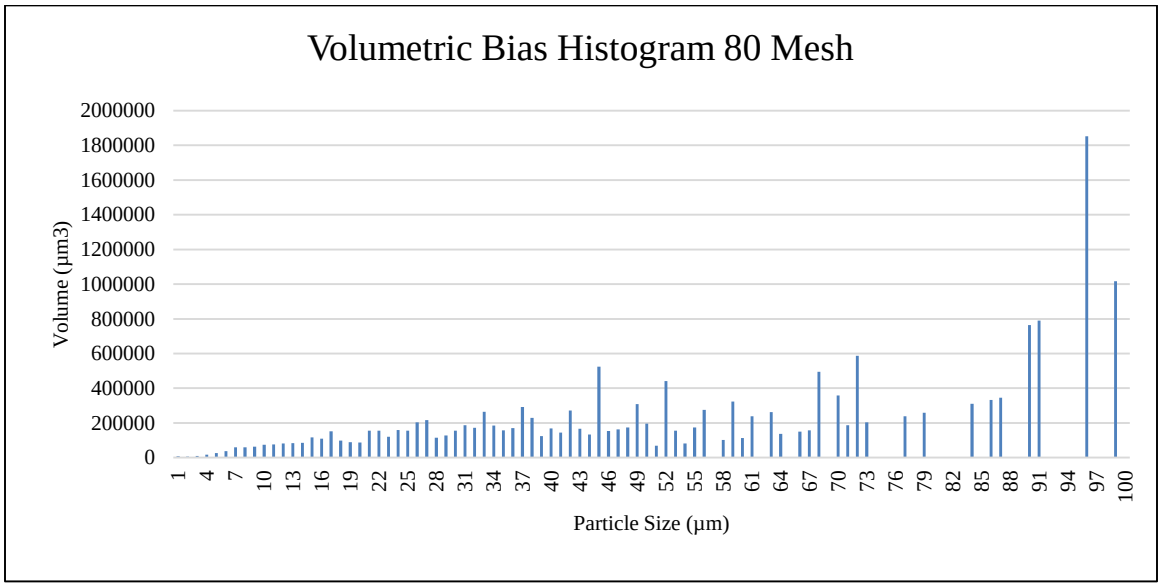

Figure 53. Volumetric bias histogram of 80 mesh.

CHAPTER IV

CONCLUSION

Particle Size Distribution

Once the particle size distributions were adjusted with a bias towards the volume that that particle size takes up, some trends can be seen. For the 80 mesh samples the distribution tended towards smaller particles seen in Figure 54.

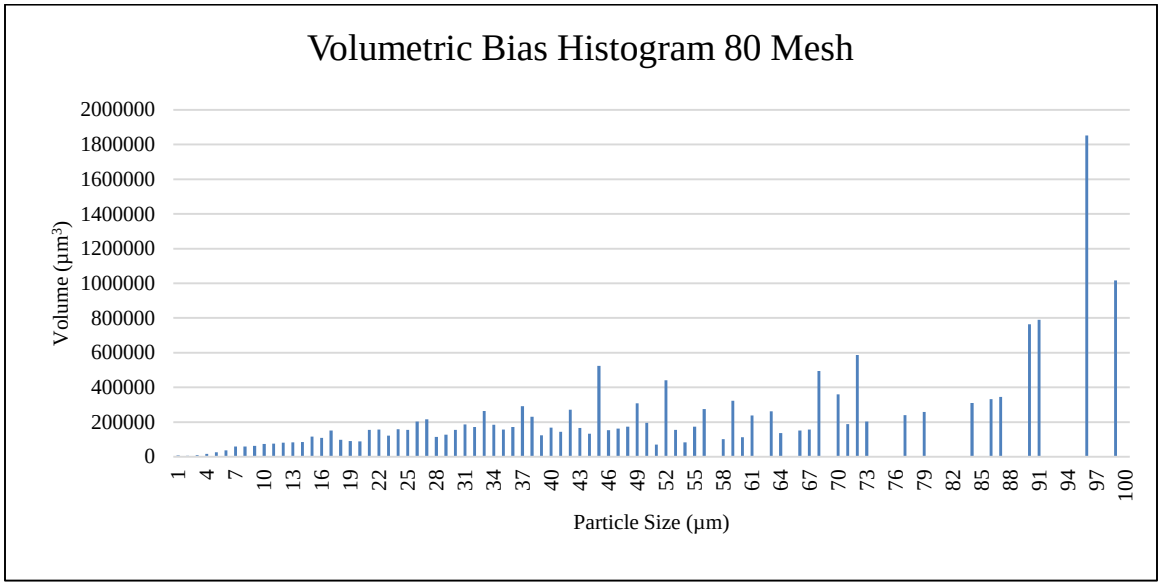

Figure 54. Volumetric bias histogram of 80 mesh.

The particles for the 80 mesh should be 0.00 inches to 0.007 inches (177.8µm). It can be seen in the histogram that there is a fairly even distribution from zero up to about 100µm for the volumetric distribution.

The 40-80 mesh samples the distribution tends towards larger particles as seen in Figure 55.

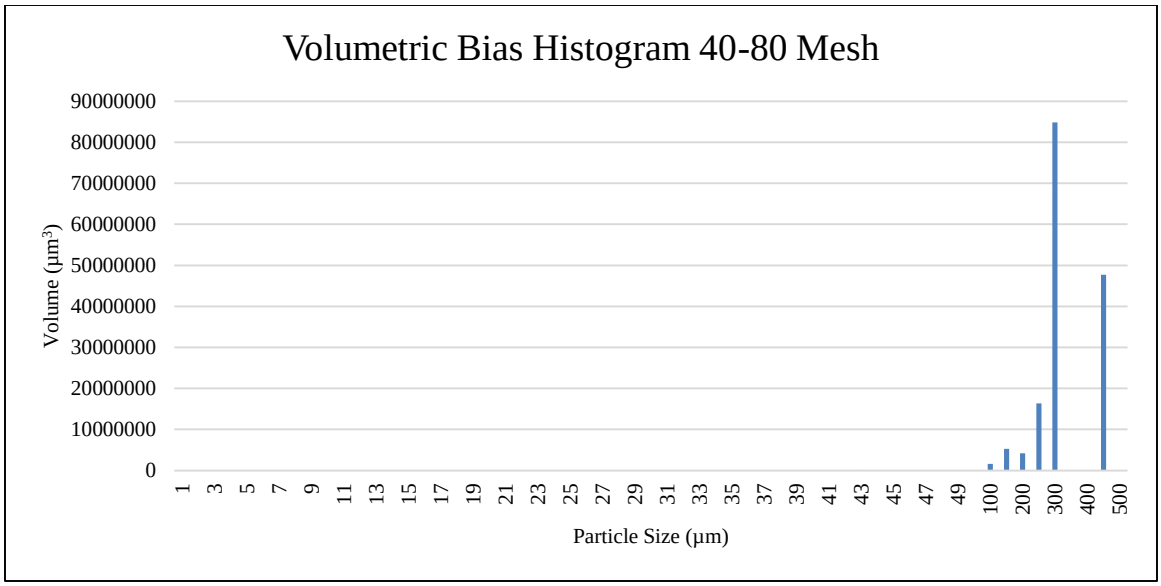

Figure 55. Volumetric bias histogram of 40-80 Mesh.

The particles for 40-80 mesh should be 0.007 inches (177.8µm) to 0.0145 inches (368µm) for 40-80 mesh. Seen in the histogram, the volumetric distribution shows that the particles land in that band of particle sizes.

The last distribution is the 40 mesh which is simply the particles that went through the 40 mesh sieve screen so the particles should span from 0.00 inches to 0.0145 inches (368µm). However, the distribution that is seen from the data is not that large as seen in Figure 56.

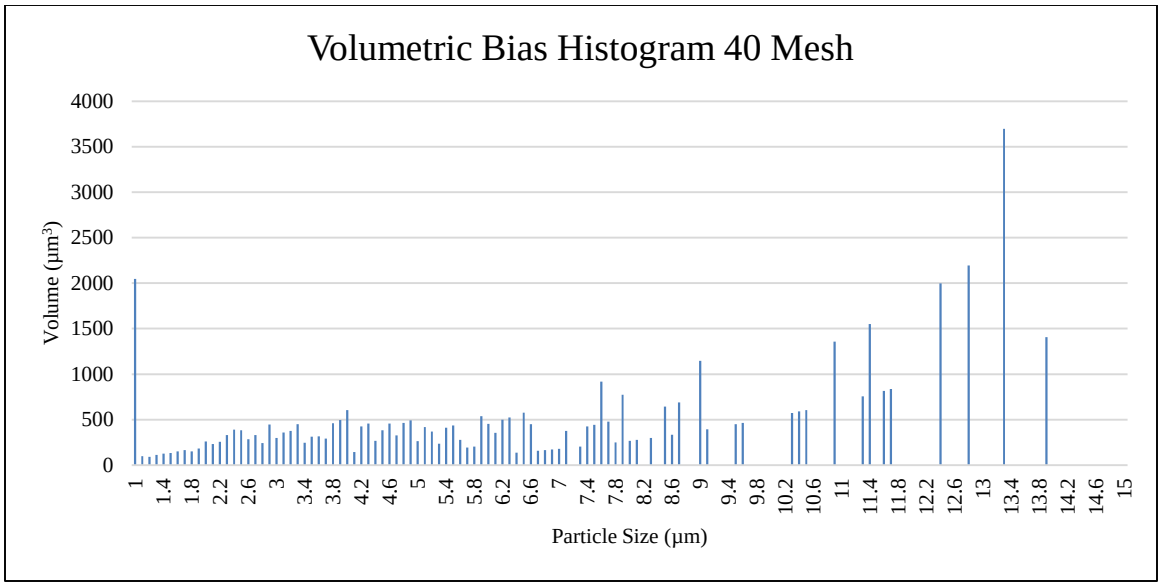

Figure 56. Volumetric bias histogram of 40-80 Mesh.

Instead the distribution that is seen is pretty uniform from zero to about 14 micrometers. Also the optical microscope pictures show that the particles in the sample look more sphere in shape. This is because this sample was the very first sample of Nextrema that was made at PAX River, and the way to make the particles was still being developed. This particular sample was made by tumbling larger chunks of Nextrema in water to create the small particles. Then the slurry that was developed was poured through the 40 mesh sieve and dried out on a glass Pyrex pan. The particles were re-tumbled dry and packaged and sent to USM for blending into the PEI. This method of creating particles was quickly abandoned due to how slowly it generated volume of Nextrema particles, and the crushing method was adopted. It is believed that the tumbling and slurry method of creating particles suspended much smaller particles in the water which resulted in a smaller distribution that can be seen in the histogram.

Epoxy

The epoxy specimen that were manufactured were made as a backup as explained earlier due to concerns with timing of the PEI specimen. The epoxy specimen were made for additional data to help understand the interactions between the matrix and the fillers. Due to the results that were found, it is believed that during the 48 hour room temperature cure, the Nextrema particles that were mixed into the epoxy settled to the bottom of the specimen. This is exceptionally prevalent in the larger particle size seen in the TMA curve in Figure 57.

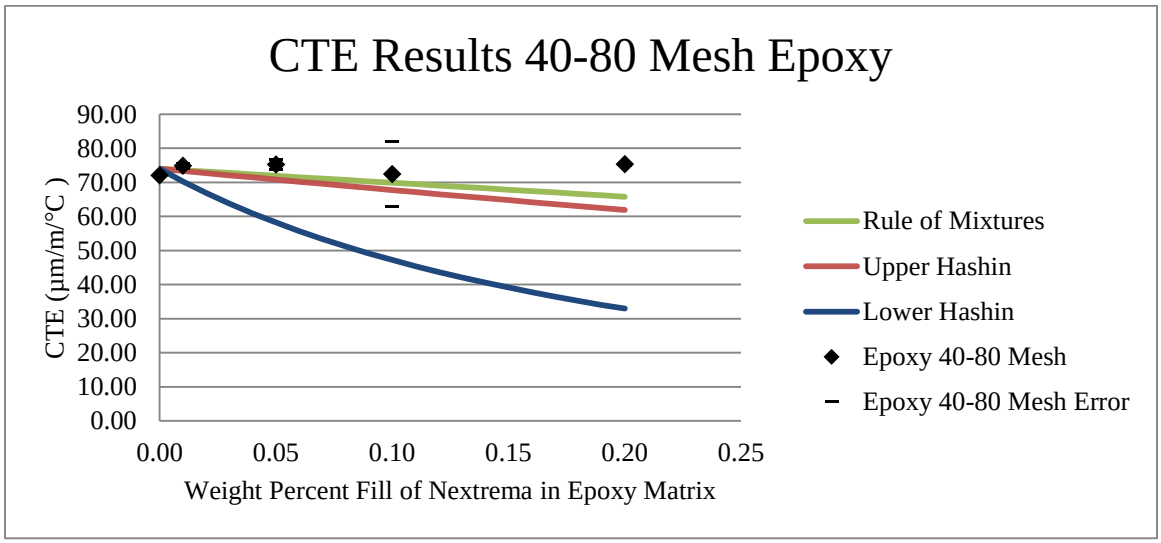

Figure 57. CTE Results 40-80 Mesh Epoxy.

It can be seen that the CTE never changed no matter how much filler was mixed into the epoxy specimen. Because the epoxy specimen were sampled out of the center of the specimen that were made, then machined flat to allow for flat surfaces for the TMA and create a thinner specimen so that the sample would be able to be heated all the way through. After collecting results, it is believed that the particles all sank to the bottom and the machining process removed most, if not all the Nextrema particles. It was attempted to get this data to get a lot of data and specimen to help to correlate the predictions that

Hashin made in order to help understand what happens at higher fill percentages because the PEI samples were limited due to the maximum allowable torque on the extruder without damaging it.

Because the epoxy is a thermoset material, no rheological data was collected, because for the purposes of this research it would not have added value to the research. For the purposes of drawing conclusions, the epoxy ended up adding little to no value to trying to figure out how to lower the CTE of FDM tooling the way the researcher originally thought it would.

Polyetherimide

The data from the PEI specimen is more useful for drawing conclusions. There were still some issues that caused some of the data to come back with unpredicted results. The second set of PEI samples were run through the extruder two extra times, for a total of three times through the extruder. The second set of specimen are all the 40-80 mesh and the 80 mesh specimen. Due to the increased thermal history on these specimen it is strongly believed that the average molecular weight was decreased due to thermal damage. The reduced molecular weight would explain why even with the filler, these range of specimen all had lower viscosity values across the temperature sweep from 325-425˚C. Figure 58 and Figure 59 show how the viscosities were measured as being lower than the neat PEI.

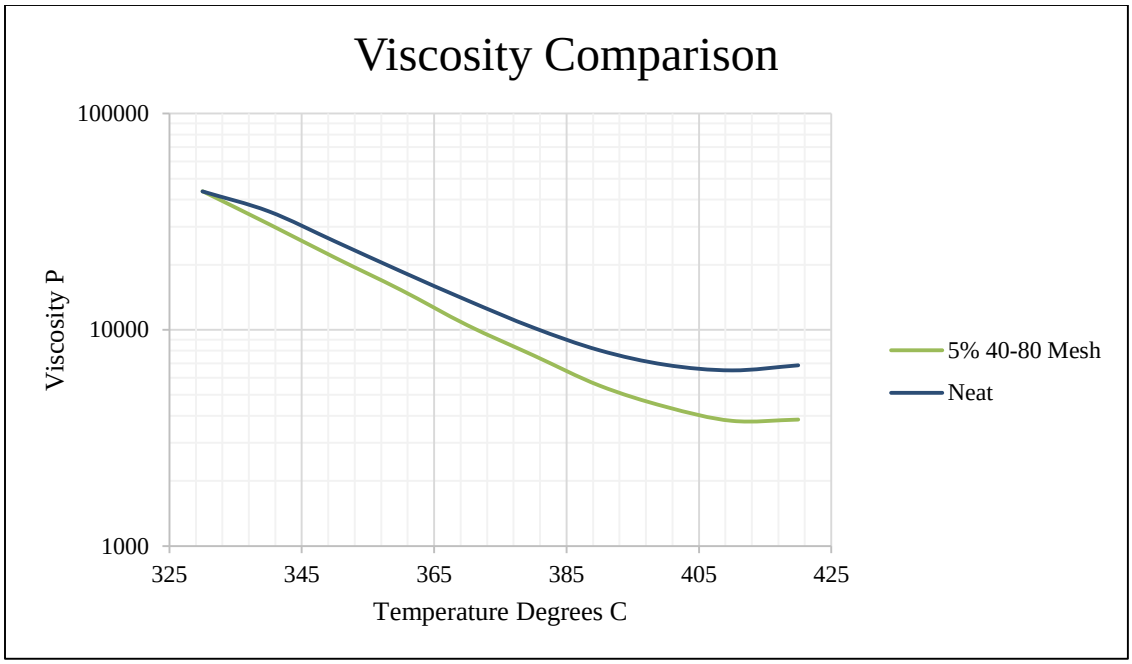

Figure 58. Viscosity Comparison 5% 40-80 Mesh vs Neat.

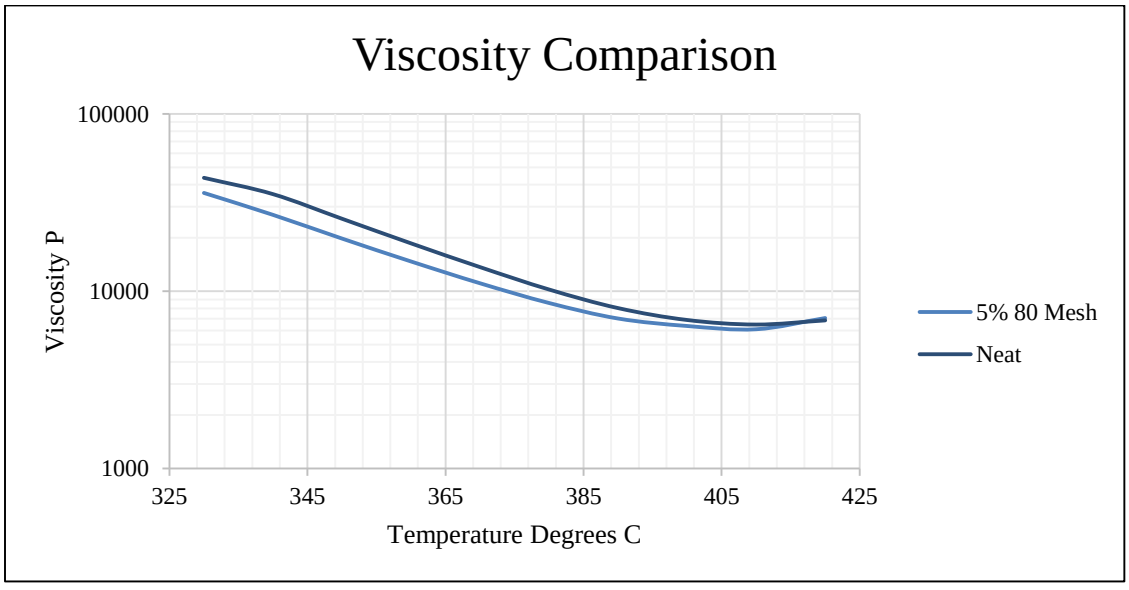

Figure 59. Viscosity Comparison 5% 80 Mesh vs Neat.

Also, the voids and color splotches that were seen in the cross sectional micrographs explain why the TMA results from the second set of specimen are not what was expected. The voids could have created space for the polymer to expand into explaining the lower than expected results in the 80 mesh specimen, also the color

blotches noticed were very likely polymer that did not mix enough in the extruder and had different percent fills of Nextrema, explaining the erratic results seen in the CTE results for the 40-80 mesh specimen. Figure 60 and Figure 61 show the CTE results showing the erratic and lower results from the damaged specimen.

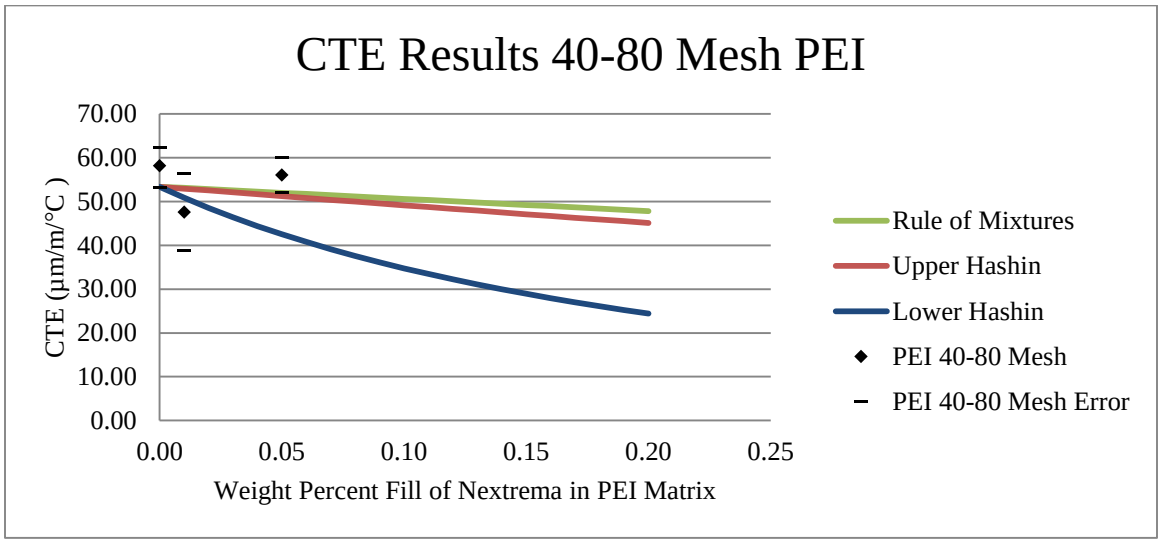

Figure 60. CTE Results 40-80 Mesh PEI.

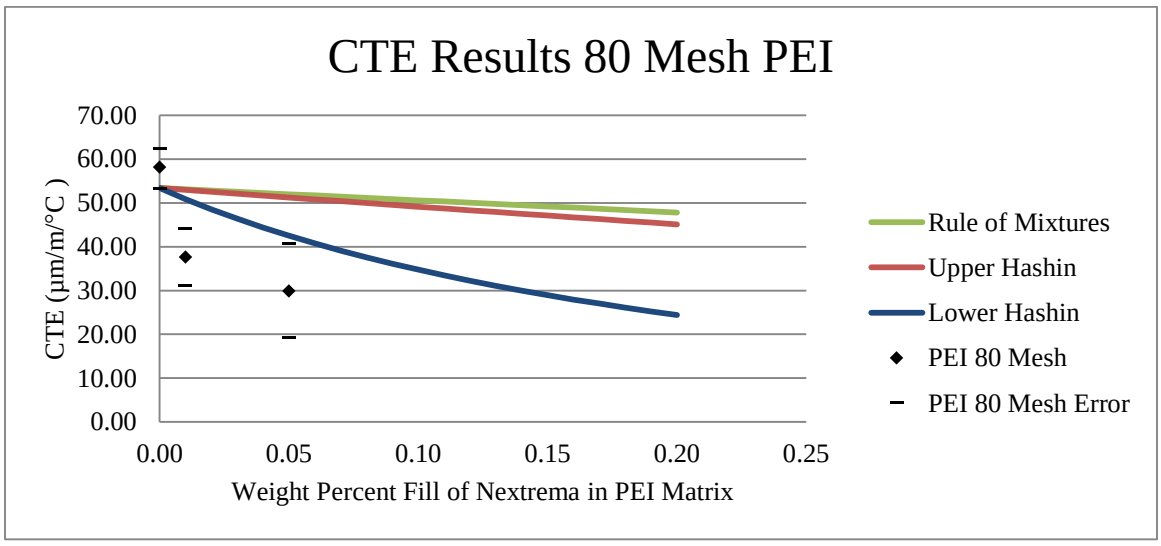

Figure 61. CTE Results 80 Mesh PEI.

The PEI material with the 40 mesh particles of Nextrema only went through the extruder once so the specimen that came from this first run had less thermal history, less

thermal damage as well as less mechanical damage from the high strain rates in the twin screw extruder runs. This lower amount of damage can be seen in the viscosity curves that were collected and generated by the RDA that was used. The results are seen in Figure 62 and Figure 63.

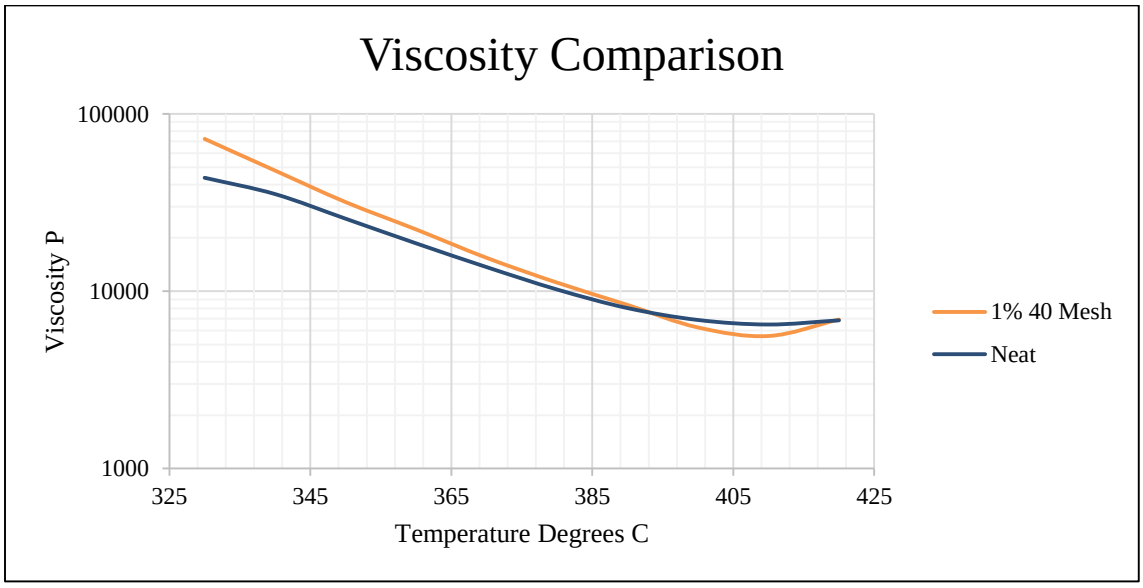

Figure 62. Viscosity comparison 1% 40 Mesh PEI vs Neat.

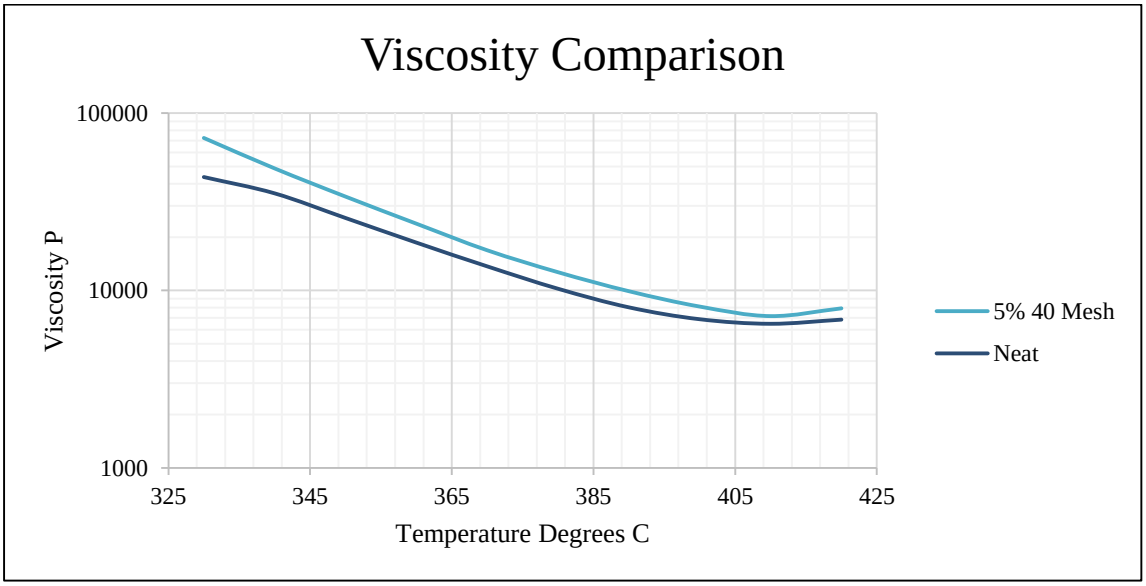

Figure 63. Viscosity comparison 5% 40 Mesh PEI vs Neat.

Table 7 shows the comparison of the viscosity data in tabular form of both the 5% and the 1% 40 mesh filled PEI specimen. From the above graph and below table, the data shows about a 5-7˚C change in temperature increase could compensate for adding 1% of the 40 mesh filler and approximately a 10˚C change in temperature increase would compensate for the viscosity difference when adding the 40 mesh Nextrema filler at about 5% by weight.

Table 7

Temperature vs Viscosity

Temperature Degrees C, Pascals										
Temperature (C)	330	340	350	360	370	380	390	400	410	420
5% 40 Mesh (P)	72473	48784	33850	23820.5	16860	12677.5	9907	8116	7169	7930
1% 40 Mesh (P)	72264	47888	31821	22305	15430	11183	8371	6246	5590	6923
Neat (P)	43632	35297	25643	18624.5	13679	10227.5	8034	6884	6490	6850

The CTE data from the 40 mesh specimens is more reliable because as stated above, the specimen saw less thermal history, therefore less thermal degradation, as well as not containing any visual voids or inconsistent colors as well as no voids found with the micrograph cross section photos that were taken. Figure 64 shows the curve comparing the results with the predicted bounds for Hashin’s equations.

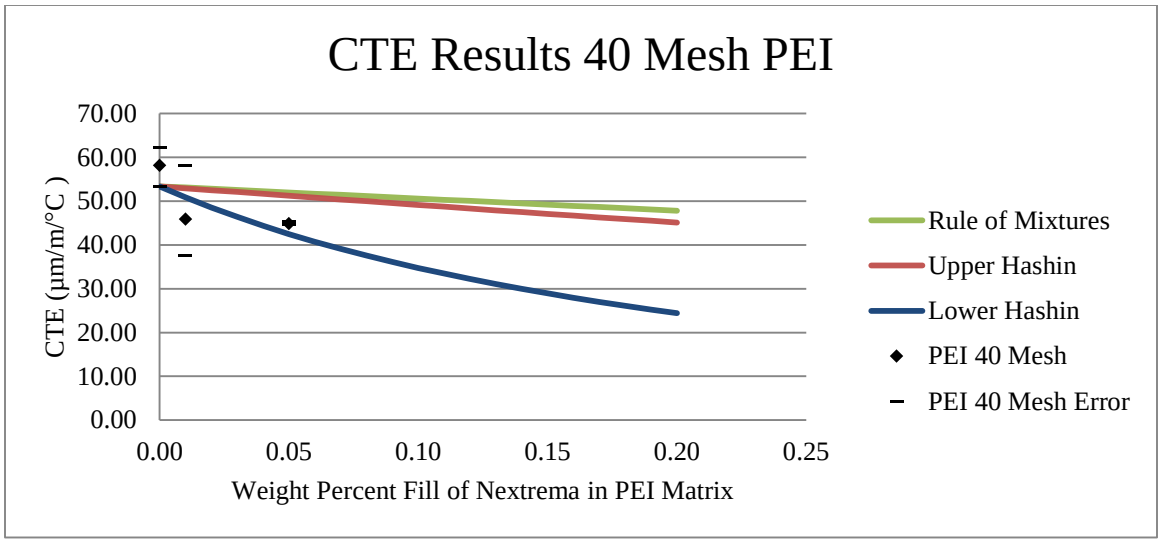

Figure 64. CTE Results 40 Mesh PEI.

The 304 stainless steel CTE is 17.3µm/m/ºC and 6061 Al is 23.6µm/m/ºC (www.matweb.com 2014). At around 20% by weight the bulk CTE is getting low enough that the tooling would behave more like a steel or aluminum piece of tooling which are well understood how to help compensate with the first two methods of compensating for CTE tooling and part mismatch which were discussed in the introduction.

Future Work

Based on the data that was generated and what was learned during this thesis, this project will be continued jointly by NAVAIR polymers and composites branch at Patuxent River NAS as well as NAVAIR polymers and composites branch at North Island NAS. There will be several steps; working with Stratasys to synthesize thread of PEI with Nextrema, Modeling, making FDM parts, and finally further testing. If that effort is successful, full scale complex shaped tool will be made and attempted curing a composite part on the tooling.

The first step of the continued work will be to partner with Stratasys. Stratasys is currently the leader in making FDM machines and developed the Fortus 400mc that

would be used at North Island NAS to make any sample coupons or, in the future, tooling. Based on what was learned in the work that was done in this thesis, the higher the percentage of Nextrema is better for reducing the bulk CTE of the material. Even though the 40 mesh appeared to give the best results in this thesis, as described in the conclusion, it is believed that this is due to the thermal history that was on the other samples. Using the smaller particles would be better for pushing material through the nozzle of the FDM machine. 80 mesh Nextrema should be used. The concentration of the Nextrema should also be limited, even though it is understood that more is better for CTE properties, too high of a concentration of particles will cause the material to get brittle and could significantly increase the viscosity making the material hard to process. At this time the suggestion would be around 20-30 percent weight fill so as not to be too high and become brittle. Based on historical work in the thermoplastic industry, about 40percent fill by volume is about the limit before significantly affecting properties negatively and impacting process-ability.

In parallel to this effort, North Island NAS will be investigating theoretically what the effect of raster fill path will have on the bulk CTE of the tooling that would be 3D printed during the FDM process. This means that North Island NAS team will be investigating how the spacing of the printed paths as well as direction of those paths and any interstitial spaces will allow the material to possibly fill into those void spaces as it expands.

Once North Island NAS has down selected to a processing fill path that they believe will be able to positively affect the CTE properties of the mold without negatively effecting the strength properties of the material, they will be supplied with material from

Stratasys to make some specimen. These specimen will then be tested on Patuxent River NAS for compressive strength at autoclave cure temperatures (150 and 177˚C) to make sure there is sufficient strength that the mold will not distort under autoclave pressures. The specimen will also be tested for CTE in the TMA.

Success in these steps will lead into full scale testing to create a complex shaped mold to attempt to cure an epoxy matrix carbon fiber reinforced composite in an autoclave.

APPENDIX A

TMA RAW DATA CURVES

This appendix records the raw data taken from the TMA Q400 V7.3 Build 9.

PEI Results

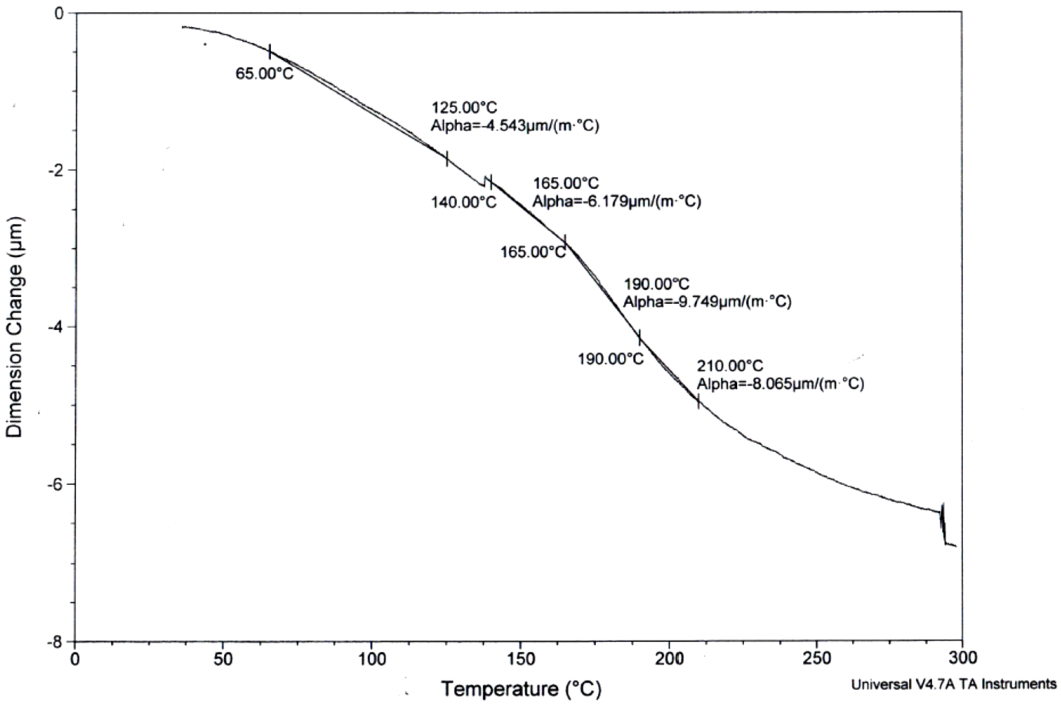

Figure 65. Negative CTE Nextrema 4.9946mm thickness.

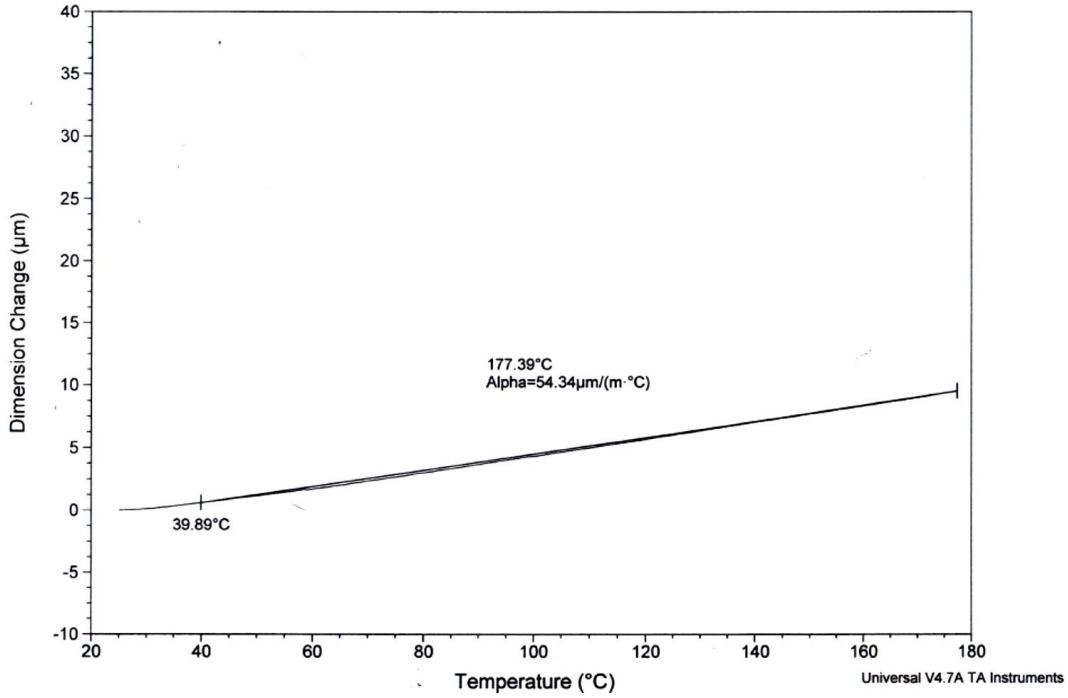

Figure 66. PEI Neat 1.1924 Thickness.

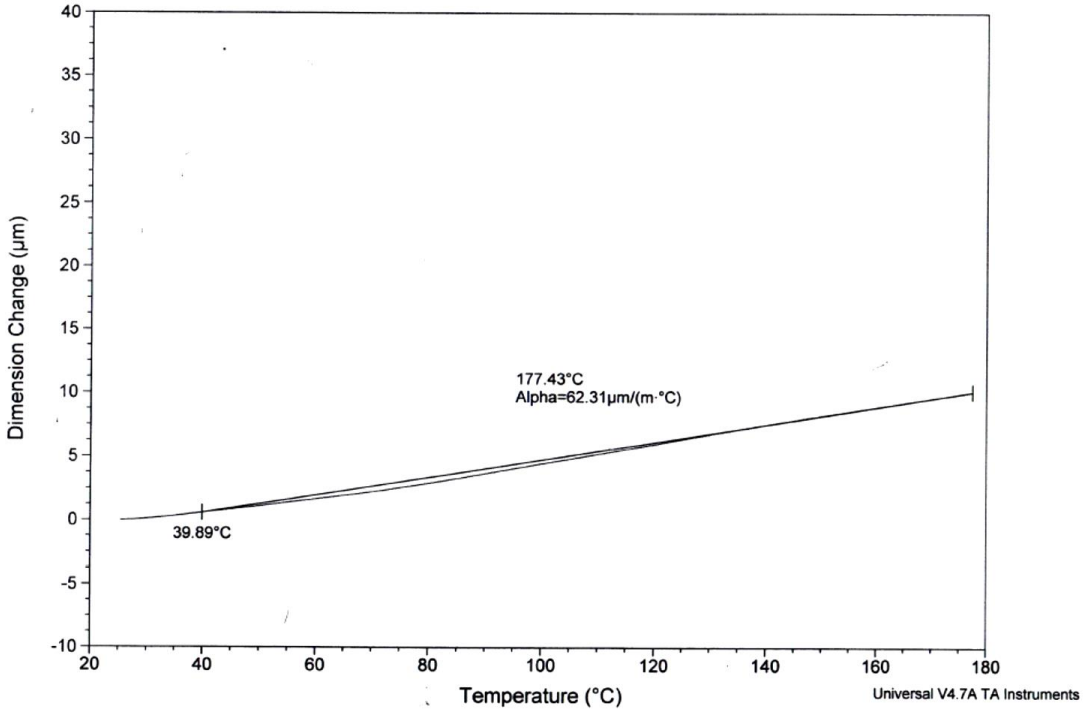

Figure 67. PEI neat 1.1102 Thickness.

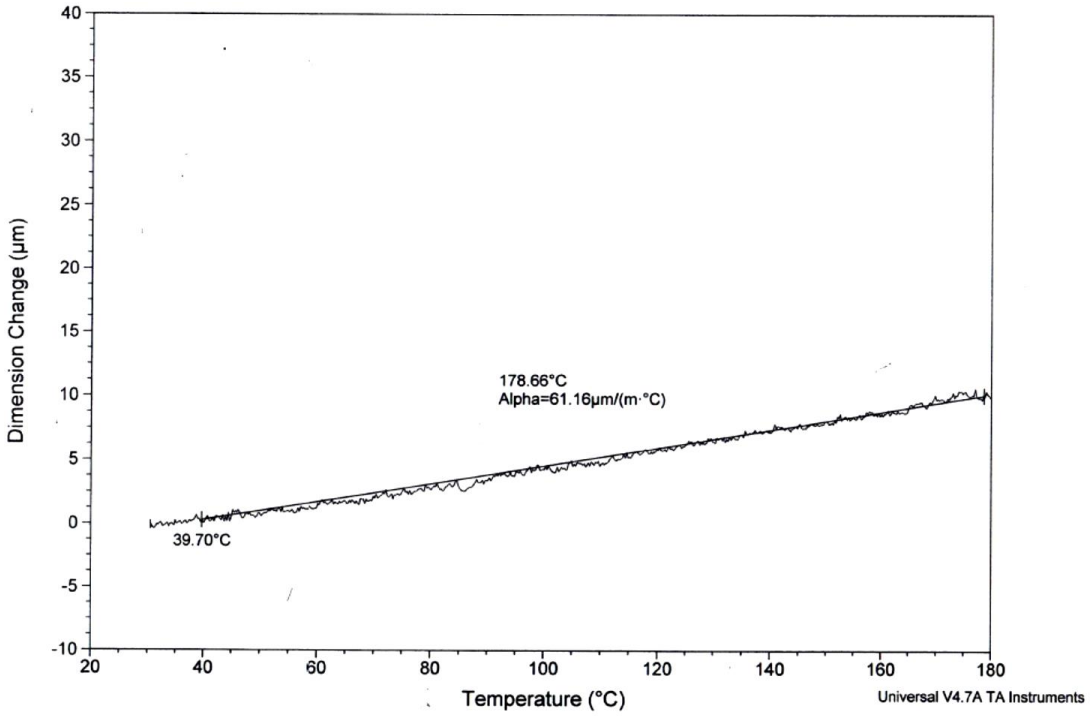

Figure 68. PEI Neat 1.1528mm Thickness.

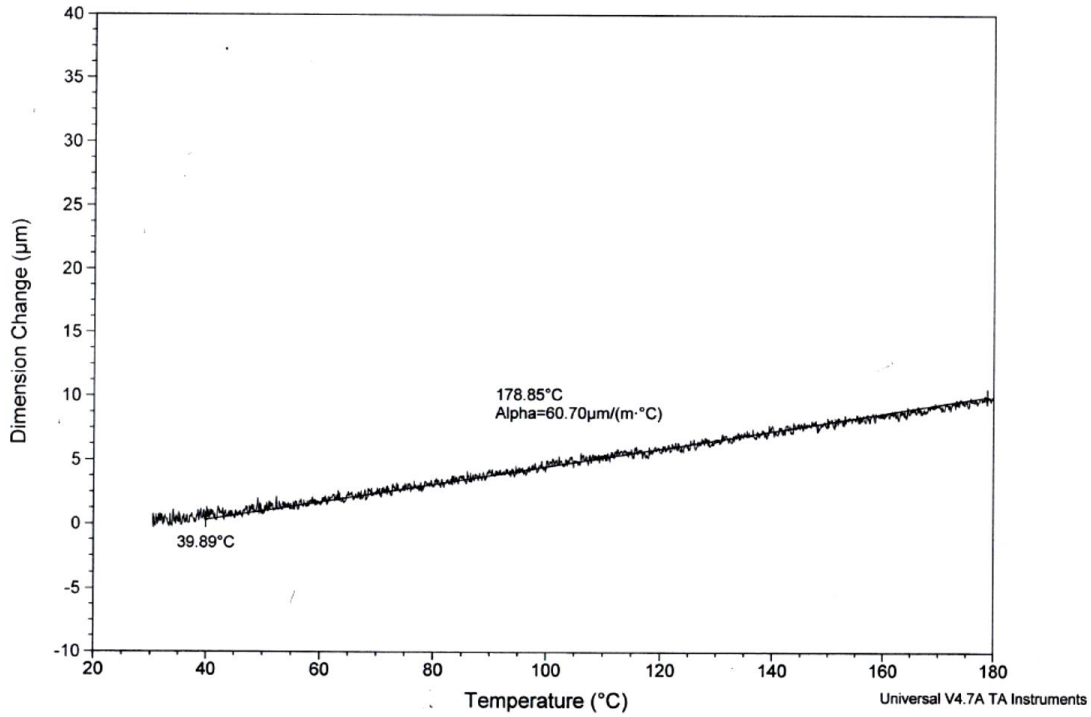

Figure 69. PEI Neat 1.1491 Thickness.

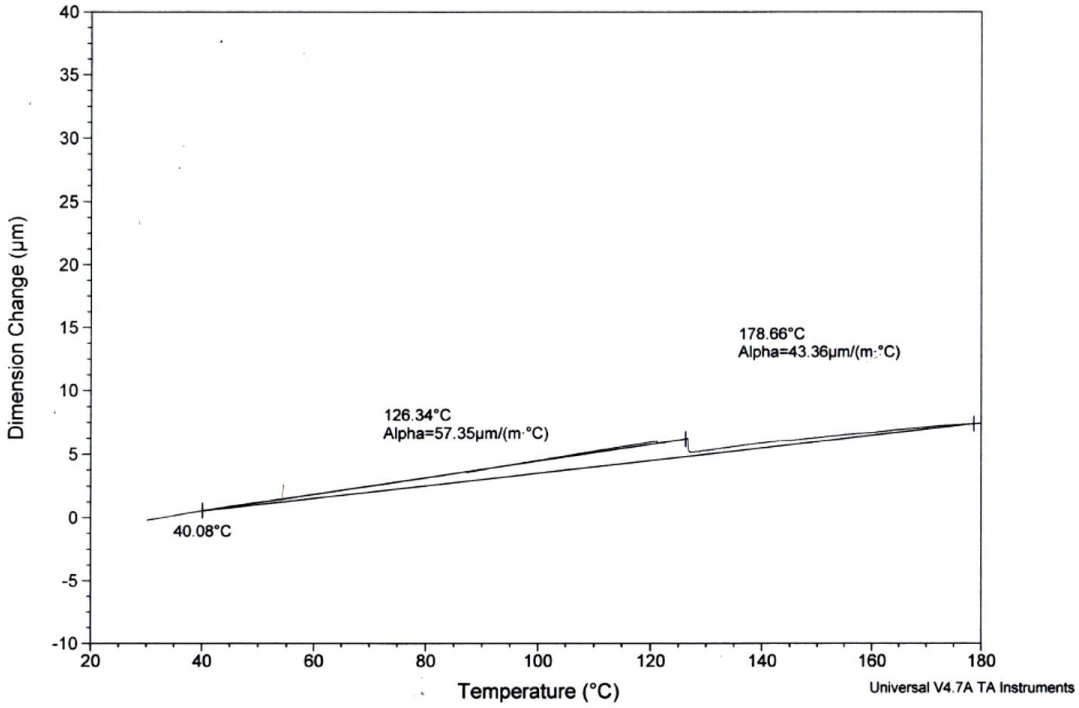

Figure 70. PEI Neat 1.1374mm Thickness.

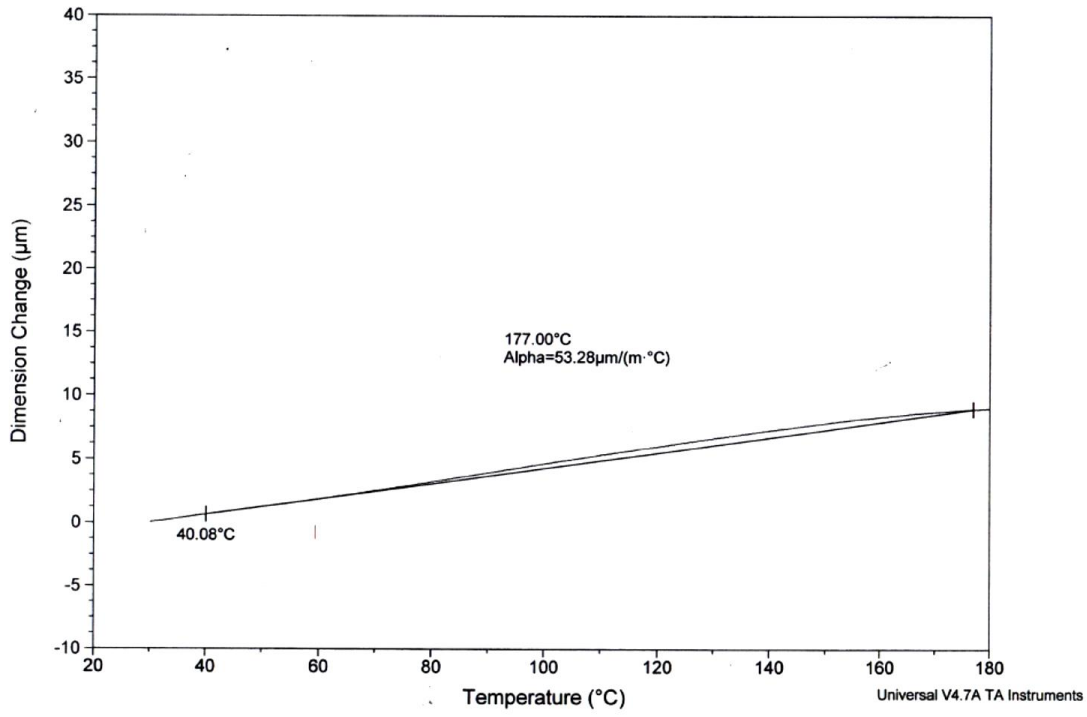

Figure 71. PEI Neat 1.1369mm Thickness.

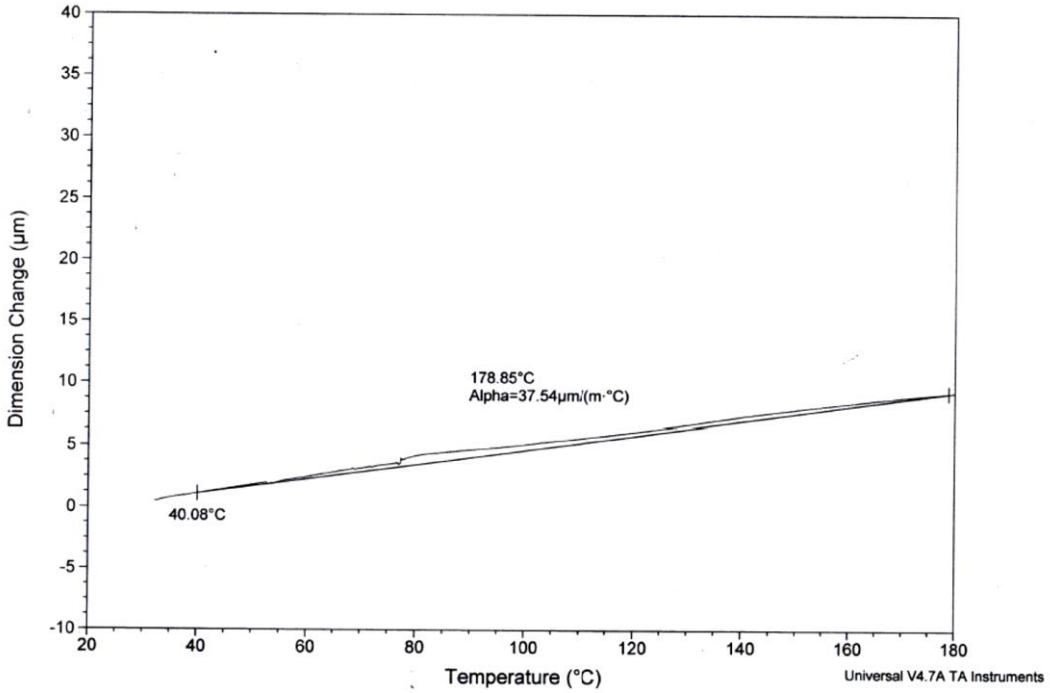

Figure 72. PEI 1% 40 1.5590mm thickness.

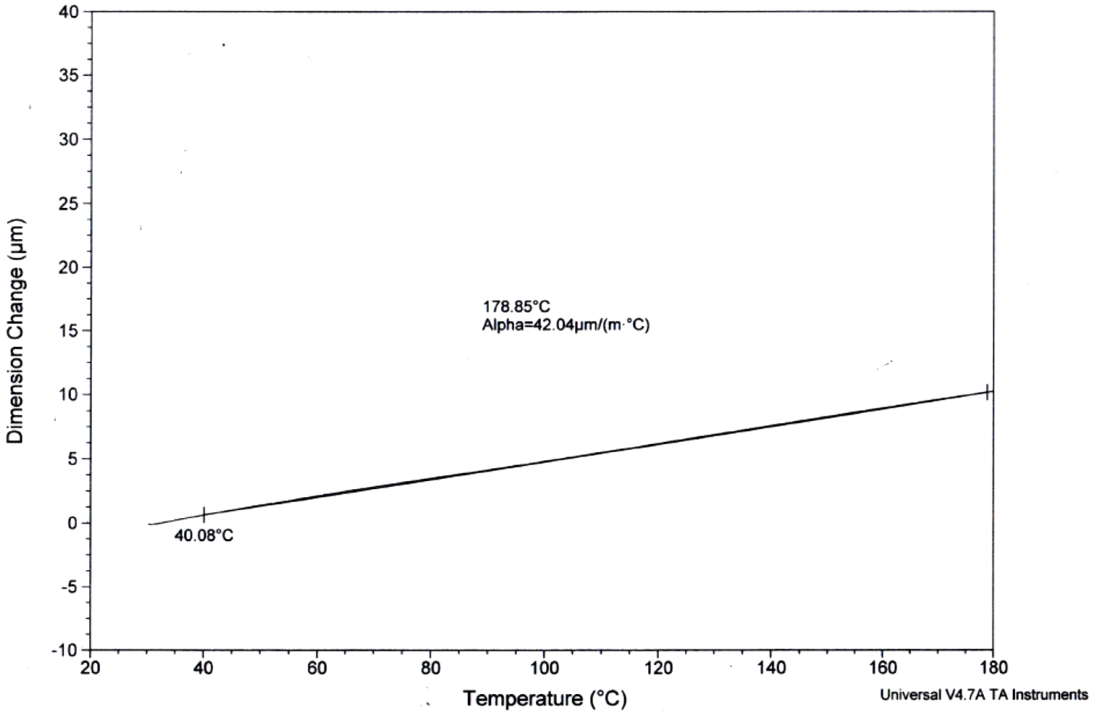

Figure 73. PEI 1%40 1.6300mm Thickness.

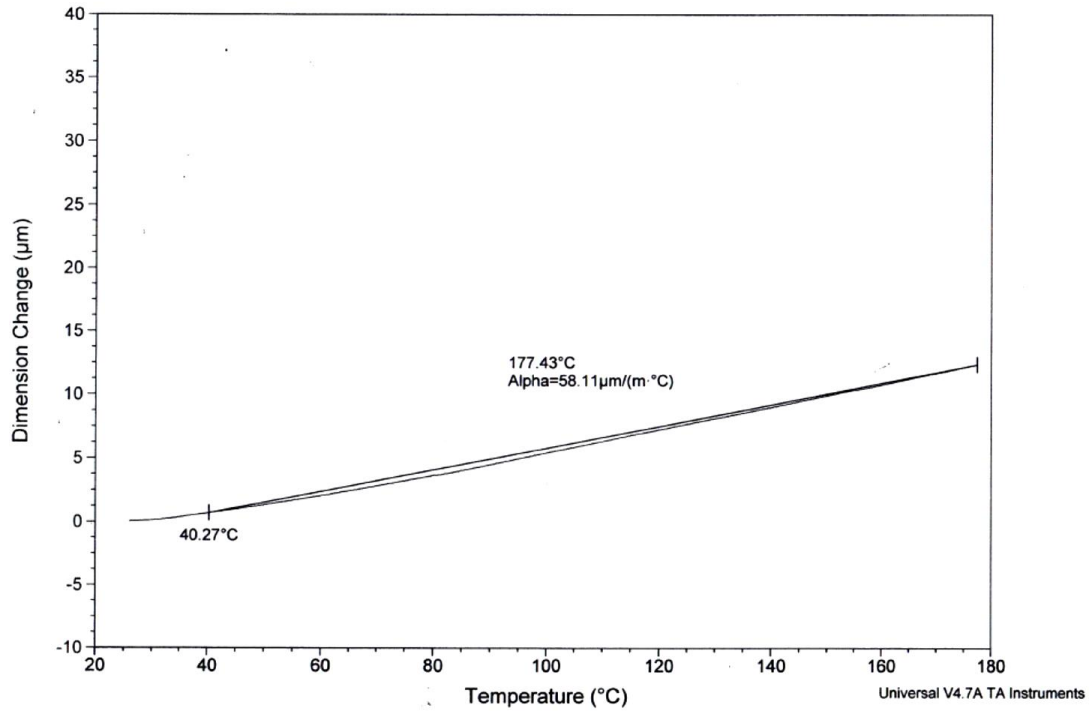

Figure 74. PEI 1% 40 1.4628 mm Thickness.

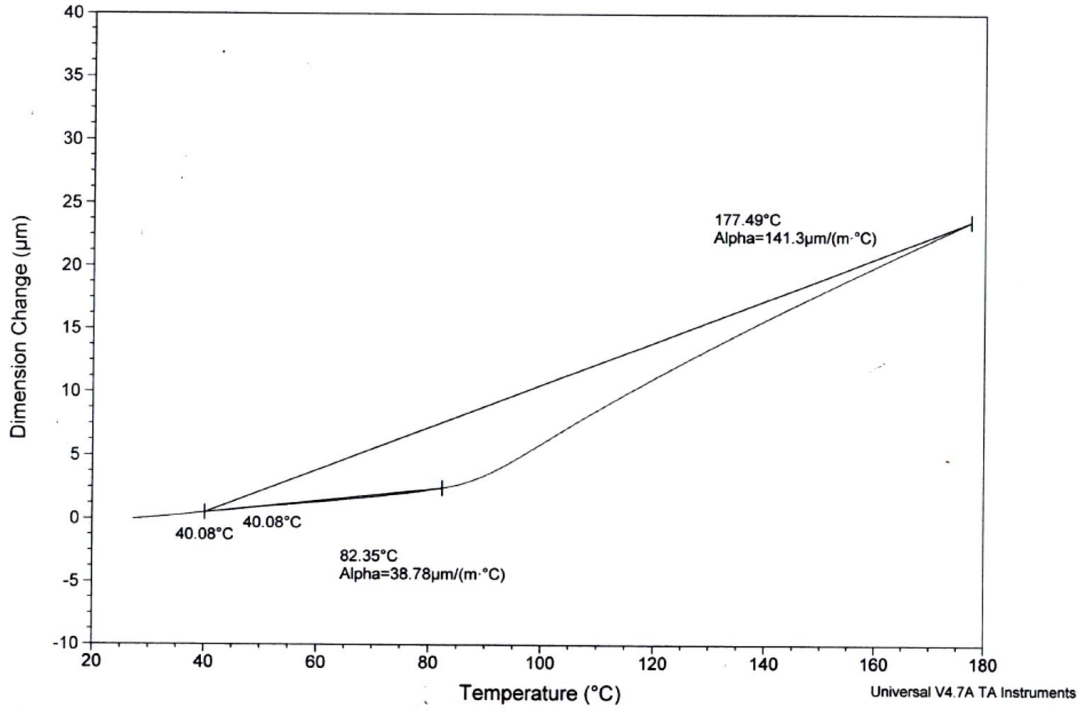

Figure 75. PEI 1%4080 1.1900mm Thickness.

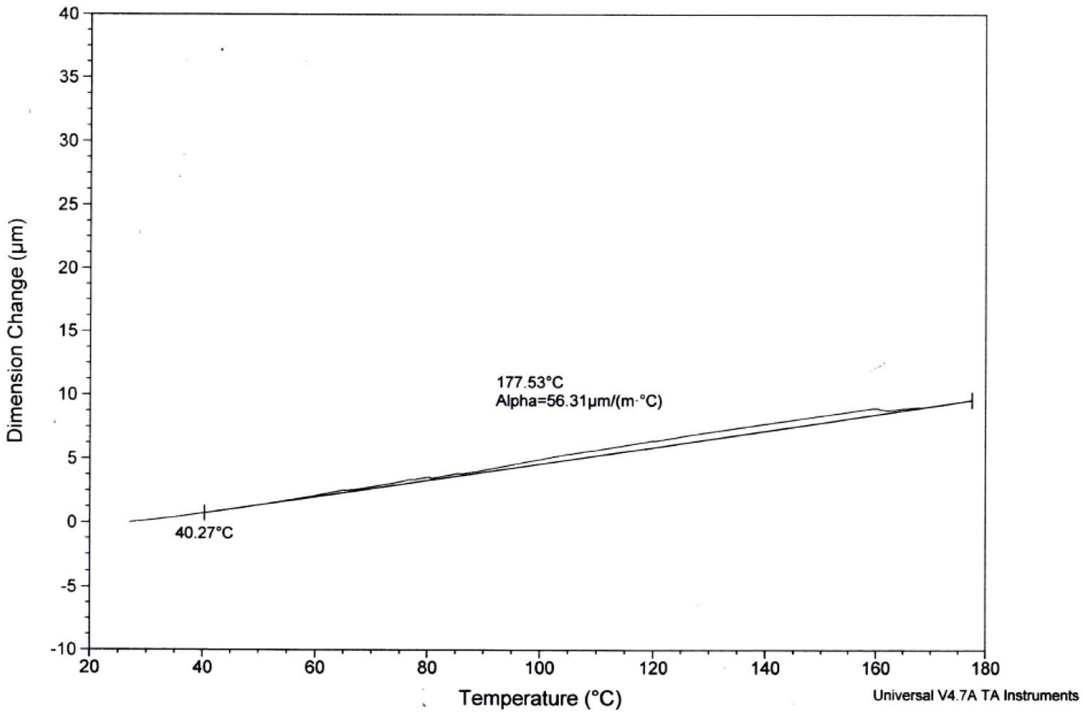

Figure 76. PEI 1%4080 1.1463 Thickness.

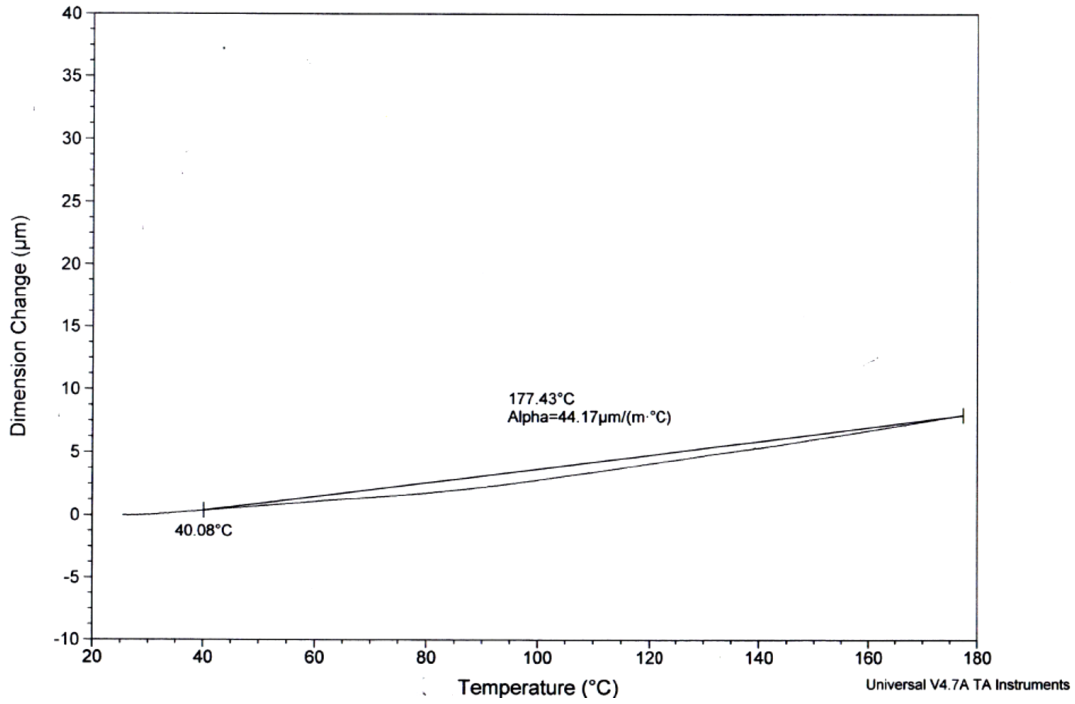

Figure 77. PEI 1%80 1.2463 mm Thickness.

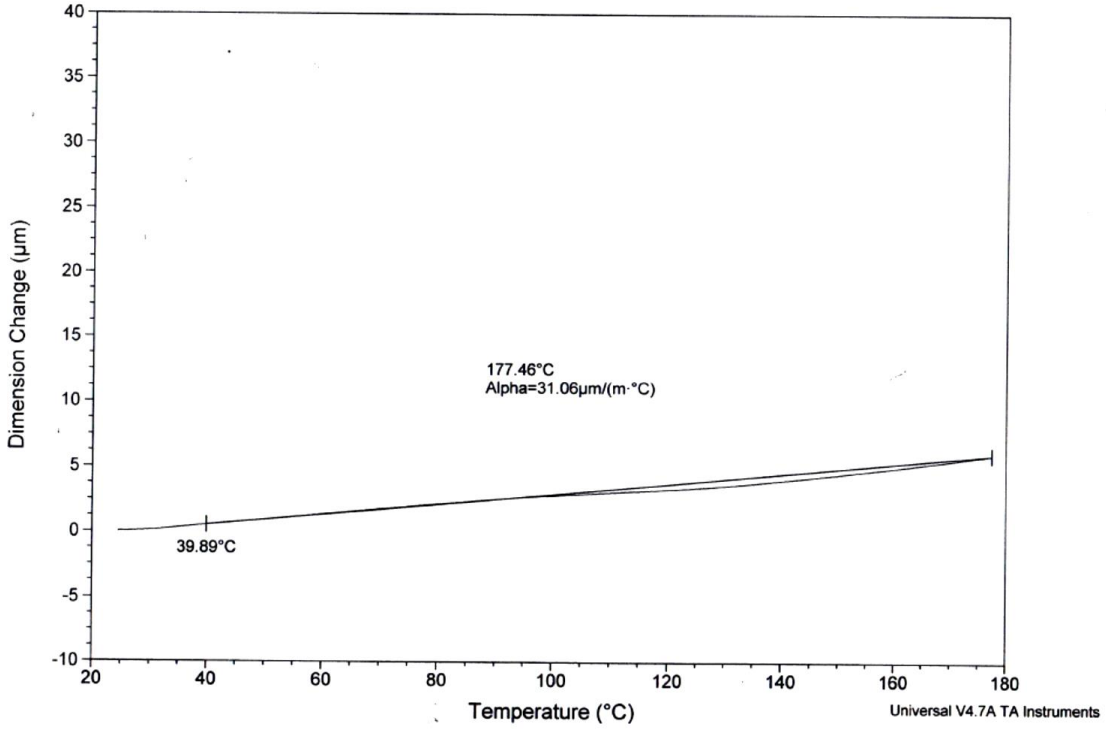

Figure 78. PEI 1% 80 1.2774 mm Thickness.

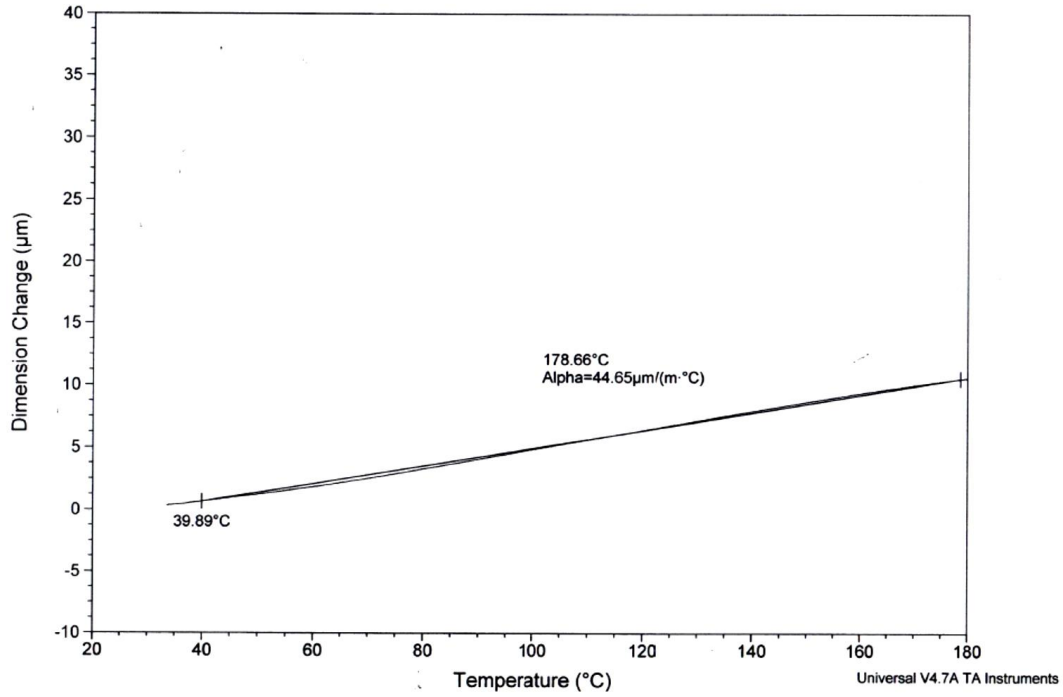

Figure 79. PEI 5% 40 1.5960 mm Thickness.

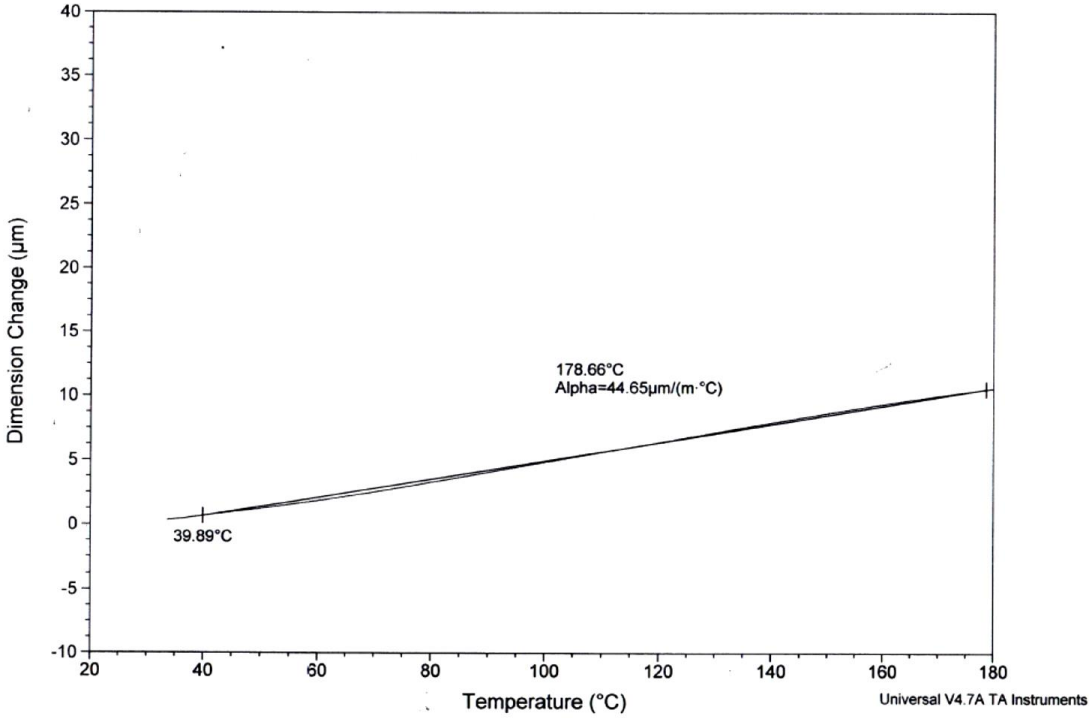

Figure 80. PEI 5% 40 1.5960 mm Thickness.

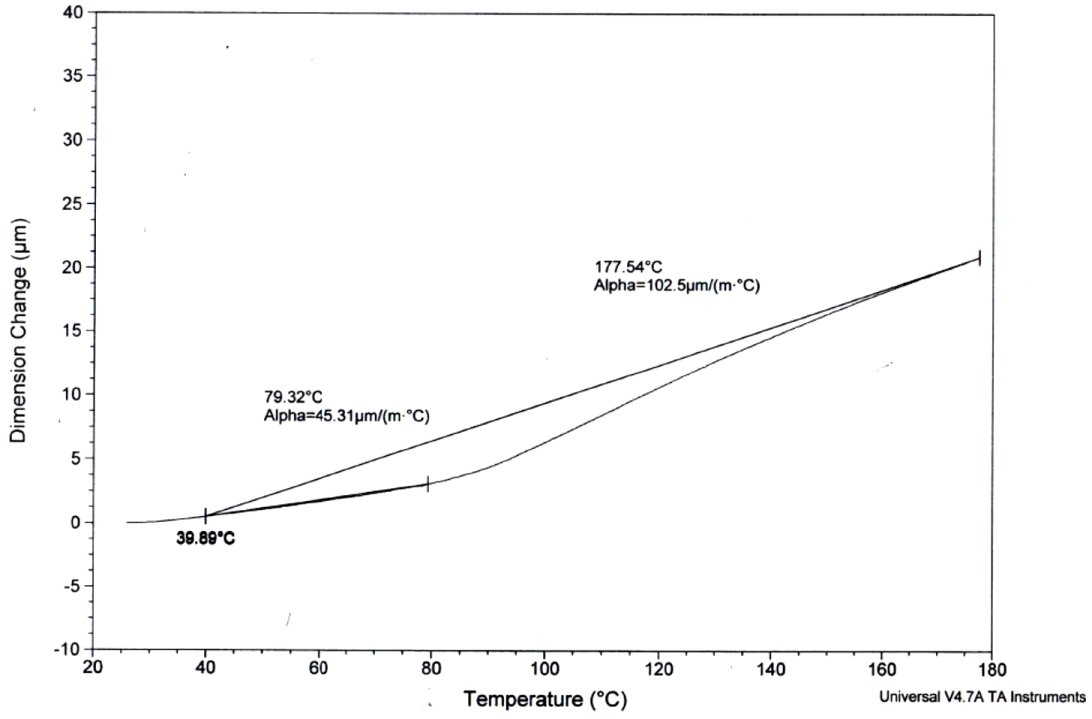

Figure 81. PEI 5% 40 1.4457mm Thickness.

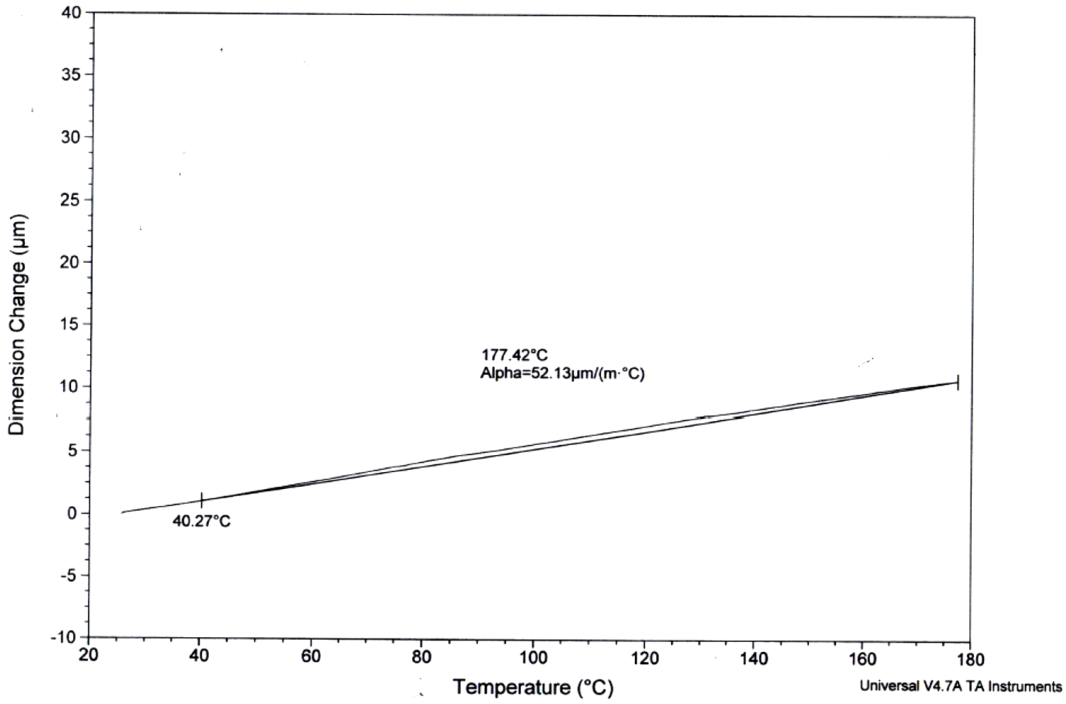

Figure 82. PEI 5%40-80 1.3499mm Thickness.

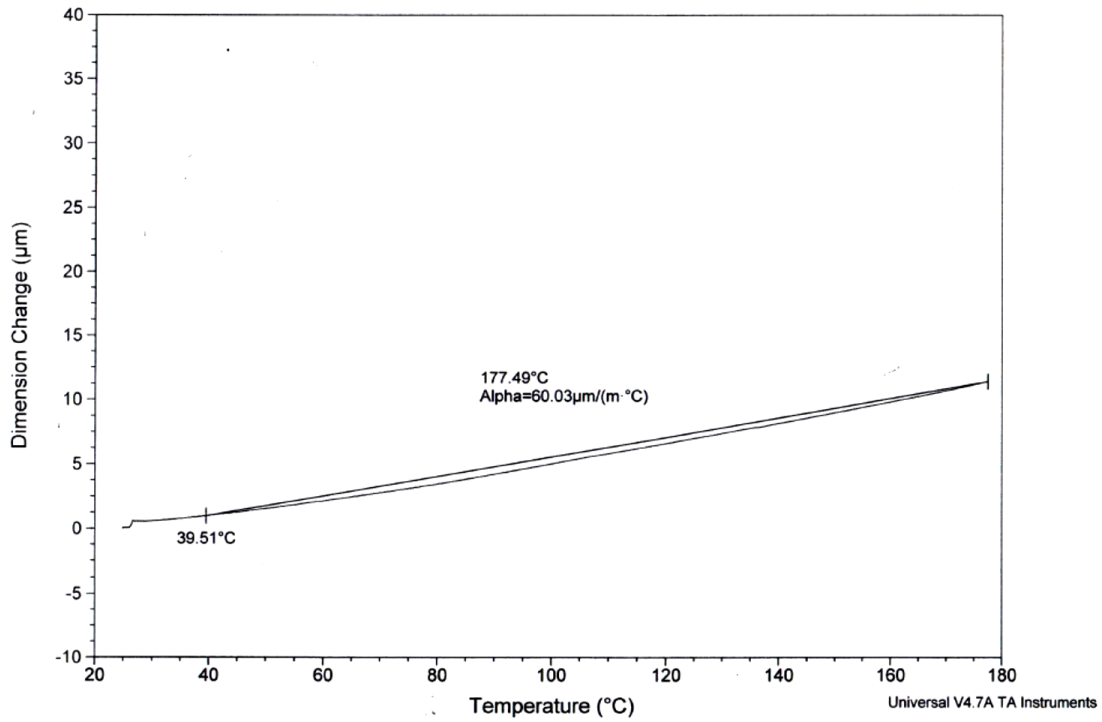

Figure 83. PEI 5% 4080 1.2583mm Thickness.

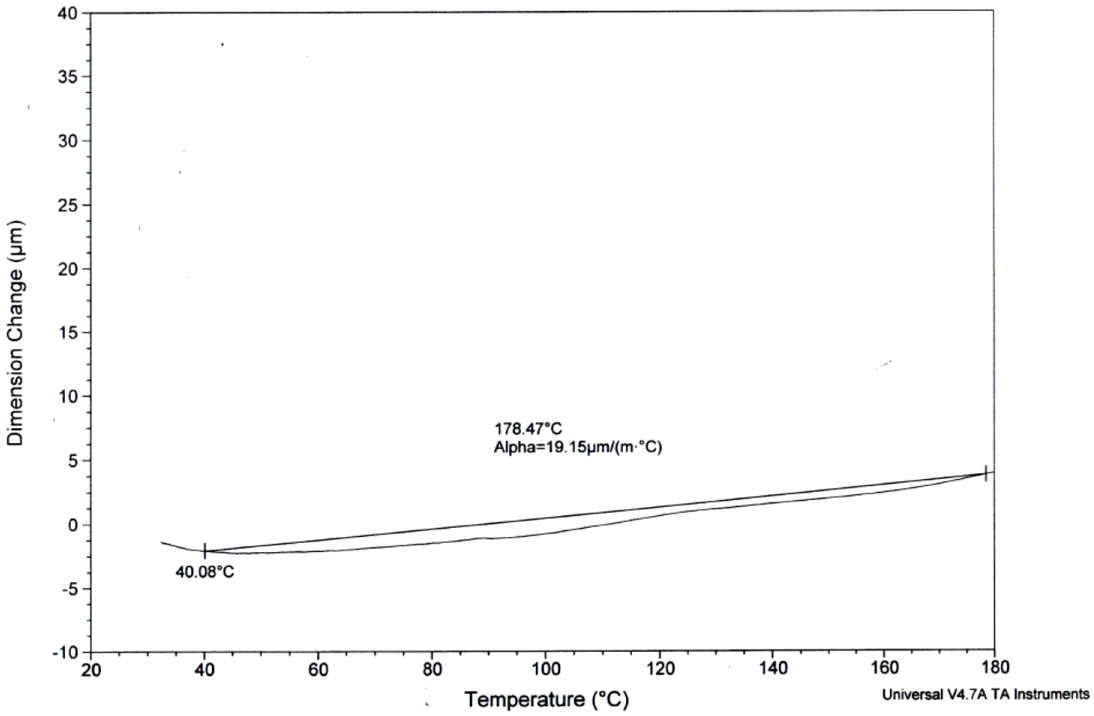

Figure 84. PEI 5% 80 2.2122 mm Thickness.

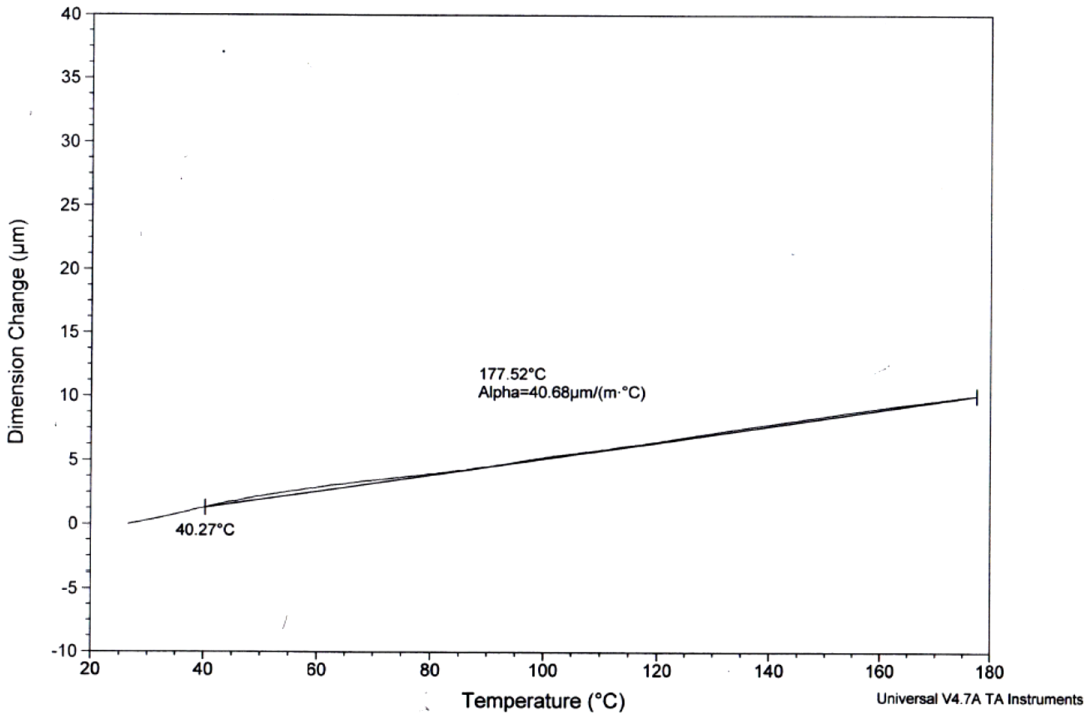

Figure 85. PEI 5% 80 1.5716mm Thickness.

Epoxy results

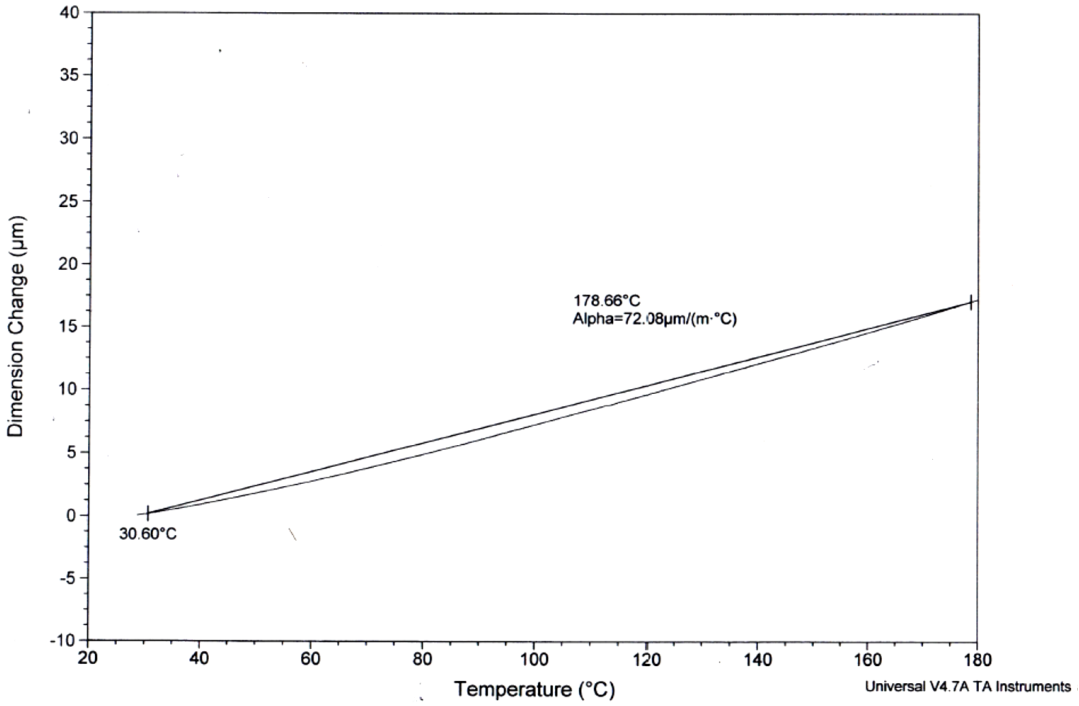

Figure 86. Epoxy Neat 1.5800 Thickness.

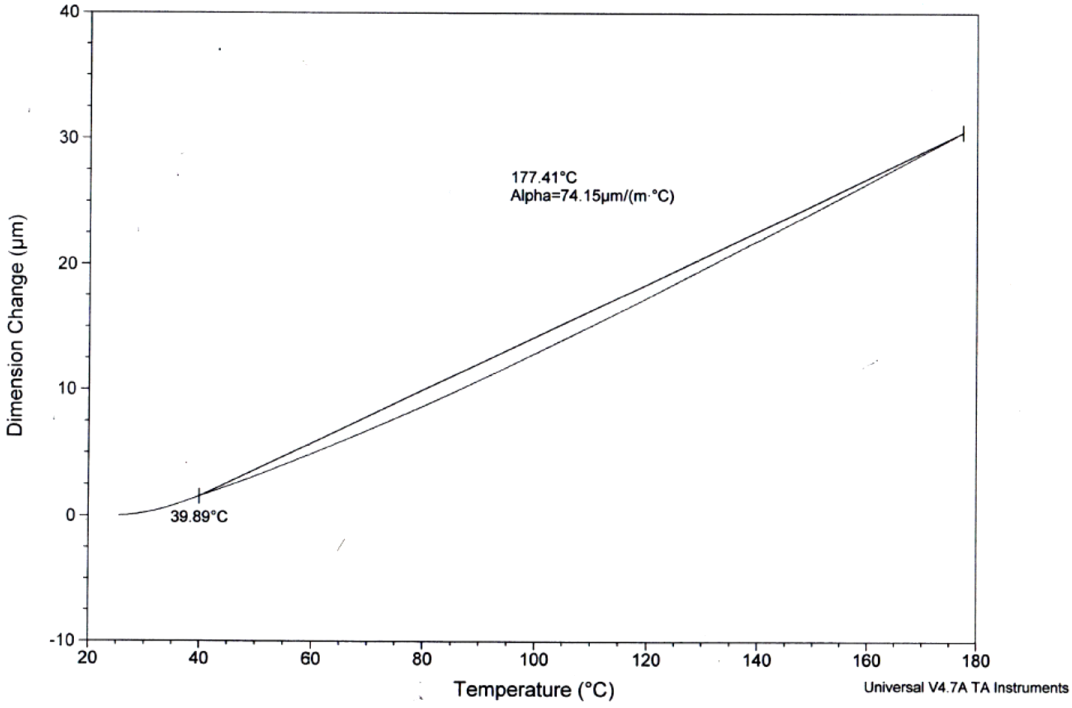

Figure 87. Epoxy 1%40-80 2.8425mm Thickness.

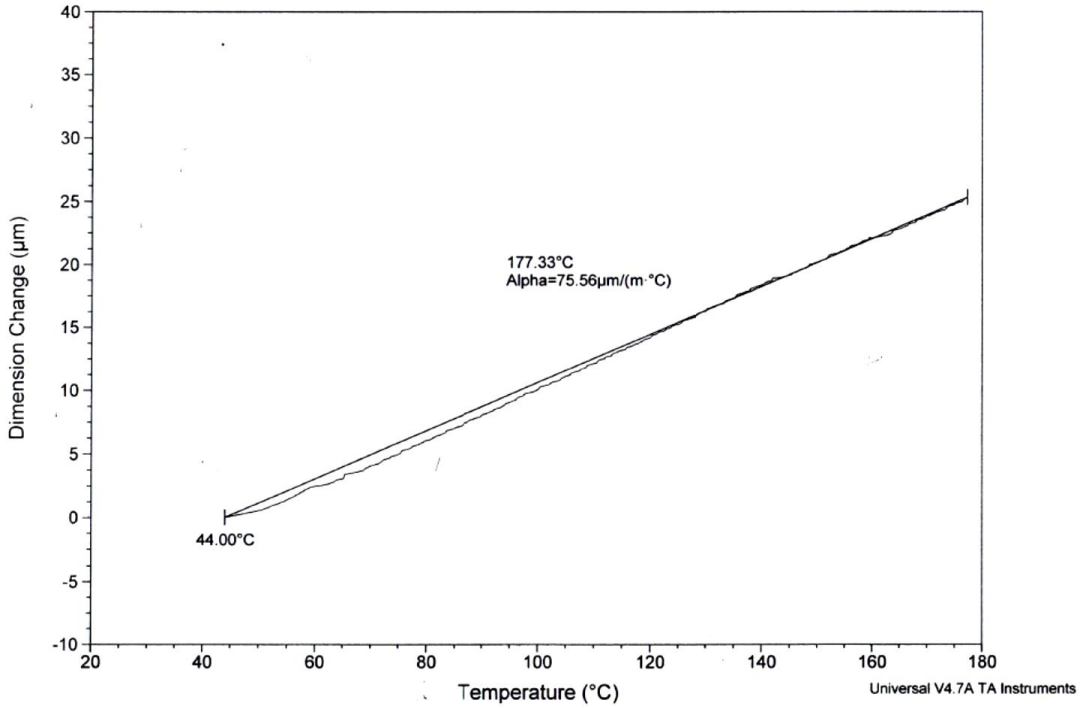

Figure 88. Epoxy 1%40-80 2.5112mm Thickness.

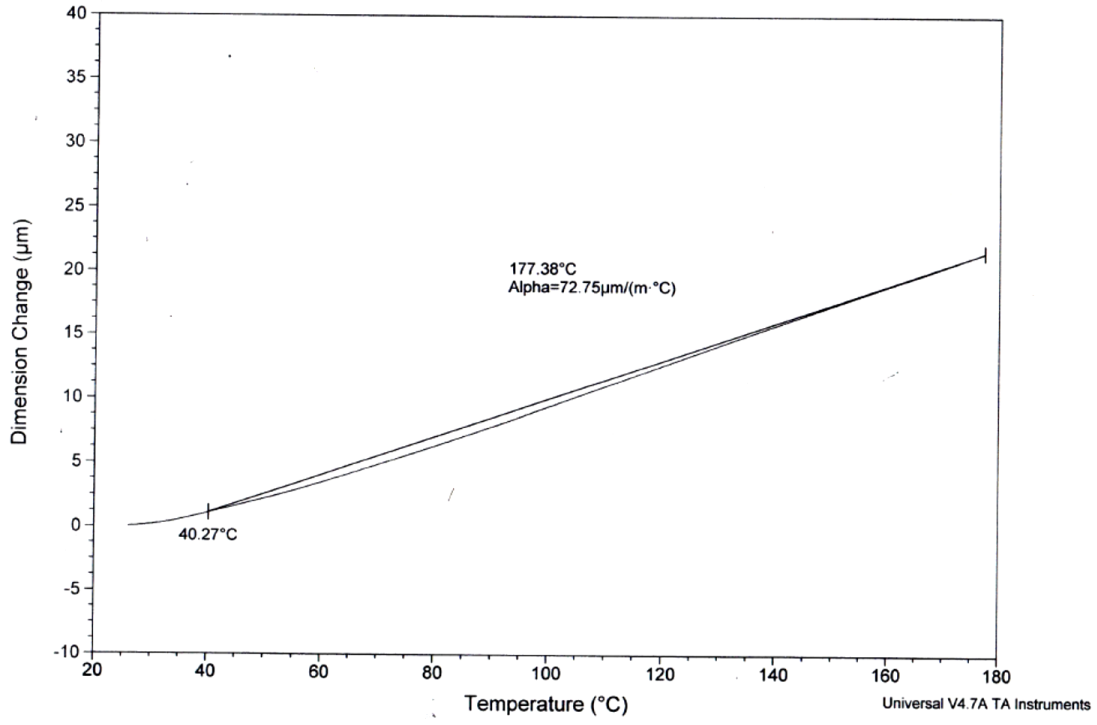

Figure 89. Epoxy 1%80 2.0511mm Thickness.

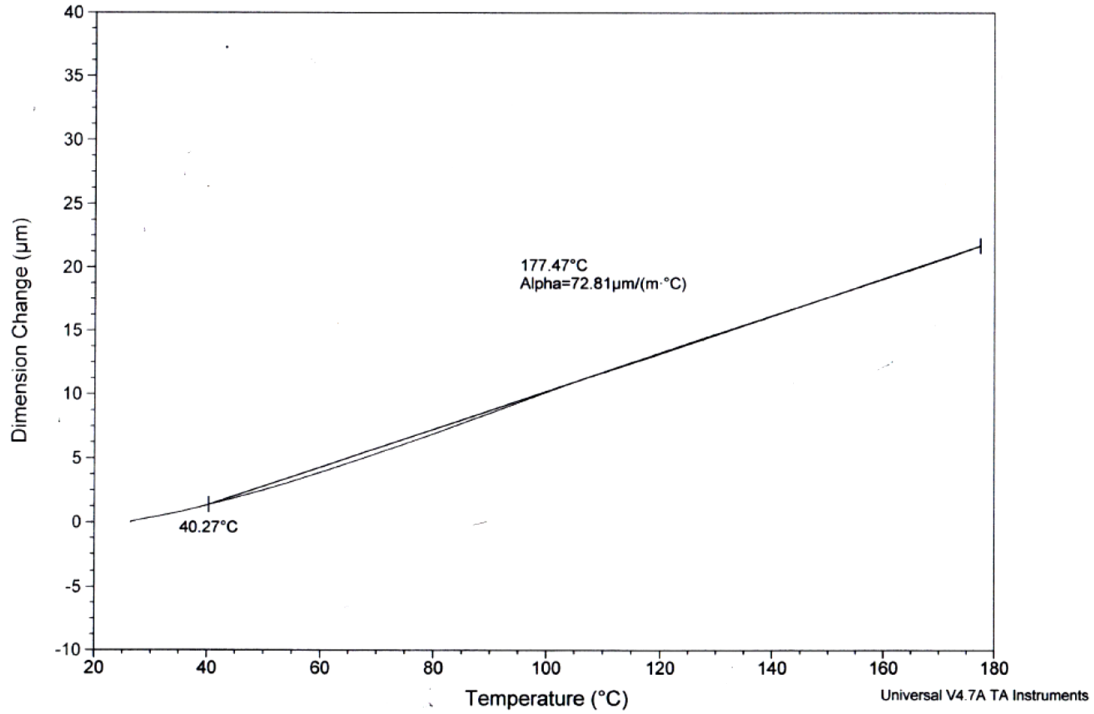

Figure 90. Epoxy 1%80 2.0355mm Thickness.

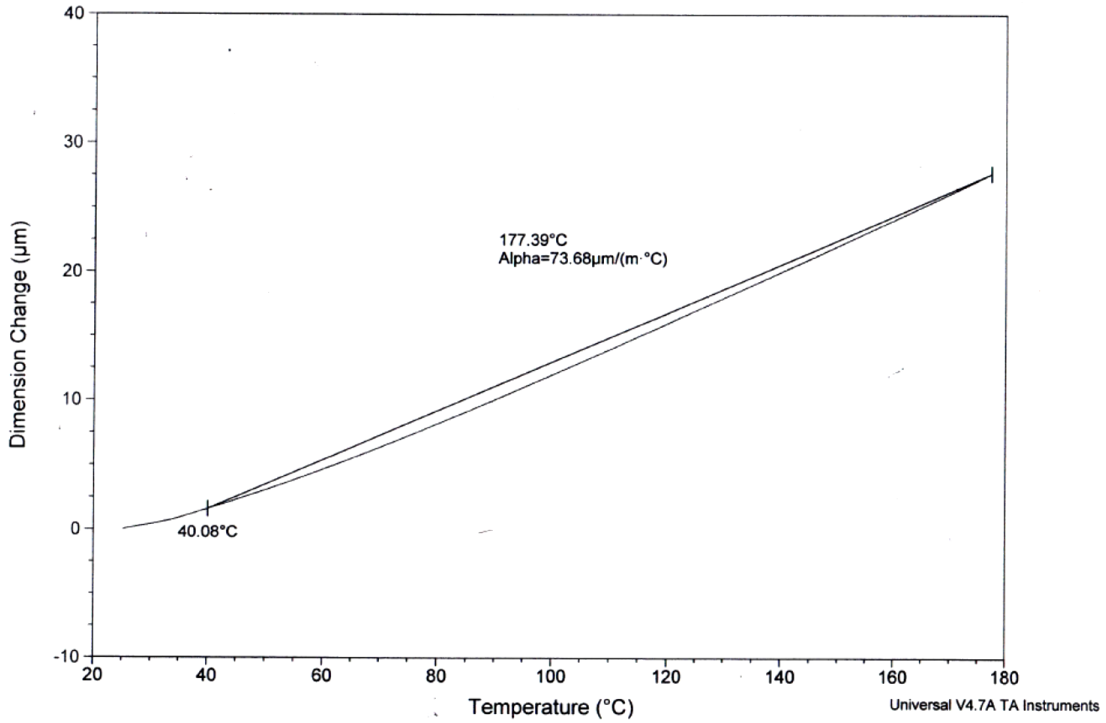

Figure 91. Epoxy 5%4080 2.5780mm Thickness.

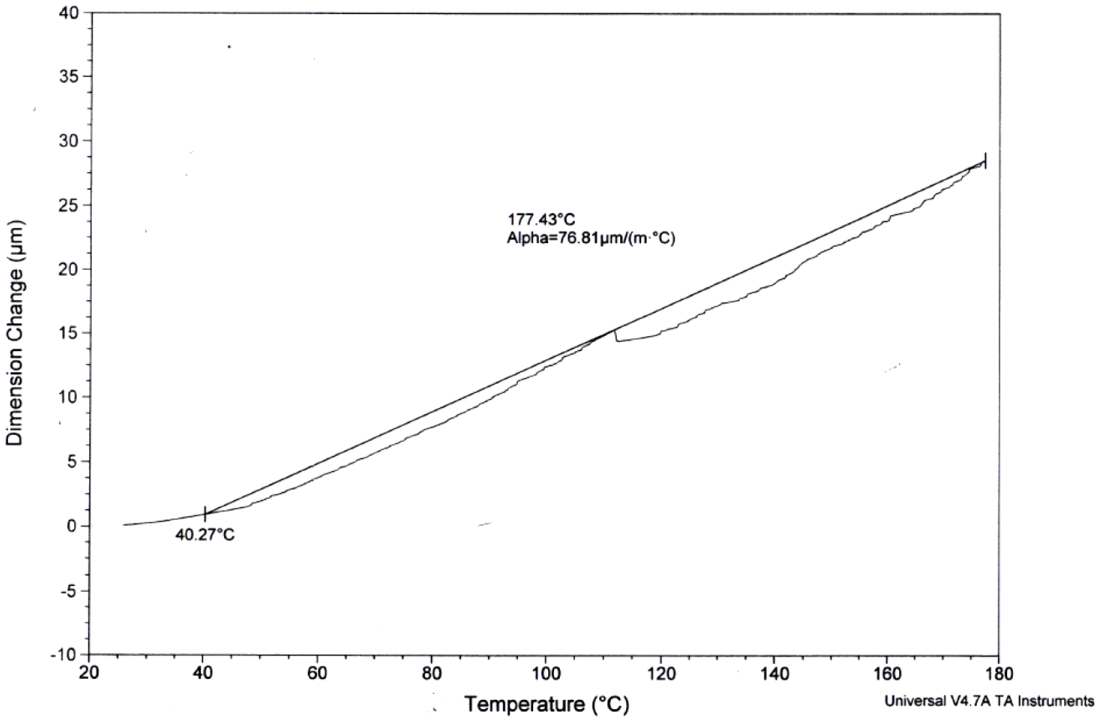

Figure 92. Epoxy 5%4080 2.6211mm Thickness.

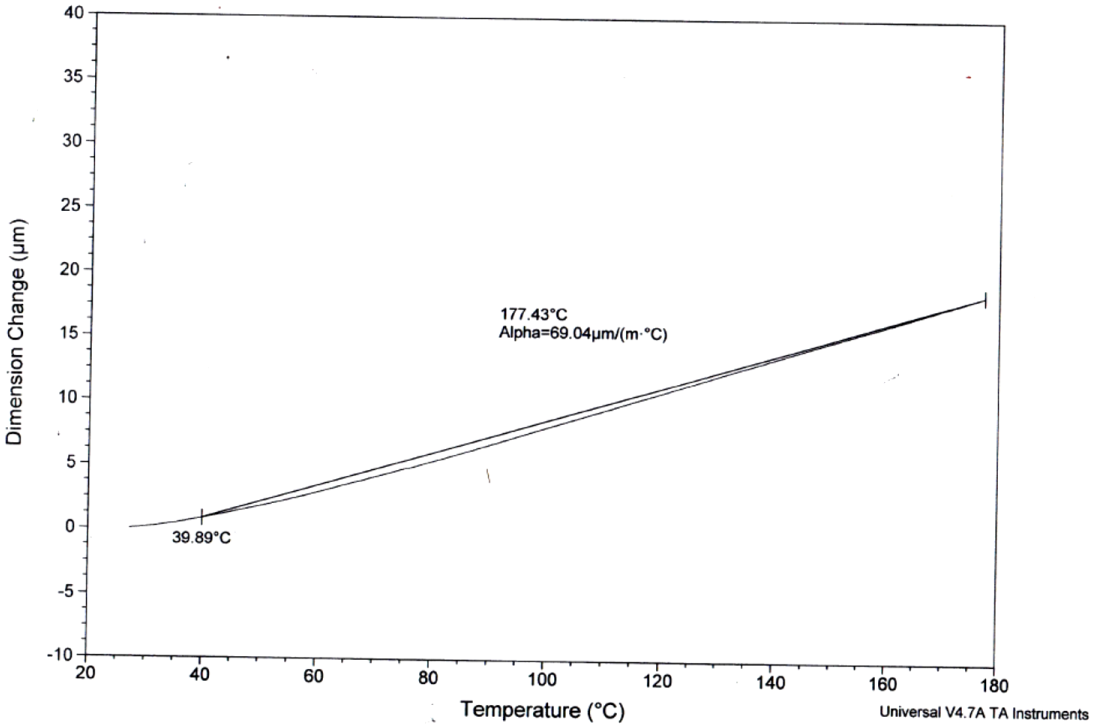

Figure 93. Epoxy 5%80 1.8663mm Thickness.

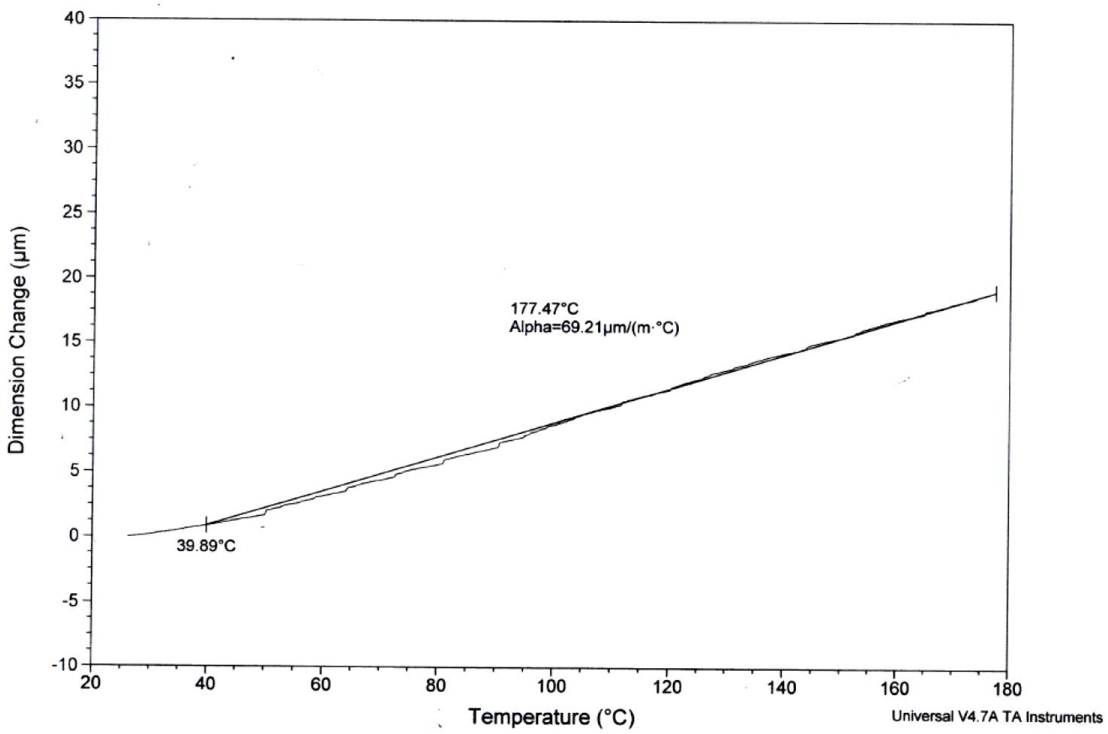

Figure 94. Epoxy 5%80 1.9177mm Thickness.

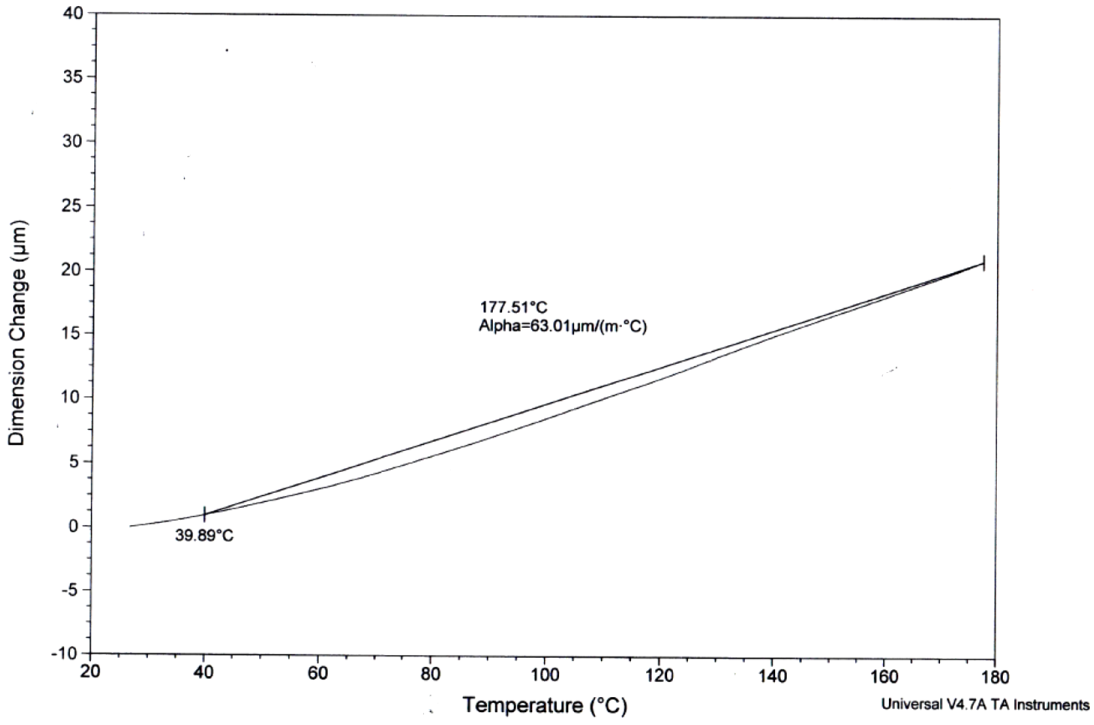

Figure 95. Epoxy 10%4080 2.3033mm Thickness.

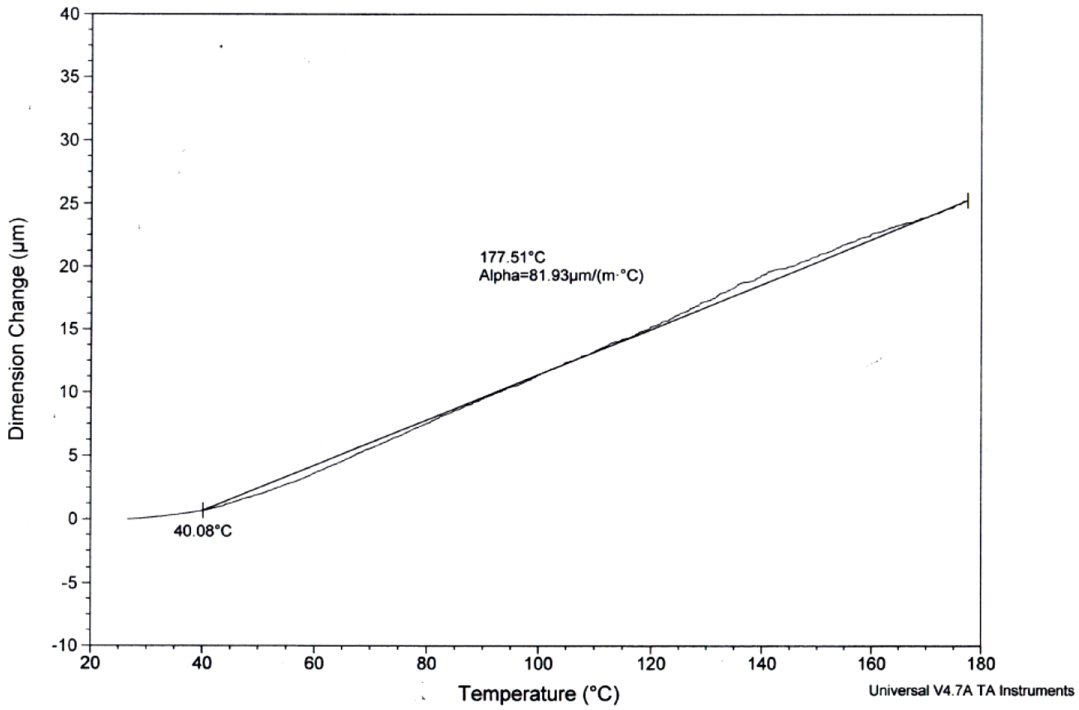

Figure 96. Epoxy 10%4080 2.1847mm Thickness.

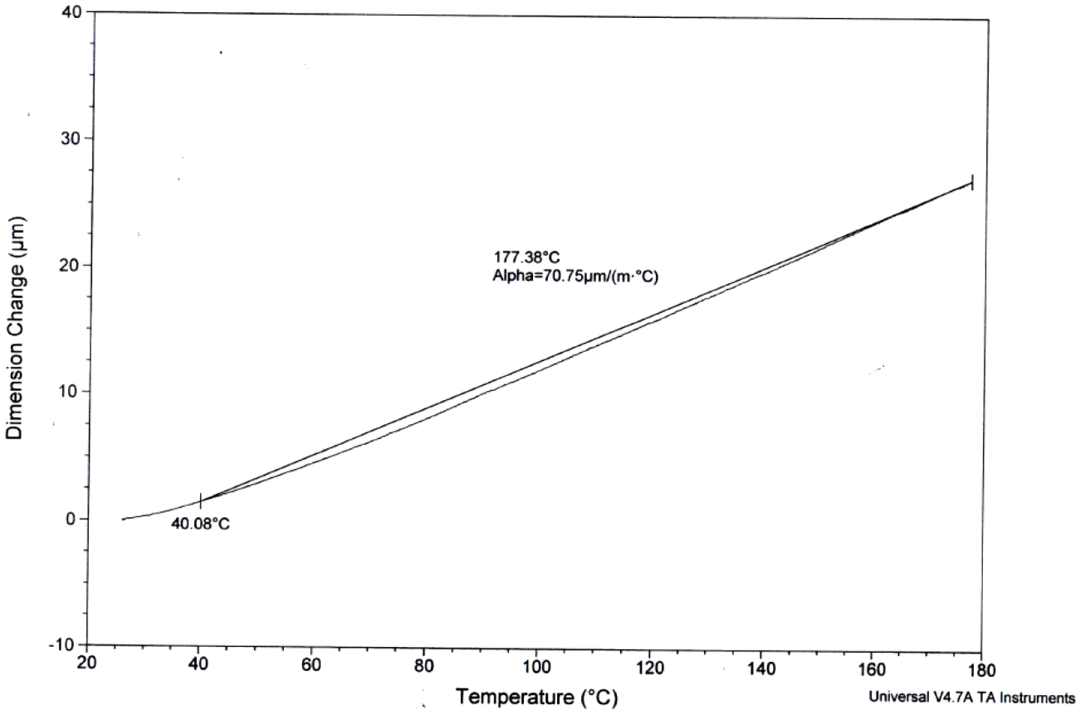

Figure 97. Epoxy 10%80 2.6429mm Thickness.

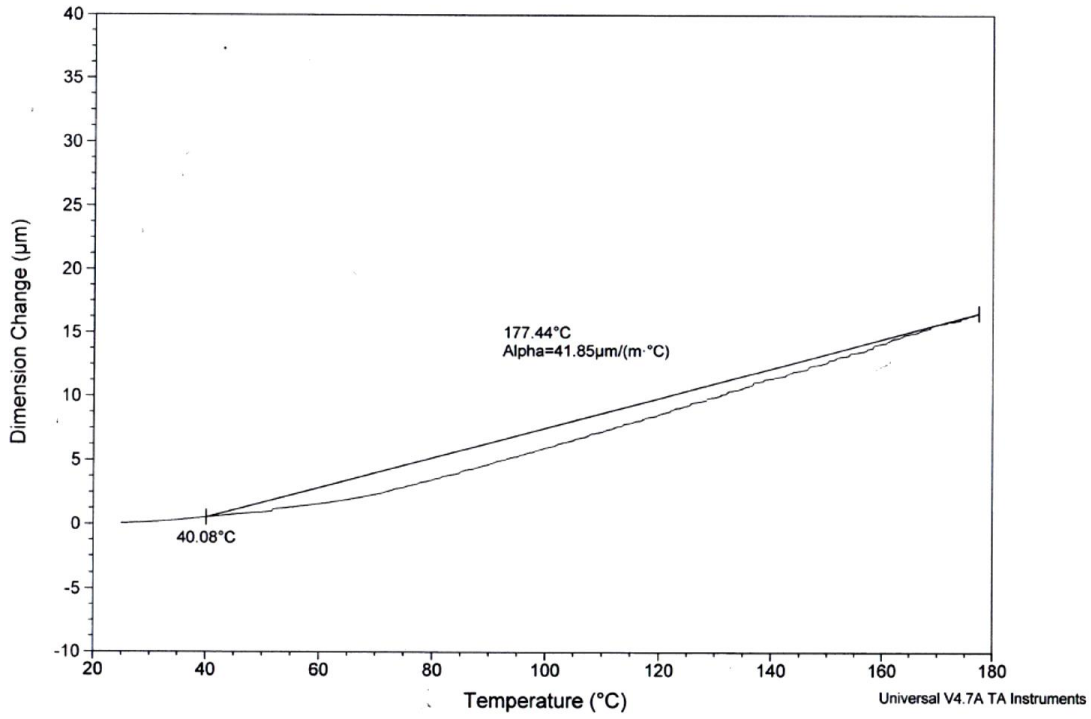

Figure 98. Epoxy 10%80 2.7868mm Thickness.

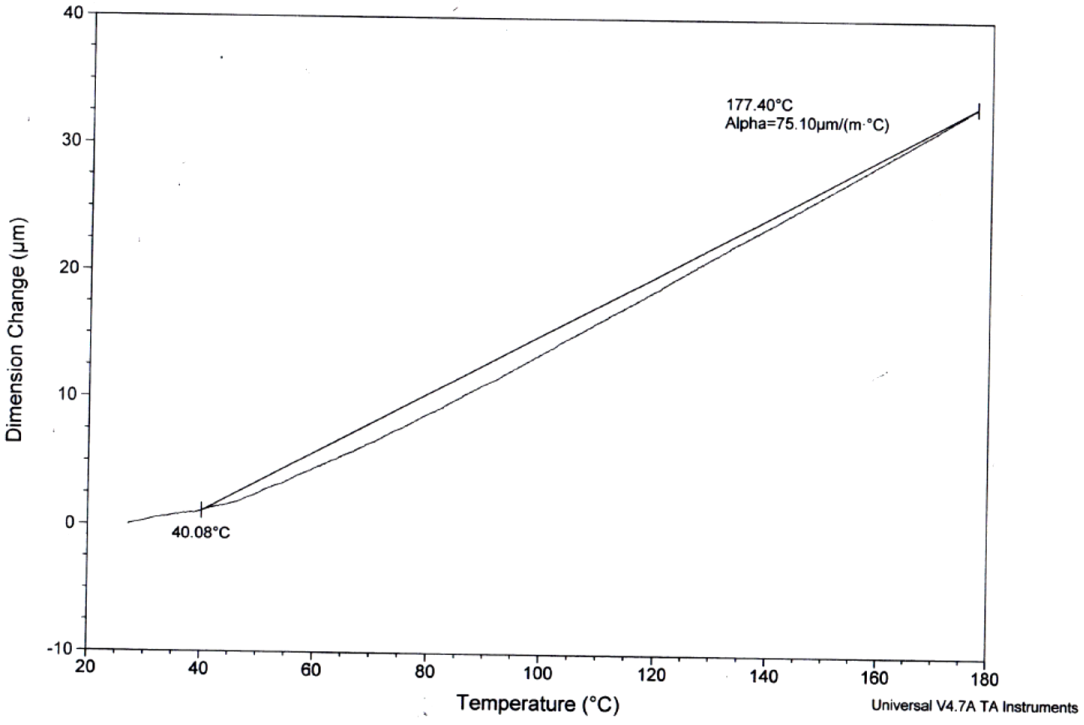

Figure 99. Epoxy 20%4080 3.1153mm Thickness.

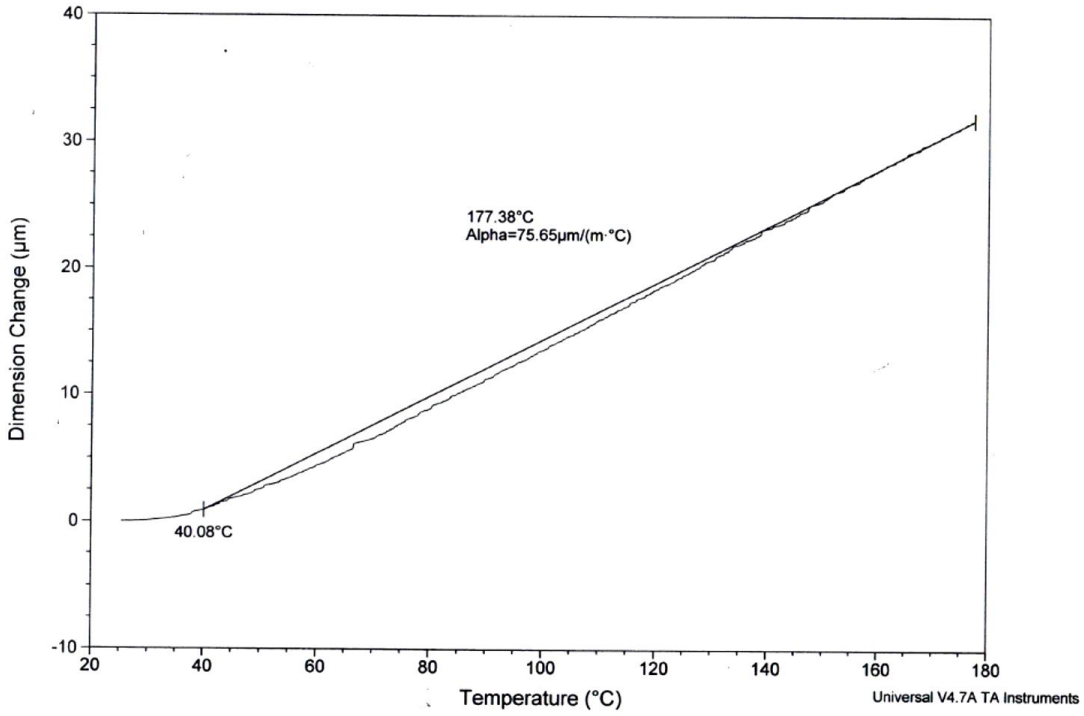

Figure 100. Epoxy 20%4080 2.9722mm Thickness.

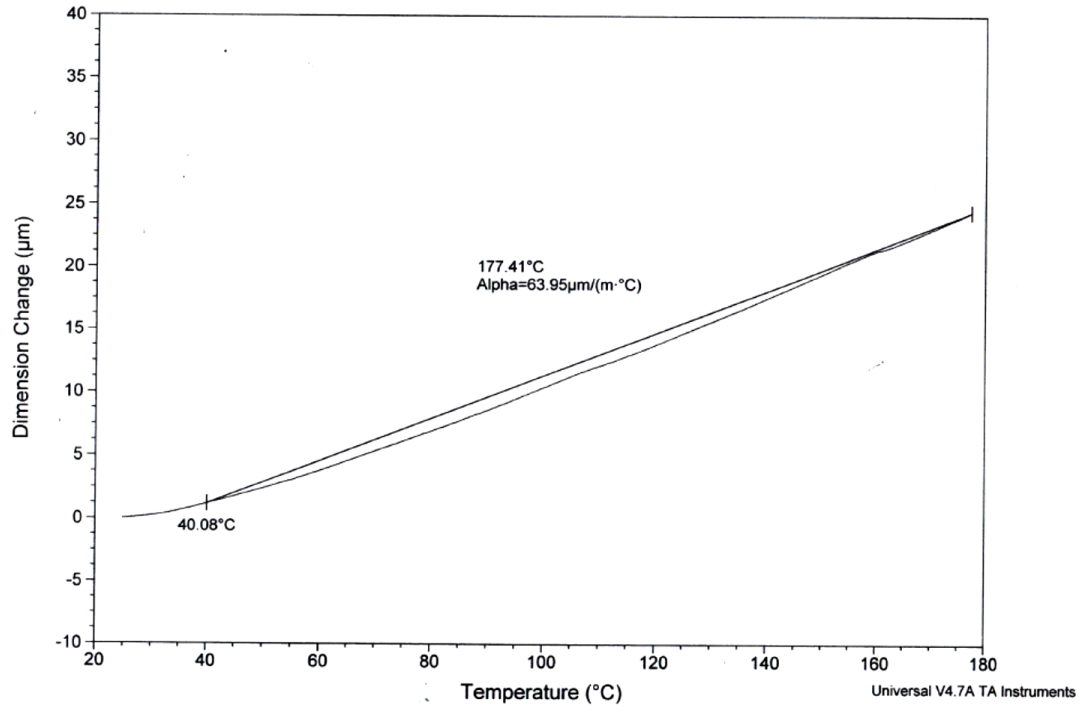

Figure 101. Epoxy 20%80 2.6457mm Thickness.

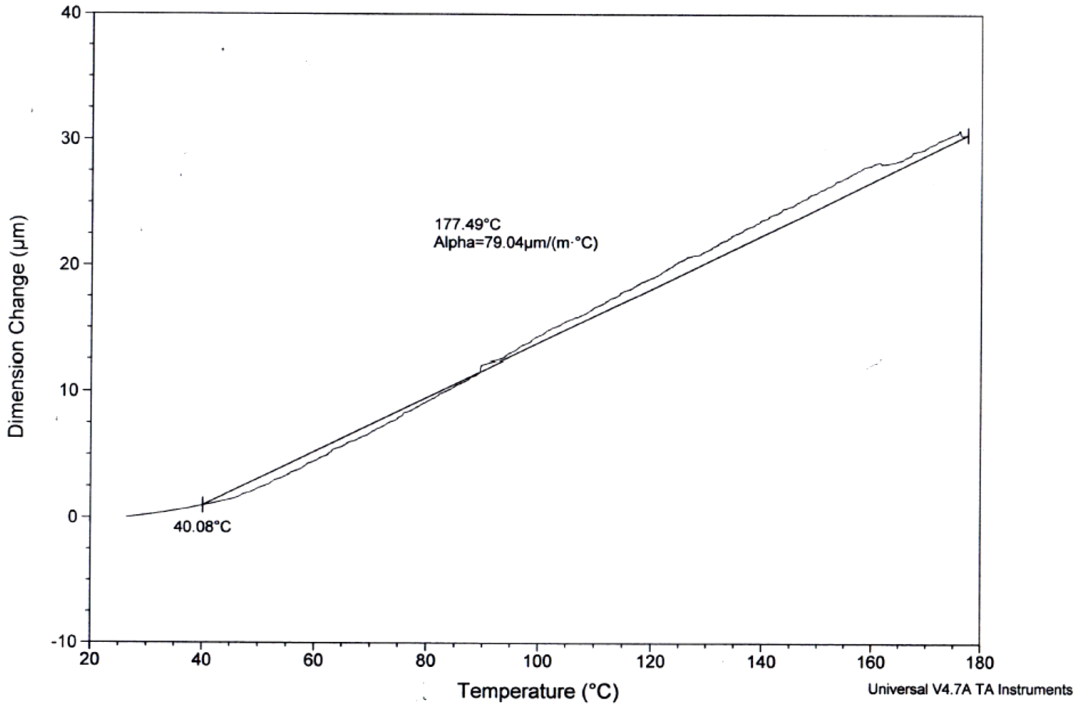

Figure 102. Epoxy 20% 80 2.7110 Thickness.

APPENDIX B

RDA RAW DATA

This appendix contains the raw data taken form the AERES TE Instruments RDA.

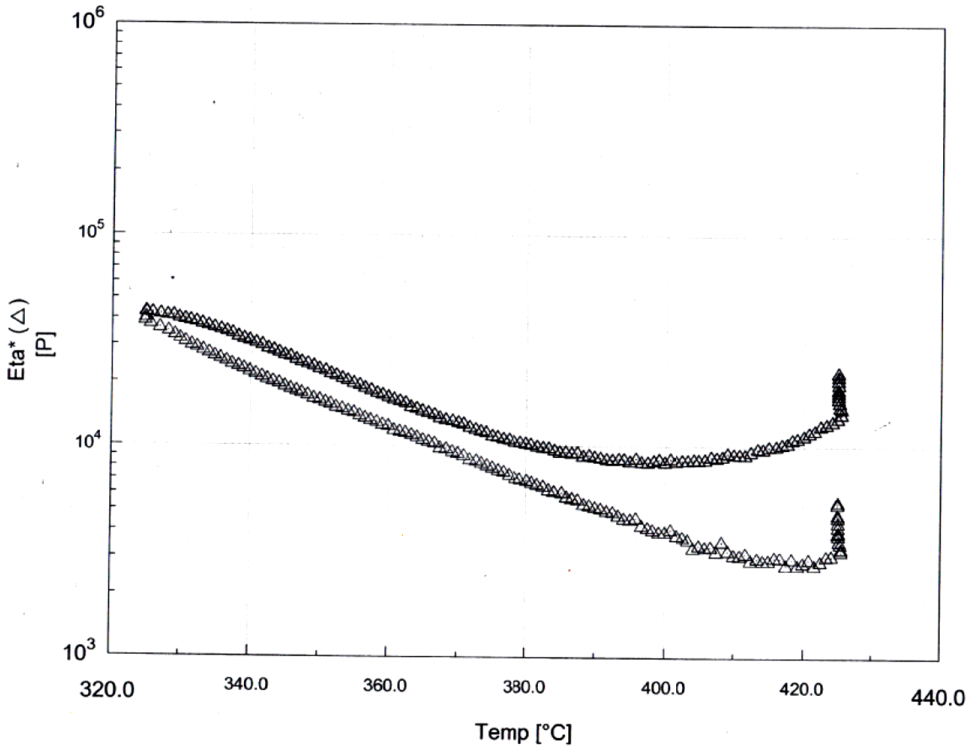

Figure 103. PEI 5%80 Two Samples.

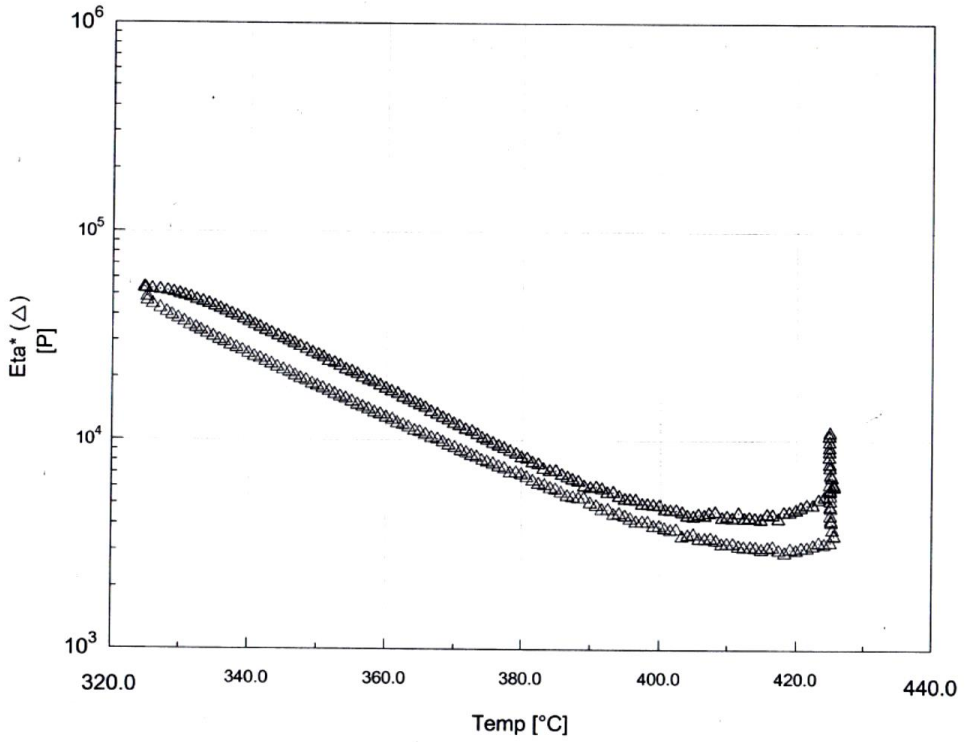

Figure 104. PEI 5%4080 Two Samples.

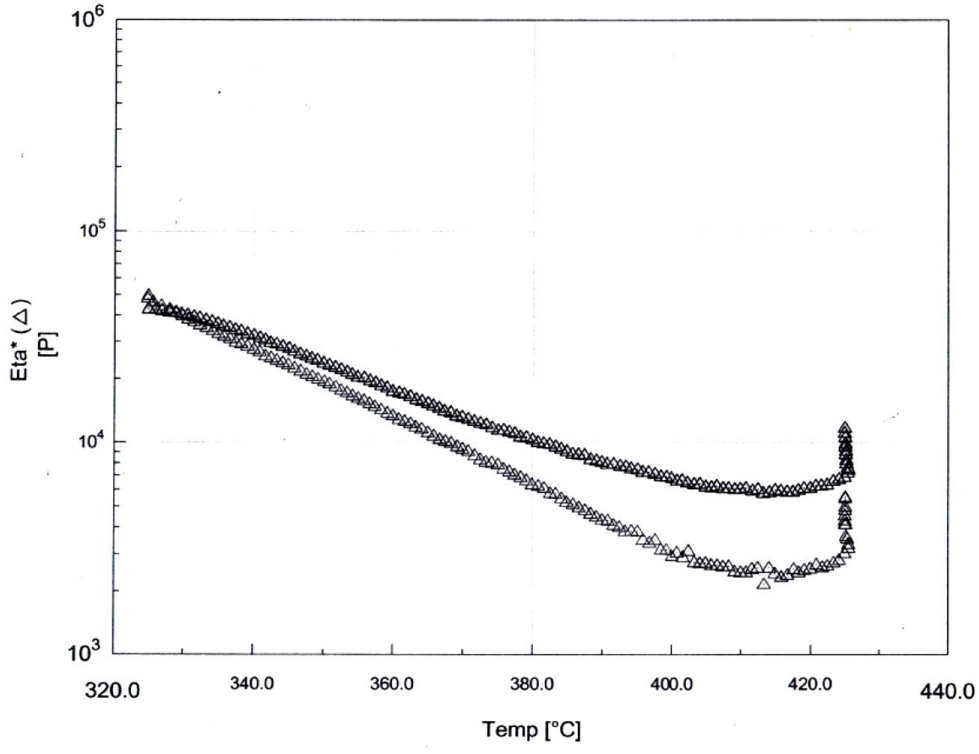

Figure 105. PEI 1%4080 Two Samples.

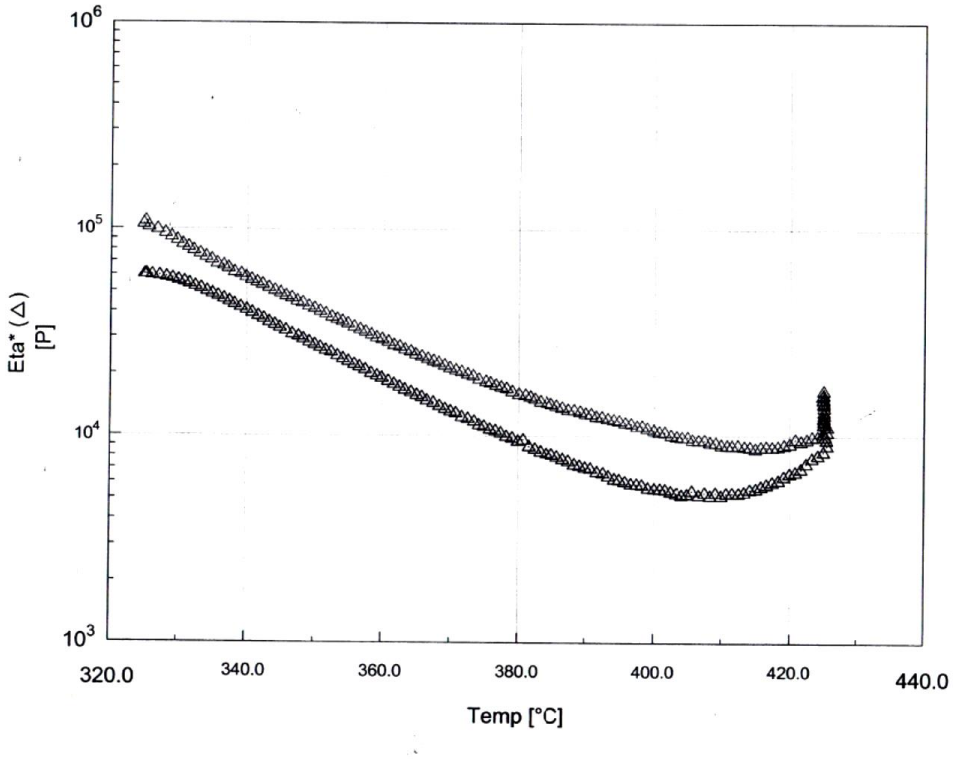

Figure 106. PEI 5%40 Two Samples.

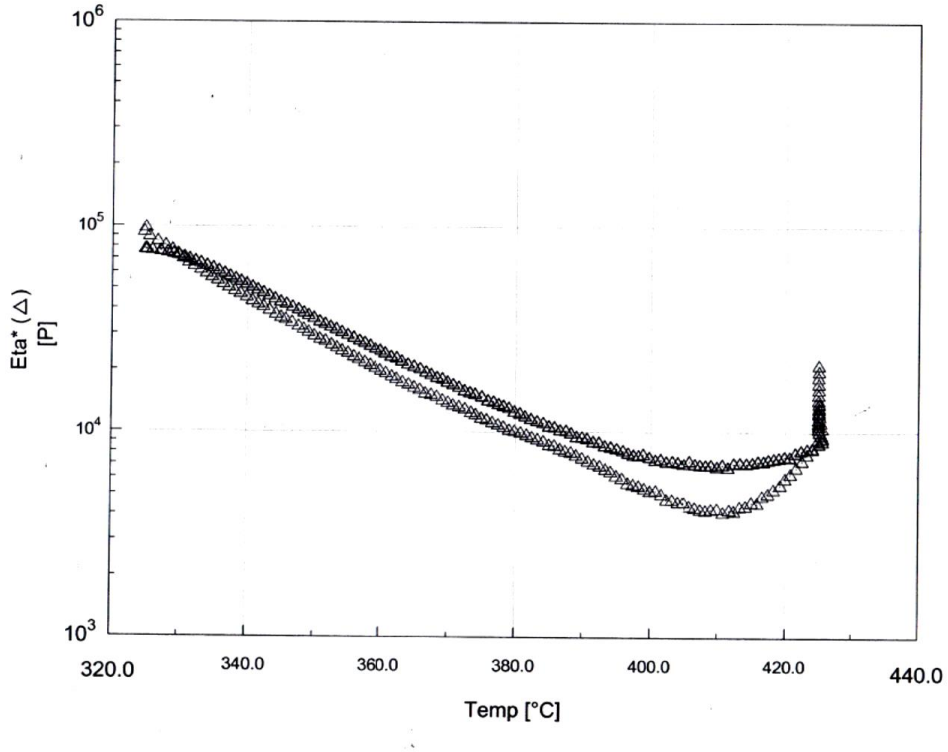

Figure 107. PEI 1%40 Two Samples.

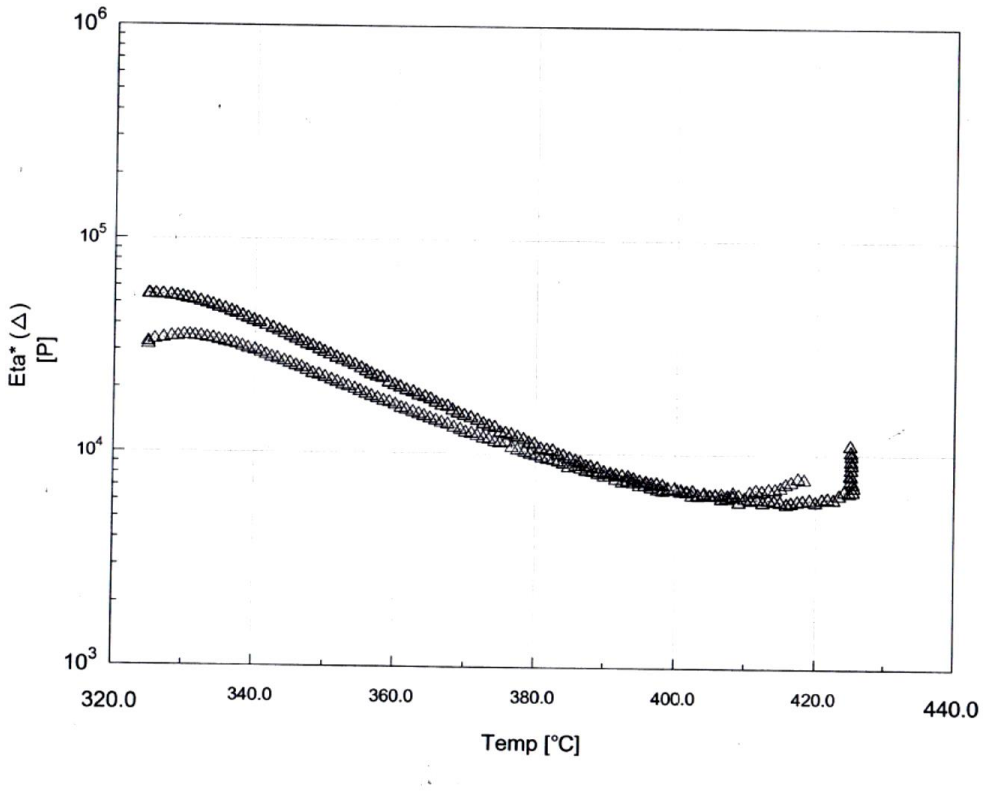

Figure 108. PEI Neat Two Samples.

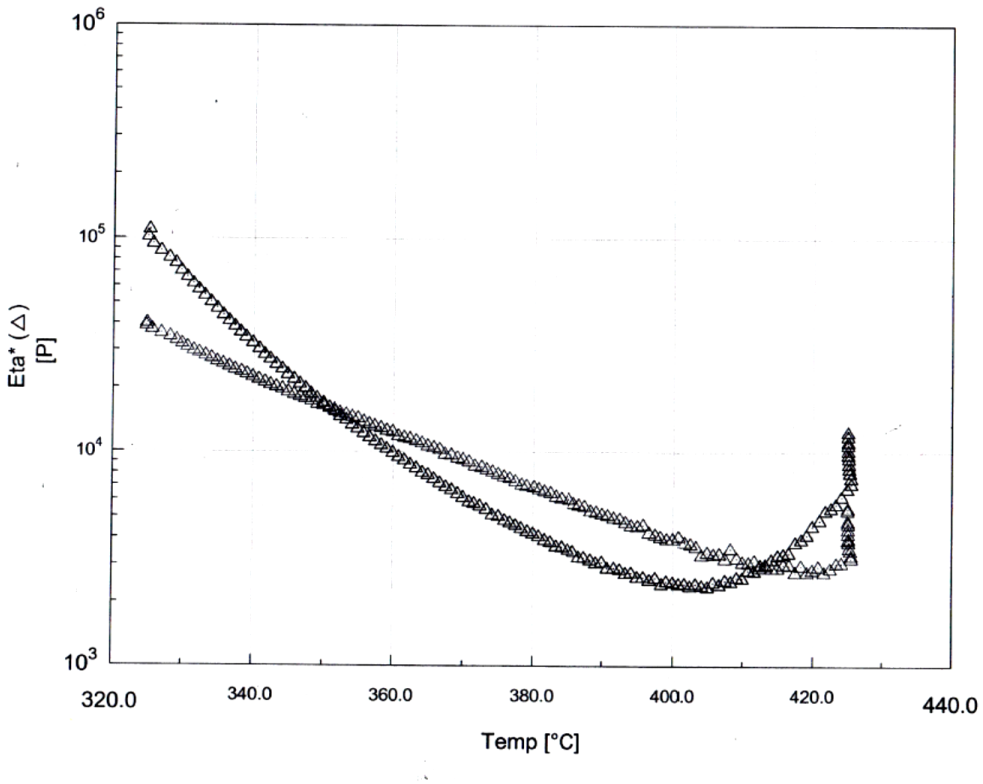

Figure 109. PEI 1%80 Two Samples.

BIBLIOGRAPHY

Campbell, D., R. A. Pethrick, and J. R. White. *Polymer Characterization Pysical Techniques.* 2nd. Boca Raton, Florida: CRC Press, 2000.

Goodfellow. “Epoxy Coposites.” Accessed January 14, 2014. www.goodfellow.com.

Hashin, Zvi. "The Elastic Moduli of Heterogeneous Materials." *Applied Machanics* (1962): 143-150.

Hashin, Zvi, and B W Rosen. "The Elastic Moduli of Fiber-reinforced Materials." *Applied Mechanics* (1964): 223-232.

Matweb. “Steel thermal Expansion.” Accessed January 14, 2014. www.matweb.com.

Massey, Justin, Ed Haris, Stephen Pacheco, and Mark Heacock. 2011. "Rapid Prototype Tooling for Hat Stiffener Repair." *NAVAIR 4.3 Conference.* North Island. 26.

Massey, Justin, Mark Heacock, and Ed Harris. "NV Composite - NAVAIR CRADA Work Update." *NAVAIR 4.3 Conference.* North Island, 2014.

Odian, George. *Principles of Polymerization.* 4th. Hoboken, New Jersey: John Wiley & Sons, Inc., 2004.

Schott. “Nextrema.” Accessed January 14, 2014. www.schott.com/nextrema

TA Instruments. "TMA." *TA Instruments.* Accessed July 14, 2014. http://www.tainstruments.com/pdf/TMA.pdf.

Tognana, S, W Salgueiro, A Somoza, J A Pomarico, and H F Ranea-Sandoval. "Influence of the Filler Content on the Thermal Expansion Behavior of an Epoxy Matrix Particulate Composite." *Materials Science and Engineering* (2009): 26-31.

Tomblin, John. *Overview of Composite Materil Trends in Aviation Manufacturing.* Report, Wichita: Wichita State University (2009).

Performance Composites. “Carbon Fiber”. Accessed January 14, 2014. www.performance-composites.com.

Wucher, B., F. Lani, T. Pardoen, C. Bailly, and P. Martiny. "Tooling geometry optimization for compensation of cure-induced distortions of a curved carbon/epoxy C-spar." *Composites* (2013): 27-35.